STRUCTURAL ANALYSIS OF A PULTRUDED COMPOSITE BEAM: SHEAR STIFFNESS DETERMINATION AND STRENGTH AND FATIGUE LIFE PREDICTIONS

Michael David Hayes

Dissertation Submitted to the Faculty of the
Virginia Polytechnic Institute and State University
in Partial Fulfillment of the Requirements for the Degree of

Doctor of Philosophy
in
Engineering Mechanics

John J. Lesko, Chair
Scott W. Case
Michael W. Hyer
Muhammad R. Hajj
Thomas E. Cousins

November 18, 2003
Blacksburg, Virginia

Keywords: FRP beam, Timoshenko shear stiffness, beam theory, strength, life, fatigue, durability, remaining strength, finite element analysis, delamination, compression

Structural Analysis of a Pultruded Composite Beam: Shear Stiffness Determination and Strength and Fatigue Life Predictions

Michael D. Hayes

John J. Lesko, Chair

Engineering Mechanics

ABSTRACT

This dissertation is focused on understanding the performance of a particular fiber-reinforced polymeric composite structural beam, a 91.4 cm (36 inch) deep pultruded double-web beam (DWB) designed for bridge construction. Part 1 focuses on calculating the Timoshenko shear stiffness of the DWB and understanding what factors may introduce error in the experimental measurement of the quantity for this and other sections. Laminated beam theory and finite element analysis (FEA) were used to estimate the shear stiffness. Several references in the literature have hypothesized an increase in the effective measured shear stiffness due to warping. A third order laminated beam theory (TLBT) was derived to explore this concept, and the warping effect was found to be negligible. Furthermore, FEA results actually indicate a decrease in the effective shear stiffness at shorter spans for simple boundary conditions. This effect was attributed to transverse compression at the load points and supports. The higher order sandwich theory of Frostig shows promise for estimating the compression related error in the shear stiffness for thin-walled beams.

Part 2 attempts to identify the failure mechanism(s) under quasi-static loading and to develop a strength prediction for the DWB. FEA was utilized to investigate two possible failure modes in the top flange: compression failure of the carbon fiber plies and delamination at the free edges or taper regions. The onset of delamination was predicted using a strength-based approach, and the stress analysis was accomplished using a successive sub-modeling approach in ANSYS™. The results of the delamination analyses were inconclusive, but the predicted strengths based on the compression failure mode show excellent agreement with the experimental data. A fatigue life prediction, assuming compression failure, was also developed

using the remaining strength and critical element concepts of Reifsnider et al. One DWB fatigued at about 30% of the ultimate capacity showed no signs of damage after 4.9 million cycles, although the predicted number of cycles to failure was 4.4 million. A test on a second beam at about 60% of the ultimate capacity was incomplete at the time of publication. Thus, the success of the fatigue life prediction was not confirmed.

ACKNOWLEDGEMENTS

Part 1: Determination of the Timoshenko Shear Stiffness of Composite Structural Beams

Table of Contents

List of Tables

List of Figures

1 Introduction

Fiber-reinforced polymeric (FRP) composites are increasingly finding use in the areas of civil infrastructure and construction. Specifically, composites are being considered for structural elements in bridge construction as lighter, more durable alternatives to steel and concrete. The design of FRP structures in infrastructure applications is typically stiffness-controlled, since large deflections can pose problems for overlay and connection durability. Furthermore, FRP structural beams will exhibit appreciable shear deformation at low aspect (span-to-depth) ratios, due to the relatively low shear modulus of FRP materials. In order to minimize cost and to design efficient structures using FRP beams, it is important for the manufacturers to be able to precisely specify stiffness design allowables. Therefore, it is imperative to be able to measure the stiffness quantities accurately in the laboratory and to be able to estimate them analytically.

Timoshenko first order shear deformable beam theory is typically utilized in the analysis of FRP beams, requiring the specification of two stiffness quantities: the bending stiffness EI and the shear stiffness, kGA. The shear correction factor k was introduced to account for the error in the shear strain energy caused by assuming a constant shear strain through the depth of the beam, as opposed to the classical parabolic distribution. The shear correction factor depends upon the cross-sectional shape, material properties, and vibration response of the beam [1]. In the case of thin-walled FRP beams, determination of kGA either experimentally or analytically can be difficult due to a number of different factors. This problem is one focus of this dissertation.

1.1 Background

The current study is motivated by the need to understand and predict the performance of a particular structural member that has been developed for the infrastructure market. Strongwell Corporation of Bristol, Virginia has developed a 91 cm (36 inch) deep pultruded double web beam (DWB) for use in bridge construction (Figure 1). The beam is a hybrid laminated composite, composed of both E-glass and carbon fibers in a vinyl ester resin. The DWB is intended for unsupported spans from 9.14 to 18.3 m (30 to 60 feet). Experimental results indicate that at the 9.14 m span, shear accounts for 15% of the total deformation under four-point loading with loads applied at the third points (1/3 and 2/3 span).

In the development phase for the 36 inch DWB, Strongwell first manufactured a 20.3 cm (8 inch) subscale prototype of the DWB. The beam was later implemented in the Tom's Creek

Bridge rehabilitation [2]. During and after the rehabilitation project, a number of 8-inch DWB's were tested to measure bending and shear stiffness, torsional stiffness, strength, and fatigue resistance [3-5]. The results of this testing were published in the first EXTREN DWB™ Design Guide [4]. The Materials Response Group at Virginia Tech recently completed a contract to add performance data and design information for the 36 inch DWB to the design manual.

Virginia Tech also collaborated with Strongwell, the Virginia Department of Transportation (VDOT), and the Virginia Transportation Research Council (VTRC) to construct a bridge using the 36 inch DWB. The team rehabilitated a short span bridge on Route 601 over Dickey Creek in Smyth County, Virginia using the 36 inch DWB as the primary girders. The original steel/timber structure was replaced with eight 36 inch DWB's over an 11.8 m (39 ft) span (Figure 2). A 13.7 cm (5-3/8 inch) deep glue-lam timber deck system with asphalt overlay was utilized atop the FRP girders. A timber and steel rail system was also employed. The FRP girders were spaced 1.1 m (42 inches) apart over the 9.1 m (30 ft) width. The target deflection criterion was L/800 (maximum deflection equal to the span length L divided by 800) [6]. Upon completion of the rehabilitation in October 2001, the new structure was field tested to assess deflections, strains, load distribution factors, and the impact factor [7]. The test results indicated a maximum service deflection of less than L/1000.

Prior to the Route 601 Bridge rehabilitation, Waldron [8] examined eleven 36 inch double-web beams in a static four-point bending geometry to measure the bending and shear stiffness values. The Timoshenko shear stiffness kGA was obtained using two different methods, the "graphical method" and the "back calculation method" (Section 1.2.3). The measured kGA value was as much as 59% less than the analytically calculated value (Section 3.1.1) for two beams tested using the graphical method. The Weibull mean value for all eleven beams tested using the back calculation method was 33% less than the analytical value, and the scatter was considerable. At the time, the error was attributed mainly to imprecision in the deflection measurements caused by the low bit resolution of the data acquisition system.

More recently, Schniepp [9] tested 15 beams at spans ranging from 9.1 m to 17.7 m (30 ft to 60 ft), corresponding to span-to-depth ratios of 10 to 19, respectively (Figure 3). The objective was to collect sufficient data to calculate design allowables for the design manual. Therefore, care was taken to obtain accurate deflection measurements. The issue of precision was alleviated greatly by switching to a higher resolution data acquisition system, and the

measured values improved slightly; the mean kGA values were higher than the analytical value by 15-27%, and the scatter was still high. The results are summarized in Table 1, where the A- and B-allowables were determined using Weibull statistics. Schniepp used the "back calculation" method exclusively. Note that the units of (stiffness x area) are used throughout this text to retain the physical significance of the quantity kGA. The test geometry was again four-point bending with loads applied at the third points through 46 cm x 23 cm (18 inches x 9 inches) load patches. Note that the average measured kGA values are inversely proportion to the span length (Figure 13).

These results highlight the difficulty in measuring the Timoshenko shear stiffness kGA. The shear deformation is small at longer spans relative to the bending deformation and therefore more difficult to measure accurately. As the span length is shortened, the measured value appears to approach the analytical value, as evidenced by Schniepp's results. However, at shorter spans, non-classical behavior at the load patches and supports may affect the deflection and the measured kGA value. For instance, out-of-plane warping due to shear deformation is thought to affect the measurement of kGA [10]. Furthermore, the patch loads present a contact problem which can cause stress concentrations, as well as transverse compression. Such deformation is not predicted using ordinary beam theory.

Thus, <u>the primary objective of this study is to analytically calculate the Timoshenko shear stiffness kGA for the 36 inch DWB and to assess what aspects of the traditional bending test impact the measured value</u>. These results may be even more important for other FRP beams in which the amount of shear deformation is greater. A review of the literature will elucidate the current understanding of shear deformation and the calculation of the Timoshenko shear stiffness.

1.2   Literature Review

1.2.1   Timoshenko Shear Stiffness

To account for shear deformation in beam theory, Timoshenko [11, 12] introduced an additional kinematic variable, ϕ, the angular rotation of the cross-section at the mid-surface. This additional degree of freedom represents a relaxation of the Kirchhoff assumption that cross-sections remain normal to the mid-surface upon deformation; the additional deformation is due to shear. In defining the shear stress resultant, Timoshenko also introduced the concept of a

shear correction factor k to correct the strain energy resulting from the assumption of a constant shear profile.

Cowper later presented an alternate derivation of Timoshenko beam theory that leads to a comprehensive definition for k [13]. His approach was to integrate the equations of three-dimensional elasticity, defining mean kinematic variables over the entire cross-section. Residual displacements were included to account for warping of the cross-section. The shear correction factor naturally appeared in the governing equations when the shear stress distribution was equated to that of a known exact solution. Cowper derived explicit formulas to calculate k for isotropic beams of solid cross and thin-walled sections. For homogeneous isotropic beams, he found that k depends only on the geometry and the Poisson's ratio, v. For a solid rectangular section, k approaches the well-known value of 5/6 as v approaches zero.

1.2.2 Analytical Methods to Calculate kGA for Composite Beams

For laminated composite beams, the material properties and therefore the shear stress will vary through the depth of the beam. Dharmarajan and McCutchen [14] extended Cowper's approach to homogeneous specially-orthotropic solid beams. The shear correction factor k was shown to be dependent upon the effective engineering properties of the beam. Similarly, Teh and Huang [15] derived equations for generally orthotropic beams and demonstrated that k deviates from 5/6 as the fiber orientation angle increases. Madabhusi-Raman and Davalos [16] later derived a form for the shear correction factor for laminated rectangular beams with symmetric or asymmetric cross-ply or angle-ply lay-ups. In this work, the shear correction factor was computed by equating the shear strain energy obtained from the constitutive relations of first order shear deformable laminated plate theory to that obtained using the "actual" shear stress distribution calculated *a posteriori*, i.e. computed using the equilibrium equations of elasticity. This is the usual approach for determining interlaminar stresses from plane-stress solutions like Classical Laminated Plate Theory (CLT) [17, 18].

Determining the value of k for a thin-walled composite beam is more difficult, since the shear stress distribution is less easily obtained. Therefore, the common practice is to estimate the shear stiffness kGA by multiplying the transverse shear modulus G by the shear area A and assuming a value of $k = 1$ [19]. However, the definition of shear area for a thin-walled beam is not always clear. It is usually considered to be only the areas of the vertical members, since thin flanges carry very little shear. However, this assumption may no longer be valid as the thickness

4

of the flanges increases. Furthermore, since the factor k is used to correct the Timoshenko strain energy as computed over the shear area, <u>k and A are coupled</u>. Of course, the shear modulus G may also vary through the depth of the beam, complicating the issue further.

To estimate values of kGA for thin-walled composite beams, Bank [10] extended Cowper's method to thin-walled beams made of anisotropic panels such as laminated FRP beams and assessed the effect of anisotropy on k. In his development, Bank neglected the out-of-plane Poisson's ratio in the flanges in order to simplify the integration of the shear flow along the beam's contour. This assumption is valid only for thin flanges. Omidvar [20] followed a similar approach to develop formulas for thin-walled beams, but did not neglect the Poisson's effect in the flanges; however, only isotropic beams were considered. Bank and Melehan [21] later extended the Cowper/Bank approach to multi-celled cross-sections without neglecting the Poisson's ratio.

In References [10, 13-16, 20, 21], <u>the shear is considered to act on the entire cross-sectional area of the beam</u>. Since the shear stress distribution in a thin-walled beam is piecewise parabolic and the shear stress is very small in the flanges, the shear correction factor k can be much smaller than that found considering only the area of the vertical members. For instance, the Mechanics of Laminated Beam (MLB) model developed by Barbero et al. [22] neglects any shear stiffness contributions from the horizontal walls, and the shear stiffness GA is simply equal to the sum of the in-plane shear stiffnesses of the vertical panel(s). Furthermore, only the shear flow over the vertical members is considered in computing the shear correction factor. The result is that the shear correction factor is approximately equal to 1 for moderately tall sections with thin flanges, as expected. The shear flow across the <u>entire</u> section is found *a posteriori* by integrating the appropriate equilibrium equation in terms of stress resultants. The shear correction factor k is found by equating the shear strain energy computed from the shear flow <u>over the web section only</u> to the Timoshenko shear strain energy. In computing the latter, the shear force is taken to be the resultant of the shear stress over the web area only. This model assumes that the walls are symmetric with off-axis plies which are balanced.

More recently, Kim and Yoon [23] derived formulas to determine k for solid, rectangular anisotropic beams and thin-walled box beams composed of angle-ply laminates. Their focus was to assess the influence of extension-shear and bending-shear coupling on the shear correction factor. These couplings arise due to the presence of the A_{16} and A_{12}/A_{22} terms in the CLT

constitutive equations. Kim and Yoon derive formulas for k by equating the shear strain energy from Timoshenko beam theory to that found from the "actual" shear stress distribution found by integrating the equations of equilibrium. Their results suggest that k can vary between 0.38 and 5/6 for a rectangular section and between 0.5 and 1.0 for the box beam, depending upon the amount of coupling.

In summary, it is important to recognize that <u>the value of k is dependent upon or coupled with the definition of the shear area</u>. Consider, for example, the shear stress distribution for an isotropic wide flange calculated using the mechanics of materials approach. The MLB model yields a value of $k \approx 1$ for a homogeneous, isotropic I-beam with an aspect ratio of 1 [22]. For the same section, Bank [10] calculates a value of $k \approx 0.3$. This example highlights the need to carefully define the shear area and to consider only the shear flow over that area in calculating k. The error caused by interchanging the k values as predicted by these different approaches could be significant.

1.2.3 Experimental Determination of kGA

It is clear that the section shear stiffness and the shear flow depend on the material properties and geometry of the beam. Therefore, simply performing coupon shear tests on the web or vertical wall material of the beam is not sufficient to accurately determine the global section shear stiffness of the beam for use in Timoshenko beam theory. Full section tests on the beam itself are preferred, and two methods are available to determine the shear stiffness kGA experimentally.

In the first method, referred to here as the "back calculation method", a single four-point bend test is performed. The bending stiffness EI is first determined from strain readings on the outer flange surfaces at mid-span (in the constant moment region):

$$EI = \frac{Mc}{\varepsilon} \tag{1-1}$$

where M is the moment from equilibrium, c is the largest distance from the neutral axis, and ε is the measured strain. Once EI is known, the measured deflection can be used to back calculate kGA from the appropriate Timoshenko equation. For instance, the Timoshenko equation for a four-point bend test with the loads applied at the third points is

$$\delta_{max} = \frac{23PL^3}{648EI} + \frac{PL}{3kGA} \qquad (1\text{-}2)$$

where P is the is the load applied at both points and L is the span length. Solving for kGA,

$$kGA = \frac{PL}{3\left(\delta_{max} - \frac{23PL^3}{648EI}\right)} \qquad (1\text{-}3)$$

This method, while quick and simple, is generally avoided as it is very sensitive to error in the deflection measurement.

In the "simultaneous method", also referred to as the "graphical" method, multiple bending tests at different spans are run for each beam. Each test generates an additional Timoshenko equation with two unknowns, EI and kGA, since the measured deflection is known. Theoretically, only two span lengths are required to solve for the two unknown stiffness parameters, but additional tests are normally run to reduce the error. If the Timoshenko equation is modified by dividing by PL^3, then the equation can be interpreted as being that of a line, with $1/L^2$ being the independent variable on the abscissa and δ_{max}/PL^3 being the dependent variable on the ordinate. This is the "graphical" interpretation of the simultaneous approach. For example, Equation (1-2) becomes

$$\frac{\delta_{max}}{PL^3} = \frac{23}{648EI} + \frac{1}{3kGA}\frac{1}{L^2} \qquad (1\text{-}4)$$

Then the deflection quantity δ_{max}/PL^3 can be plotted versus $1/L^2$ for different tests run at different spans, L. The slope of a fitted line will be proportional to the kGA and the intercept will be proportional to the EI (see Figure 4). Alternately, one can divide the Timoshenko equation by PL, and the slope and intercept will be proportional to EI and kGA, respectively. The simultaneous method has been used by a number of researchers to characterize solid beams, thin-walled beams, and sandwich panels (e.g. [1, 24-29]).

1.2.4 Experimental Error

Both experimental methods are very sensitive to error in the deflection measurement. Furthermore, the inherent limitations of Timoshenko beam theory may introduce additional error. Non-classical effects caused by warping, transverse flexibility, and complex boundary conditions are neglected by Timoshenko beam theory and will affect deflections slightly. For example, "warping incompatibilities" caused by loading and boundary conditions or non-uniform bending cause additional axial displacements or warpings [30]. Through the strain-displacement relations, these warping displacements cause a local increase in the outer fiber axial strains and a reduction in the shear strain. The effect decays over a finite length, which depends upon the test geometry, beam geometry (aspect ratio), and material properties (degree of anisotropy). For a solid orthotropic beam, this decay length is simple to estimate (refer to Dufort's parameter ω in [31]). The task of computing the decay parameter for a thin-walled laminated beam is addressed in the current study.

The local reduction in shear strain caused by an incompatibility can be viewed as an increase in the local <u>apparent</u> Timoshenko shear stiffness, leading to an increase in the <u>effective</u> shear stiffness for the beam as a whole. Alternately, one can view the increase in axial strain as a decrease in the apparent bending stiffness. This view was taken by Lopez-Anido and GangaRao [32]. They developed a thin-walled beam theory including out-of-plane warping and calculated an effective axial modulus, which varies along the length of the beam. The effective modulus is shown to decrease in the vicinity of load points, and the effect decays in the far field. According to the authors, this observation explains why so many researchers have difficulty calculating the shear stiffness using Timoshenko beam theory. This argument was again echoed by Bank [10] in the context of calculating the shear correction factor. These results reinforce the concept of an effective Timoshenko shear stiffness which depends upon the loading geometry.

1.2.5 Local Effects under Transverse Loading

1.2.5.1 Simple Beams

The issue of local effects under concentrated, transverse loads has been addressed extensively in the literature for solid, rectangular section beams. The bulk of this research has focused on the limitations of the standardized shear tests, such as the ASTM D-790 flexural test method, the ASTM D-2344 Short Beam Shear (SBS) test, and the ASTM D-5379 V-notched beam method or Iosipescu shear test. For example, Whitney [33] developed an analytical stress

analysis based on 2-D elasticity theory to predict shear and normal stress distributions in the vicinity of the applied loads in orthotropic beams under three- and four-point bending. The surface traction was assumed to be a uniformly distributed load and was represented using a Fourier expansion. The shear stress was found to be skewed near both the supports and load points, and the compressive stress was also found to be significant in both locations.

Yoshida et al. [34] conducted a similar study but represented the concentrated load using a cosine distribution. Their results confirmed the normal and shear stress concentrations, as well as large increases in the axial stress. They also employed the photoelastic film coating technique and finite element analysis (FEA) to verify their results. Ming and Adams [35] used a finite element contact analysis to analyze the stress state under the loading pins.

Traction-induced distortion of the shear stress profile, as well as transverse flexibility, has also been addressed in the sandwich panel literature for soft, compressible core structures. In Frostig's "higher-order sandwich theory" [36], the faces are modeled as beams and the core is considered to be an elastic medium that carries no axial stress, represented by the 2-D equations of equilibrium. The in-plane stresses in the face sheets and the transverse stresses at the face/core interface are shown to be consistent with an elasticity solution and finite element results. Again, high concentrations in axial stresses (in the face sheets), compressive stresses (core), and shear stresses (core) are found under the load points and above the supports.

Dufort et al. [31] utilized Moiré interferometry to capture the effects of warping and crushing in orthotropic beams under three-point bending. They then derived a third order beam model to predict cross-section warping due to transverse shear [37]. Their work demonstrated that the third order kinematics permit a realistic smooth continuity of strains at mid-span caused by warping locking, as opposed to Timoshenko beam theory which predicts a discontinuity. Their results suggest that warping locking (warping restraint at a symmetry condition) leads to an apparent stiffening of the beam, while crushing leads to an apparent softening of the beam. They also conclude that warping can affect the beam deflection by as much as 6% for an orthotropy ratio of E_{11}/G_{13} greater than 35 and an aspect ratio (L/h) less than 5.

1.2.5.2 Laminated Beams

A number of analytical beam theories specific to thin-walled laminated beams have been developed over the past 20 years, mainly for the analysis of helicopter rotor blades. The focus of much of this work has been torsion, although some attention has been given to bending related

warping. The earliest models adapted Vlasov's thin-walled beam theory to open section laminated composite beams using CLT to calculate wall properties, e.g. Bauld and Tzeng [38]. This approach did not account for shear deformation, but was later modified to incorporate shear by Chandra and Chopra [39].   Rehfield [40] used St. Venant's approach to capture out-of-plane warping due to torsion. Bauchau [30] modified the St. Venant approach using Reissner's variational principle to include eigenwarpings. These warping effects decay over a length determined by the aspect ratio of the beam, as well as the degree of orthotropy.   The decay length can be as high as 15 times the beam height [41]. Bauchau's theory captures the warping by expanding the axial displacement kinematics in a series of eigenwarpings and using energy principles to derive the governing equations. However, the model requires a finite element solution.

Similarly, Hjelmstad [42] studied the warping restraint effect that occurs when the end of a thin-walled beam is restrained from rotation, such as at a clamped end of a cantilever beam. He expressed the axial displacement as a series expansion in terms of a set of independent basis functions, and found that the shear strain was coupled with the warping intensity. This leads to a "shear anomaly" in which warping can occur solely due to a shear gradient. (This effect was first observed by Foutch and Chang [43]). The implication is that warping can occur even for beams with simple or free boundary conditions, as long as there is some change in the resultant shear force, as in the case of a simply-supported beam with a uniformly distributed load, for example. In fact, the two warping effects oppose each other.

In their model, Lopez-Anido and GangaRao [32] used a macroelement approach to derive a thin-walled beam theory with warping. Similar to the previous studies, this approach requires expressing the axial displacement as a Fourier polynomial series expansion in terms of basis functions. However, no form for the kinematic expressions is assumed *a priori*. The loading must also be represented as a Fourier series. The multiple walls or "macroelements" are connected via continuity and equilibrium at the common nodal lines, and explicit solutions for box beams are possible. This model is capable of capturing shear lag along the length of the beams, as well as across the width of the flanges.

Other models have been developed to provide more exact solutions to the torsion warping problem and to incorporate coupling effects for the bending and vibration problems [44-48]. Kim and White [49] also incorporated transverse shear effects in the walls to more accurately

model thick-wall beams. However, because of the extra refinements, all of these models require finite element solutions.

All of the models discussed in this section, while helpful in understanding the mechanisms of warping in simple thin-walled beams, are not readily applicable to open sections with arbitrary construction and wall lay-ups. Most are designed for closed, box sections with simple and often uniform lay-ups around a single contour. One exception, the laminated beam theory of Barbero et al. [22] described in Section 1.2.2, is capable of modeling laminated beams with arbitrary cross-sections and lay-up, although the model is limited to Timoshenko kinematics. However, the authors point out that the kinematics could easily be modified to account for warping.

1.2.6 Sandwich theories

Although higher order beam models can capture warping effects and the resulting localized stress concentrations, they cannot capture the transverse compression that occurs under concentrated loads. Furthermore, they do not accurately represent the boundary conditions which usually consist of surface tractions or specified displacements at the top and bottom flanges. However, such effects are of great concern in the sandwich panel literature, where soft inner cores are susceptible to local indentation under concentrated loads. The most relevant papers in this field are considered next.

The original sandwich theory by Allen [29] and Plantema [50] used a Timoshenko-type approach to account for shear deformation by assuming that the face sheets carry all of the axial load (the so-called "weak core" assumption) and that the core carries all of the shear loading. Compressive deformation was not considered. However, local perturbations in the deformation due to warping constraint could be captured. Later attempts to capture the transverse flexibility used a beam on elastic foundation approach, e.g. Reference [51]. This approach did not couple the two face sheets together, so that the global response was not accurately predicted.

Frostig et al. [36] developed a 2-D sandwich model for isotropic face sheets and core (discussed previously) that could account for stress concentrations under loads and over supports. The model was later extended to orthotropic laminated sheets [52, 53]. This "higher order sandwich model" follows the weak-core assumption. Swanson presented solutions for a uniform distributed load and concentrated loads [54]. Frostig and Baruch [55] and Swanson [53]

also derived a solution to the higher order sandwich model equations for arbitrary loading using a Fourier expansion for the loading, similar to the Navier solution for a simply supported plate.

An alternate approach is the elasticity solution of Pagano [56] and Srinivas and Rao [57]. Each layer in the structure is modeled as an elastic continuum, and the 3-D governing equations of equilibrium are expressed for each layer. Displacement and stress continuity are imposed as interface conditions for each layer, and the ends of each layer are assumed to be simply-supported. The solution is found using a Fourier expansion for the loading and by solving the system of constraint equations. For a sandwich panel or beam, the web is represented using its effective ply properties, and the core layer can be modeled as weak or "strong" (i.e. carrying axial stress). The primary advantage of this approach is that no limitations are placed on the thickness or stress state of the layers. However, for more than a few layers or loading terms, the computational requirements become prohibitive.

1.2.7 Summary

Since the introduction of shear deformable beam theory by Timoshenko in the 1920's, exact solutions for determining the shear correction factor of general solid beams have been developed. Approximate analytical solutions for thin-walled laminated beams have also been introduced. These solutions permit accurate predictions of the global beam response for most engineering applications. However, experimental determination of the Timoshenko shear stiffness has proven to be more difficult. This difficulty is likely a direct result of the type of non-classical behaviors that Euler and Timoshenko beam theories neglect, including warping and transverse flexibility. While several authors have acknowledged the importance of these factors, few have attempted to quantify the effects.

1.3 Objectives

The first objective of Part 1 of this dissertation is to accurately determine the Timoshenko shear stiffness kGA of the 36 inch DWB. Based on the experience and contributions of past researchers, kGA will be calculated using several analytical methods which take into account the thin-walled cross-section of the beam and the anisotropy of the wall panels. The second objective of Part 1 is generally to understand the difficulties in measuring kGA experimentally. In particular, the effects of boundary conditions, loading conditions, and test geometry are considered. It is hypothesized that these factors influence the beam response primarily through

warping and warping restraint, so means of quantifying the warping effect are explored. Finite element analysis and analytical models are utilized to test this hypothesis. The effects of transverse compressibility are also considered. The third objective of this study is to develop guidelines for the practicing engineer to estimate error in the *kGA* measurement caused by the non-classical effects. Observations from the finite element analysis and analytical models are used to compare different loading cases and the effect of the beam design on the error.

2   Analytical Methods

2.1   Shear stiffness determination

The Timoshenko shear stiffness kGA of the 36 inch DWB was calculated using three different approaches: 1) the Mechanics of Laminated Beam model, 2) the Cowper/Bank approach, and 3) finite element analysis (FEA). The lay-up of the 36 inch DWB was estimated using the fiber thread-up schematics provided by the manufacturer, and the ply-level engineering properties were estimated using standard micromechanics models. While the lay-up is proprietary, the web is essentially a quasi-isotropic panel with some random-fiber continuous strand mat (CSM). The flanges are comprised of two sub-laminates: the outer sub-laminate, which consists of carbon fiber and CSM, and half of the web panel material which is folded 90 degrees to form the inner sub-laminate. This all-glass portion terminates at two external tapers (Figure 1). The ply properties used to model the DWB are summarized in Table 2.

2.1.1   Thin-Walled Laminated Beam Theory

The global beam properties were determined using the MLB model of Barbero et al. [22]. In the MLB model, the constitutive behavior of the panels is determined using CLT, and first order shear deformable (Timoshenko) kinematics are specified for the beam's cross-section. The stiffness quantities for the beam are calculated by equating the sum of the strain energies of each individual wall in terms of each wall's constitutive equations to the total strain energy of the beam in terms of the unknown global stiffness quantities. The global stiffness quantities are then solved for in terms of the local wall stiffness quantities. The shear stiffness of the flanges (generally, any horizontal members) is neglected, and the total shear stiffness is simply equal to the sum of the in-plane shear stiffness values of the vertical members, GA. The derivation and resulting equations are not presented here, but the reader is referred to the third order laminate beam theory derived in Appendix A. The MLB solution can be obtained from the third order development by simply omitting the third order term in the kinematics and the resulting higher order quantities in the energy expressions and stiffness quantities.

The theory also provides a means of determining the shear correction factor, k, for application in Timoshenko beam equations. Following the definition, k is found by equating the shear strain energy predicted by Timoshenko beam theory to that obtained from the "actual" shear stress distribution over the cross-section. The Timoshenko strain energy is simply

$$U_{Timoshenko}(z) = \frac{1}{2}V_y(z)\gamma_{yz}(z) \qquad (2\text{-}1)$$

where V_y is the resultant shear force over the cross-section. In Barbero et al. [22], the z-direction is along the length of the beam, and the y-direction is through the depth of the beam. Using the constitutive behavior, Equation (2-1) becomes

$$U_{Timoshenko}(z) = \frac{1}{2}\frac{(V_y(z))^2}{kGA} \qquad (2\text{-}2)$$

The shear strain energy due to the actual shear stress distribution is calculated as the sum of the individual shear strain energies of the n walls comprising the cross-section:

$$U_{actual} = \frac{1}{2}\sum_{i=1}^{n}\int_{-b_i/2}^{b_i/2} \overline{N}_{sz}^*(s_i,z)\overline{\gamma}_{sz}^*(s_i,z)\sin^2\phi_i ds_i \qquad (2\text{-}3)$$

where $\overline{N}_{sz}^*$ is the local laminate shear stress resultant and $\overline{\gamma}_{sz}^*$ is the local laminate shear strain. The s-coordinate is the local laminate transverse direction (y in usual laminate notation), determined by the orientation angle ϕ_i of the ith panel (see Figure A.2, Appendix A). For the web panel, s is related to y, while for the flanges, s is related to x. Also note that b_i is the width of the ith laminate.

Because the MLB analysis neglects shear deformation in the flanges and assumes a constant shear strain distribution through the web, the actual wall shear stress resultant and shear strain across all walls is estimated *a posteriori* by integrating the z-direction resultant force equilibrium equation for each panel:

$$\overline{N}_{z,z} + \overline{N}_{sz,s_i}^* = 0 \qquad (2\text{-}4)$$

where $\overline{N}_z$ is the axial stress resultant in the wall. Integrating Equation (2-4) and applying Bredt's formula for closed cross-sections results in the actual shear flow $\overline{N}_{sz}^*$ over the cross-section contour. The actual wall shear strain is then found by

$$\gamma_{xz}^*(s_i, z) = \frac{\overline{N}_{sz}^*}{F_i} \tag{2-5}$$

Substituting $\overline{N}_{sz}^*$ and γ_{xz}^* into Equation (2-4), the shear correction factor is found by equating Equations (2-2) and (2-3) and solving for k.

Barbero et al. [22] give a general equation for k in terms of wall stiffness parameters and the contour definition. It is important to note that to be consistent with the underlying assumptions of MLB, <u>only the shear flow over the web panels is used to compute k</u>. That is, only part of the total shear flow is used to compute the shear strain energy in Equation (2-3), as signified by the use of the $sin^2\phi$ term. Furthermore, <u>the shear resultant force</u> used in Equations (2-1) and (2-2) <u>is actually slightly less than the total shear force</u>:

$$V_y(z) = \sum_{i=1}^{n} \int_{-b_i/2}^{b/2} \overline{N}_{sz}^* \sin\phi_i \, ds_i \tag{2-6}$$

These are subtle but important details which can cause large errors in the k calculation, if they are not carefully considered.

2.1.2 Cowper/Bank Method

Next, the approach developed by Cowper for calculating k for isotropic thin-walled beams and then modified by Bank for thin-walled beams composed of laminated panels was utilized. The standard equations for I- and box-sections were adapted to the DWB by neglecting the contribution of the sub-flanges. The DWB was modeled as an I-beam by representing the double web panels as a single web panel of double thickness. The shear stiffness GA_{tot} based on the total cross-section area was calculated assuming a uniform thickness of 1.75 cm (0.688 inch)

for the web panels, and a uniform thickness of 2.33 cm (0.917 inch) for the flange. This latter value is roughly equal to the average thickness of the flange, taking into account the taper.

2.1.3   Finite Element Analysis

2.1.3.1   Element Types

The 36 inch DWB was modeled in ANSYS$^{\circledR}$ using the SOLID46 8-noded, 3-D layered solid element. The SOLID46 element is essentially a 3-D version of the layered SHELL99 element type designed to model thick layered shells or solids. In both cases, the full 3-D ply-level constitutive equations are utilized to calculate an integrated stiffness matrix for the entire layered shell or solid. The resulting stiffness matrix, strain measures, and stress resultants are identical to those calculated in shell or plate theory for layered composite materials, with the addition of higher order terms to permit warping of the cross-section. For instance, in the case of a flat plate, the integrated constitutive equations become

$$\begin{Bmatrix} \{\overline{N}\} \\ \{\overline{M}\} \end{Bmatrix} = \begin{bmatrix} [A] & [B] & [E] \\ [B] & [D] & [F] \end{bmatrix} \begin{Bmatrix} \{\overline{\varepsilon}^{(0)}\} \\ \{\overline{\varepsilon}^{(1)}\} \\ \{\overline{\varepsilon}^{(3)}\} \end{Bmatrix} \quad \text{and} \quad \begin{Bmatrix} \{\overline{Q}\} \\ \{\overline{R}\} \end{Bmatrix} = \begin{bmatrix} [\overline{A}] & [\overline{D}] \\ [\overline{D}] & [\overline{F}] \end{bmatrix} \begin{Bmatrix} \overline{\gamma}^{(0)} \\ \gamma^{(2)} \end{Bmatrix} \tag{2-7}$$

where

$$\left(A_{ij}, B_{ij}, D_{ij}, E_{ij}, F_{ij} \right) = \sum_{k=1}^{N} \int_{z} \overline{Q}_{ij}^{(k)} \left(1, z, z^2, z^3, z^4 \right) dz \quad i,j = 1,2,..,6$$

$$\left(A_{ij}, B_{ij}, F_{ij} \right) = \sum_{k=1}^{N} \int_{z} \overline{Q}_{ij}^{(k)} \left(1, z^2, z^6 \right) dz \quad i,j = 1,2,..,6 \tag{2-8}$$

Note that each submatrix [A], [B], etc. has dimensions 6 x 6, reflecting the assumption of a full 3-D stress state.

SOLID46 is recommended over SHELL99 for calculating interlaminar stresses, primarily because multiple SOLID46 elements can be stacked to allow through-the-thickness deformation slope discontinuities. The SHELL99 element was developed assuming that the shear disappears at the top and bottom surfaces of the element, while the SOLID46 element uses no such assumption. In the SOLID46 formulation, effective thickness-direction properties are calculated using thickness averaging. The result is that the interlaminar stresses are relatively constant though the element thickness. To calculate accurate interlaminar stresses, multiple SOLID46

elements stacked through the thickness are recommended [58]. For both parts of this dissertation, the SOLID46 element was used to model the DWB wall panels. However, shell elements would likely have sufficed for the Part 1 study, because accurate stresses were not required for the current investigation.

2.1.3.2   DWB Model

To accurately simulate the real test conditions, the load patches were modeled in detail. In the experiments, the load was applied to the beams via stroke-controlled hydraulic actuators. The cylindrical head of the actuators impinged on stout wide-flange beams, which in turn were welded to 5.1 cm (2 inch) thick steel plates to produce uniform rectangular load patches on the beam flange's surface. Elastomeric bearing pads measuring 6.03 cm (2.38 inch) in thickness were inserted between the steel plates and the beam to protect the composite material against severe load concentrations at the plate edges, and to ensure a more uniform pressure distribution. The resulting load patch dimensions were 45.7 cm x 22.9 cm (18 inches x 9 inches), where the dimensions measure across the flange width and along the beam length, respectively. In some simulations, the bearing pads at the supports were also modeled.

The bearing pads were custom ordered to meet specifications for bearing pads in bridge applications, and they were identical to the pads used in the Route 601 Bridge between the concrete abutments and the DWB girders. The rubber pads are reinforced with four steel shims and designed to allow sufficient shearing and rotation for the beam motion, while maintaining structural integrity under high cycle fatigue. The rubber is a 50 duro (Shore) hardness neoprene rubber with a tensile strength of 6.9 MPa (1000 psi) and an elongation to failure of 350%. The material is non-linear as exhibited by stress-hardening at moderate strains in tensile test data.

To simplify the analysis, the rubber was assumed to linear elastic with a Young's modulus equal to a low strain (30%) value provided by the manufacturer, 1.03 MPa (150 psi), and a Poisson's ratio of 0.4999. The modulus value was chosen to force the FEA pad deflections to match the actual deflections of the bearing pads at the supports in the 12.2 m (40 ft) geometry as closely as possible. With these properties, the maximum predicted pad compression is 0.955 cm (0.376 inches) and the average outer corner pad deflection is 0.305 cm (0.120 inches). The

measured values were 0.963 cm (0.379 inches) and 0.250 cm (0.098 inches), respectively[1]. Analysis of the FEA results later indicated that the pad strains were as high as 340%, suggesting that a higher modulus might be more appropriate.

Each layer in the pad was modeled as a separate volume and meshed using 0.254 cm thick SOLID45 elements (the isotropic version of the SOLID46 element). This dimension was chosen based on convergence of the pad deformations. Although the layers in the actual pad are not bonded, it is assumed that under high normal force, the frictional force will be sufficient to prevent inter-layer sliding. Therefore, the layers were assumed to be perfectly bonded, and coupling between the interfaces was accomplished using the VGLUE feature in ANSYS®. The 5.08 cm (2 inch) thick steel plates were modeled as isotropic volumes bonded to the pad (with 0.254 cm or 0.1 inch thick SOLID45 elements). The loads were then applied to the steel plates using uniform pressure traction across the top face of the plates.

A full length FE model was constructed for the 12.2 m (40 ft) long beam under four-point bending with the loads applied near the third points (see Figure 5). The walls of the beam were modeled such that one SOLID46 element comprises the entire thickness, except in the flange where the two sublaminates were modeled individually. The ply definitions were input to ANSYS®, which calculates the constitutive equations for the element as described previously. The mesh was sufficiently refined in the other directions to provide convergence on the mid-span deflection, calculated on the bottom surface of the bottom flange. Note that the fillets and flange tapers were not modeled.

In order to estimate the shear correction factor from FEA, the shear strain distribution through the depth of the beam in the far-field (at the quarter point) was determined. Using the effective shear modulus G of the web panels (calculated using CLT), the average shear stress distribution was then estimated. The term "average" is used because the shear stresses actually vary from ply to ply. The "actual" shear strain energy was then equated to the Timoshenko value, following the approach of Barbero et al. [22] to calculate k (discussed previously in Section 2.1.1). Following the discussion surrounding Equation (2-6), the average shear stress was integrated over the web panels only to calculate the resultant shear force for use in the Timoshenko shear strain energy calculation. Similarly, the "actual" shear strain energy was

---

[1] In Schniepp's testing, the deflections of the DWB bottom flange over the four corners of the two bearing pads were measured using displacement transducers. The maximum value reported above is the average of the two inner edge corners.

computed using only the average shear stresses over the web panels. A second estimate of k based on the entire cross-section was then computed by repeating this process using the total resultant shear force and the "average" shear stress distribution over the entire cross-section.

2.2   Non-Classical Effects and Effective Shear Stiffness

Previously, the concept of apparent shear stiffness was introduced. This local phenomenon is caused by a discontinuity or gradient in the resultant shear force. Depending upon the strength of the disturbances, which are controlled by the lay-up and geometry of the beam, the effects of these local changes in kGA integrated over the entire beam may impact the effective kGA. This effective shear stiffness is the quantity measured in experiments, and it should depend upon the loading and geometry. For instance, a beam loaded in three-point bending might exhibit a different effective kGA than a beam of equal length under four-point loading. In addition, distributed loads should have a different effect than concentrated loads. In this way, the Timoshenko shear stiffness is viewed as being not only a material or structural property, but also a geometry-dependent quantity.

The simplest way to characterize the impact of these non-classical effects on the shear response is to measure the change in deflection when the loading conditions are changed. FEA provides a means of simulating this process analytically. Unlike beam theory, FEA can account for actual loading conditions and boundary conditions, and it provides the real three-dimensional response of the beam. Of course, the user must be careful to accurately model loads and supports and to sufficiently refine the mesh to ensure convergence of the solution.

In this study, the effect of supporting the ends of the beam at the bottom surface or at the neutral axis was investigated using FEA. The use of pads at the load points and supports was also explored, and the influence of beam overhang was considered. Specifically, the stress-strain behavior near loading points and supports was observed to study local effects such as web compressibility and warping. In order to quantify the effective kGA for each loading case, the "back calculation method" was applied to the maximum predicted deflection, simulating the procedure used to determine kGA from experimental data. The bending stiffness was calculated using Equation (1-1), with the axial strain from the outer surface of the top flange. This value was checked using the theoretical bending stiffness calculated with MLB beam theory. This analysis was conducted for the three spans tested by Schniepp [9], as well as two additional span

lengths (6.1 and 15.2 m, or 20 and 50 ft), and the analytical results were compared to the experimental results. The models were constructed in the same manner described above for the 12.2 m test. Boundary conditions were varied as described below. A primary advantage of applying this approach to FEA results is that errors due to inaccurate deflection measurements are eliminated (assuming that the mesh is sufficiently refined).

2.2.1 Sensitivity Analysis

In order to demonstrate the sensitivity of the *kGA* calculation to errors in deflection measurements, a simple sensitivity analysis was conducted. The back calculation method was applied to typical deflection values at 9.14 and 12.2 m (30 and 40 ft) which were adjusted for small errors in the deflection. The resulting change in effective *kGA* was calculated, and the error in the calculated *kGA* value due to the error in deflection measurement was determined.

2.2.2 Effects of Boundary Conditions and Overhang

Four different boundary conditions were considered: 1) simply-supported boundary conditions at the neutral axis of the beam, 2) simply-supported conditions at the bottom edge of the beam, 3) pad supported with no overhang, and 4) pad supported with an overhang equal to 53.3 cm (21 inches). The first condition is meant to represent beam theory, where the boundary conditions can only be specified for the neutral axis. The third and fourth conditions are meant to represent the actual test geometry. The second condition is meant to be a compromise between the simplicity of the first condition and the actual location of the constraint.

The first condition was achieved by fixing displacements at nodes on the two web panels along the centerline of the beam. The second condition was achieved by specifying fixity to all of the nodes along the bottom edge of the bottom flange. The third and fourth conditions were achieved by bonding the bearing pad to the bottom flange and specifying fixity of displacements to the bottom face nodes on the pad. In all cases, the "pin-roller" type of conditions were emulated by restricting axial displacements on one end, while allowing free expansion or contraction at the other end. All four cases are shown in Figure 6.

2.2.3 Effects of Loading and Sensitivity to Definitions of Span and Shear Span

The effect of representing the loads as concentrated loads in the Timoshenko equations, as opposed to patch loads, was also investigated. Again, the back calculation method was applied to the FE predicted deflections determine *kGA*. The Timoshenko equation for patch

loading was derived by using uniformly distributed loads over the length of the bearing pads (22.3 cm or 9 inches). While this effect is expected to be minor, the author wishes to quantify all sources of error in the calculation of kGA. The presence of pad supports also complicates the situation in that the total span length and shear span length (support to load point) are not clearly defined. Therefore, the effect of the choice of span lengths on the effective kGA was also investigated.

2.2.4 Shear Warping - Third Order Laminated Beam Theory

The effect of warping on the deflection of FRP beams and the subsequent difficulty in determining kGA was considered next. To capture warping effects, third order kinematics following Reddy [59, 60] were utilized to derive a third order laminated beam theory (TLBT) for thin-walled beams composed of anisotropic, laminated panels. The use of third-order kinematics permits a non-linear distribution of axial displacement and strain through the beam depth (warping) and subsequently, through the strain-displacement relations, a quadratic variation of shear strain. Furthermore, the shear strains and stresses vanish at the free surfaces. This result eliminates the need for a shear correction factor and captures warping-related effects, such as the continuity of strains at a load point.

The laminated beam approach of Barbero et al. [22] was modified to permit third order kinematics and the resulting higher order constitutive equations. The energy equivalence approach employed in the MLB model was followed to develop global beam stiffness and coupling quantities in terms of the laminated wall properties, as determined using first order shear deformation theory (FSDT). The governing equations were then found using variational principles, and a solution technique employed by Dufort et al. [37] was followed to provide analytical solutions. An overview of the derivation is presented here; the full details are available in Appendix A.

2.2.4.1 Assumptions

Following the assumptions/restrictions made by Barbero et al. [22] in their Mechanics of Laminated Beam (MLB) theory, it is assumed that loading is applied through the shear center to decouple bending from torsion, and the bending is symmetric. In addition, the panels are assumed to be either vertical (web) or horizontal (flanges) to simplify the development. The beam is also assumed to be symmetric. Unlike the MLB model, this model accounts for shear deformation through the thickness of the flanges using first order (Timoshenko) kinematics.

2.2.4.2 Kinematics and Strain-Displacement Relations

The global coordinate system (different than that used by Barbero et al.) is oriented as shown in Appendix A, Figures A.1 and A.2. The global x-axis runs parallel to the longitudinal beam axis, the global y-axis is across the width of the beam, and the global z-axis is the transverse (bending) direction. The local coordinate system of the flange panels is oriented such that the local x-axis is parallel to the global x-axis, and the local z-axis is parallel to the global z-axis. The direction of the local y-axis is determined by the orientation angle θ and the right hand rule. Following the notation and convention of Reddy [59], the kinematics for a cross-section of the beam are as follows:

$$u(x,z) = u_o(x) + z\phi(x) - \alpha z^3 \left(\phi(x) + w_{o,x}(x)\right)$$
$$w(x,z) = w_o(x)$$

(2-9)

where α and β are geometric factors:

$$\alpha = \frac{4}{3h^2}$$
$$\beta = 3\alpha = \frac{4}{h^2}$$

and h is the height of the beam. The variable $\phi(x)$ is the usual Timoshenko rotation of the cross-section due to mid-plane curvature and shear deformation. The third term accounts for warping and permits a parabolic shear strain distribution. Assuming small deformations, the strain-displacement relationships become

$$\varepsilon_x(x,z) = \varepsilon_x^{(0)} + z\varepsilon_x^{(1)} + z^3\varepsilon_x^{(3)}$$
$$\gamma_{xz}(x,z) = \gamma_{xz}^{(0)} + z^2\gamma_{xz}^{(2)}$$

(2-10)

where

$$\varepsilon_x^{(0)} = u_{o,x}(x)$$
$$\varepsilon_x^{(1)} = \phi_{x,x}(x)$$
$$\varepsilon_x^{(3)} = -\alpha\left(\phi_{x,x}(x) + w_{o,xx}(x)\right)$$

and

$$\gamma_{xz}^{(0)} = \phi_x(x) + w_{o,x}(x)$$
$$\gamma_{xz}^{(2)} = -\beta\left(\phi_x(x) + w_{o,x}(x)\right)$$

In order to capture the shear strain in the flange panels, we assume first order shear deformable kinematics in the flanges. This assumption yields an additional refinement beyond the theory of Barbero et al. [22], which neglects any shear deformation in the flanges. In the case of a moderately thick-walled beam, this strain may not be negligible. Introducing the global coordinate $\bar{z}$ which is defined as the distance from the neutral axis to the flange's mid-surface and the local panel coordinate z',

$$z = \bar{z} + z'\cos\theta \tag{2-11}$$

the local flange mid-surface displacements become

$$\bar{u}_o(x) = u(x,\bar{z}) = u_o(x) + \bar{z}\phi(x) - \alpha\bar{z}^3\left(\phi(x) + w_{o,x}(x)\right) \tag{2-12}$$
$$\bar{w}_o(x) = w(x)\cos\theta_i = w_o(x)\cos\theta_i$$

The local rotation $\bar{\phi}$ is defined in terms of the global kinematics variables by calculating the global value of u at two points within the flange and solving the resulting equations for the two unknowns, $\bar{u}_o$ and $\bar{\phi}$ (see Appendix A). For moderately thick flanges, the local flange strain measures become

$$\bar{\varepsilon}_x(x,z) = \bar{\varepsilon}_x^{(0)} + z'\bar{\varepsilon}_x^{(1)}$$
$$\bar{\gamma}_{xz}(x,z) = \gamma_{xz}^{(0)} + \bar{z}^2\gamma_{xz}^{(2)} = \gamma_{xz}(x,\bar{z})$$
where
$$\bar{\varepsilon}_x^{(0)}(x) = \varepsilon_x(x,\bar{z}) = \varepsilon_x^{(0)} + \bar{z}\varepsilon_x^{(1)} + \bar{z}^3\varepsilon_x^{(3)}$$
$$\bar{\varepsilon}_x^{(1)} = \bar{\phi}'(x) = \left(\varepsilon_x^{(1)} + 3\bar{z}^2\varepsilon_x^{(3)}\right)\cos\theta$$

<div align="right">(2-13)</div>

Thus, the shear strain in the flanges is approximately linear through their thickness in accordance with the local Timoshenko assumption, and the flange value can be determined from the global shear strain expression.

The web kinematics are identical to the global kinematics, as the centroid of a web panel is assumed to be located at the neutral axis of the beam. However, since the web panels are oriented vertically, the displacements at the mid-surface vary across the width of the panel, b. Introducing the local coordinate across the width of the panel, s,

$$z(s) = s + \bar{z}$$
$$\frac{-b}{2} \leq s \leq \frac{b}{2}$$

(2-14)

the strains become

$$\bar{\varepsilon}_z^{(0)}(x,s) = \varepsilon_x^{(0)} + (s + \bar{z})\varepsilon_x^{(1)} + (s + \bar{z})^3 \varepsilon_x^{(3)}$$
$$\bar{\gamma}_{xz}^{(0)}(x,s) = \gamma_{xz}^{(0)} + (s + \bar{z})^2 \gamma_{xz}^{(2)}$$

(2-15)

Out of plane (through the laminate thickness) curvature in the web panels is neglected, following Barbero's approach.

2.2.4.3   Constitutive Behavior

From first order shear deformable plate theory, the constitutive behavior of the flange panels, expressed in terms of mid-plane values and resultant quantities is

$$\left\{ \begin{matrix} \{\bar{N}\} \\ \{\bar{M}\} \end{matrix} \right\} = \begin{bmatrix} [A] & [B] \\ [B] & [D] \end{bmatrix} \left\{ \begin{matrix} \{\bar{\varepsilon}^{(0)}\} \\ \{\bar{\varepsilon}^{(1)}\} \end{matrix} \right\}$$

(2-16)

$$\{\bar{Q}\} = \begin{bmatrix} A_{44} & A_{45} \\ A_{45} & A_{55} \end{bmatrix} \{\bar{\gamma}^{(0)}\}$$

25

where $\overline{N}, \overline{M},$ and $\overline{Q}$ are defined as

$$\{\overline{N}\} = \begin{Bmatrix} N_{xx} \\ N_{yy} \\ N_{xy} \end{Bmatrix} = \int_{-t/2}^{t/2} \begin{Bmatrix} \sigma_{xx} \\ \sigma_{yy} \\ \sigma_{xy} \end{Bmatrix} dz, \quad \{\overline{M}\} = \begin{Bmatrix} M_{xx} \\ M_{yy} \\ M_{xy} \end{Bmatrix} = \int_{-t/2}^{t/2} \begin{Bmatrix} \sigma_{xx} \\ \sigma_{yy} \\ \sigma_{xy} \end{Bmatrix} z \, dz,$$

(2-17)

$$\{\overline{Q}\} = \begin{Bmatrix} Q_x \\ Q_y \end{Bmatrix} = k \int_{-t/2}^{t/2} \begin{Bmatrix} \sigma_{xz} \\ \sigma_{yz} \end{Bmatrix} dz$$

where t is the panel thickness, and [A], [B], and [D] are defined as

$$\left(A_{ij}, B_{ij}, D_{ij} \right) = \sum_{k=1}^{N} \int_z \overline{Q}_{ij}^{(k)} \left(1, z, z^2 \right) dz$$

(2-18)

The web is modeled as an orthotropic panel with moduli E_x and G_{xz} (in global coordinates). E_x is the longitudinal modulus E_1 (local coordinates) and G_{xz} is the in-plane shear modulus G_{12}, as calculated using CLT. The web is assumed to carry only axial stress and shear stress. Curvatures and curvature-related force resultants acting through the thickness of the web are neglected. Thus, all higher-order through-the-thickness effects are neglected. The constitutive equations become

$$\overline{N}_x = A_{11} \varepsilon_x^{(0)}$$

(2-19)

$$\begin{Bmatrix} \overline{Q}_x \\ \overline{R}_x \end{Bmatrix} = \begin{bmatrix} \overline{A}_{xz} & \overline{D}_{xz} \\ \overline{D}_{xz} & \overline{F}_{xz} \end{bmatrix} \begin{Bmatrix} \overline{\gamma}_{xz}^{(0)} \\ \gamma_{xz}^{(2)} \end{Bmatrix}$$

where

$$\overline{A}_{xz} = \int G_{xz} dA = G_{xz} A_{web}$$

$$\overline{D}_{xz} = \int G_{xz} z^2 dA = G_{xz} I_{web}^{(2)} \qquad \text{(2-20)}$$

$$\overline{F}_{xz} = \int G_{xz} z^4 dA = G_{xz} I_{web}^{(4)}$$

following the notation of Reddy et al. [60].

Similarly, the global constitutive equations for the beam are expressed in terms of unknown global stiffness quantities:

$$\begin{Bmatrix} N_{xx} \\ M_{xx} \\ P_{xx} \end{Bmatrix} = \begin{bmatrix} A_{xx} & B_{xx} & E_{xx} \\ B_{xx} & D_{xx} & F_{xx} \\ E_{xx} & F_{xx} & H_{xx} \end{bmatrix} \begin{Bmatrix} \varepsilon_x^{(0)} \\ \varepsilon_x^{(1)} \\ \varepsilon_x^{(3)} \end{Bmatrix} \qquad \text{(2-21)}$$

$$\begin{Bmatrix} Q_x \\ R_x \end{Bmatrix} = \begin{bmatrix} A_{xz} & D_{xz} \\ D_{xz} & F_{xz} \end{bmatrix} \begin{Bmatrix} \gamma_{xz}^{(0)} \\ \gamma_{xz}^{(2)} \end{Bmatrix}$$

The definition of the beam stiffness coefficients are derived from energy principles, as shown in Appendix A. The total strain energy in terms of <u>local</u> panel stiffness quantities and <u>global</u> kinematics is found to be

$$U = \frac{1}{2} \int_x \left[\overline{A} \left(b(u_{o,x})^2 + \left(\frac{b^3}{12} \right) (\phi_{x,x})^2 - \alpha \left(\frac{b^5}{80} \right) \phi_{x,x} (\phi_{x,x} + w_{o,xx}) + \alpha^2 \left(\frac{b^7}{448} \right) (\phi_{x,x} + w_{o,xx})^2 \right) \right] dx$$

$$+ \frac{1}{2} b \int_x \left[\overline{A}_{xz} (\phi_x + w_{o,x})^2 - 2\overline{D}_{xz} \beta (\phi_x + w_{o,x})^2 + \overline{F}_{xz} \beta^2 (\phi_x + w_{o,x})^2 \right] dx$$

(2-22)

The total strain energy in terms of <u>global</u> stiffness quantities and <u>global</u> kinematics is

$$U = \frac{1}{2} \int_x \left[\begin{array}{l} A_{xx} (u_{o,x})^2 + 2B_{xx} u_{o,x} \phi_{x,x} + D_{xx} (\phi_{x,x})^2 - 2E_{xx} u_{o,x} \alpha (\phi_{x,x} + w_{o,xx}) - 2F_{xx} \phi_{x,x} \alpha (\phi_{x,x} + w_{o,xx}) \\ + H_{xx} \alpha^2 (\phi_{x,x} + w_{o,x})^2 + A_{xz} (\phi_x + w_{o,x})^2 - 2D_{xz} \beta (\phi_x + w_{o,x})^2 + F_{xz} \beta^2 (\phi_x + w_{o,x})^2 \end{array} \right] dx$$

(2-23)

Finally, the global beam stiffness coefficients are defined by equating like terms in Equation (2-21) to those in Equation (2-22):

$$A_{xx} = \sum_{i=1}^{nflanges} \overline{A}_i b_i + \sum_{i=1}^{nwebs} \overline{A}_i b_i$$

$$B_{xx} = \sum_{i=1}^{nflanges} \left(\overline{A}_i \overline{z}_i + \overline{B}_i \cos\theta_i \right) b_i$$

$$D_{xx} = \sum_{i=1}^{nflanges} \left(\overline{A}_i \overline{z}_i^2 + 2\overline{B}_i \overline{z}_i \cos\theta_i + \overline{D}_i \cos^2\theta_i \right) b_i + \sum_{i=1}^{nwebs} \overline{A}_i \left(\frac{b_i^3}{12} \right)$$

$$E_{xx} = \sum_{i=1}^{nflanges} \left(\overline{A}\overline{z}^3 - 2\overline{B}\overline{z}^2 \cos\theta \right) b_i$$

$$F_{xx} = \sum_{i=1}^{nflanges} \left(\overline{A}\overline{z}^4 - 2\overline{B}\overline{z}^3 \cos\theta - 3\overline{D}\overline{z}^2 \cos^2\theta \right) b_i + \sum_{i=1}^{nwebs} \overline{A}_i \left(\frac{b_i^5}{80} \right)$$

$$H_{xx} = \sum_{i=1}^{nflanges} \left(\overline{A}\overline{z}^6 - 6\overline{B}\overline{z}^5 \cos\theta + 9\overline{D}\overline{z}^4 \cos^2\theta \right) b_i + \sum_{i=1}^{nwebs} \overline{A}_i \left(\frac{b_i^7}{448} \right)$$

$$A_{xz} = \sum_{i=1}^{nwebs} \overline{A}_{xz} b_i + \sum_{i=1}^{nflanges} k_f \overline{A}_{xz,i} b_i \left(1 - \frac{4\overline{z}_i^2}{h^2} \right)^2$$

$$D_{xz} = \sum_{i=1}^{nwebs} \overline{D}_{xz}$$

$$F_{xz} = \sum_{i=1}^{nwebs} \overline{F}_{xz}$$

(2-24)

The significance of each stiffness quantity is given in Appendix A.

2.2.4.4 Governing Equations

Using the definitions of the global stress resultants in Equation (2-20), the total potential energy of the beam under distributed load q and concentrated load P is

28

$$\pi = \frac{1}{2}\int_0^L \left[N_{xx} u_{o,x} + M_{xx} \phi_{x,x} + P_{xx}(-\alpha)(\phi_{x,x} + w_{o,xx}) + Q_x(\phi_x + w_{o,x}) + R_x(-\beta)(\phi_x + w_{o,x}) \right] dx$$

$$- \int_0^L q w_o(x) dx - P w_o(x_P)$$

Equation (2-25)

Applying the Principle of Virtual Displacements, the governing equations are found to be

$$N_{xx,x} = 0$$
$$Q_{x,x} - \beta R_{x,x} + \alpha P_{xx,xx} + q = 0 \qquad (2\text{-}26)$$
$$M_{xx,x} - \alpha P_{xx,x} - Q_x + \beta R_x = 0$$

and the boundary conditions are

Either
u_o specified
w_o specified
ϕ_x specified
$w_{o,x}$ specified

or

$N_{xx} = 0$
$Q_x - \beta R_x + \alpha P_{xx,x} + (-P) = 0$
$M_{xx} - \alpha P_{xx} = 0$
$-\alpha P_{xx} = 0$

(2-27)

The P terms in parentheses are added for the case of a point load at either of the boundaries.

2.2.4.5 Solution of the Governing Equations

Here, the governing equations are solved following the approach of Dufort et al. [37], but Reddy [60] demonstrated how to derive the solution for any loading from the corresponding Euler beam solution. In the former approach, the governing equations are rewritten in terms of the displacement quantities and then reduced to one equation in one variable, the mid-surface shear strain (see Appendix A):

$$\gamma_{xz,xx}^0 - \omega^2 \gamma_{xz}^0 = \frac{(D_{xx} - \alpha F_{xx})}{\alpha^2 (D_{xx} H_{xx} - F_{xx}^2)}(A1 + qx) \qquad (2\text{-}28)$$

where

$$\omega = \sqrt{\frac{D_{xx}\left(A_{xz} - 2\beta D_{xz} + \beta^2 F_{xz}\right)}{\alpha^2 \left(D_{xx} H_{xx} - F_{xx}^2\right)}} \tag{2-29}$$

The solution to Equation (2-27) is found to be:

$$\gamma_{xz}^0(x) = \left(A_1 + qx\right)\frac{D_{xx} - \alpha F_{xx}}{D_{xx}\left(A_{xz} - 2\beta D_{xz} + \beta^2 F_{xz}\right)} + A_2 Cosh(\omega x) + A_3 Sinh(\omega x) \tag{2-30}$$

The other kinematic variables are found by substitution:

$$\phi_x(x) = A_4 + A_5 x - \frac{1}{6}\frac{x^2}{D_{xx}}\left(3A_1 + qx\right) + A_2 \frac{F_{xx}}{D_{xx}}\alpha Cosh(\omega x) + A_3 \frac{F_{xx}}{D_{xx}}\alpha Sinh(\omega x)$$

$$w_o(x) = A_6 - \frac{1}{2}A_5 x^2 - \left[A_4 + \frac{\left(D_{xx} - \alpha F_{xx}\right)}{D_{xx}\left(A_{xz} - 2\beta D_{xz} + \beta^2 F_{xz}\right)}A_1\right]x + \frac{D_{xx} - \alpha F_{xx}}{D_{xx}\omega}\left[A_3 Cosh(\omega x) + A_2 Sinh(\omega x)\right] +$$

$$\frac{A_1}{6D_{xx}}x^3 + q\left[\frac{x^4}{24D_{xx}} + \frac{\left(D_{xx} - \alpha F_{xx}\right)}{D_{xx}\left(A_{xz} - 2\beta D_{xz} + \beta^2 F_{xz}\right)}x^2\right]$$

$$\tag{2-31}$$

The parameter ω is a constant which characterizes the decay length of the higher order effects caused by a warping restraint or a shear gradient. For instance, at the location of a concentrated load, the resultant shear force undergoes a discontinuity. This discontinuity results in a warping of the cross section, which causes a local increase in the outer fiber axial strain. Moving away from the load point, decay in this strain concentration is balanced by an increase in the local shear strain. The length of the region over which this transition occurs is controlled by ω. Noting that the transcendental functions in Equations (2-29) and (2-30) can be rewritten in terms of a decaying exponential function, $e^{-\omega x/L}$, we can define a shear decay length $\delta = 1/\omega$, which corresponds to the length required for the shear to decay to 37% of the maximum, far-field

30

value under concentrated loading. It follows that 99% transfer/decay occurs at 6δ. For the case of a rectangular, orthotropic beam modeled using third-order (cubic) kinematics, Dufort et al.[37] showed that ω becomes

$$\omega = \sqrt{\frac{70GA}{EI}} = \sqrt{840\frac{1}{h^2}\frac{G_{13}}{E_{11}}} \tag{2-32}$$

Thus, the decay parameter becomes

$$\delta = \frac{1}{\sqrt{70}}\sqrt{\frac{EI}{GA}} = \frac{h}{\sqrt{840}}\sqrt{\frac{E_{11}}{G_{13}}} \tag{2-33}$$

and is controlled by the ratio of effective bending stiffness to shear stiffness and the aspect ratio, i.e. the degree of orthotropy.

The decay parameter ω is identical to the parameter λ^2 in Reddy's third order model [60], and it is similar to the quantity λ^2 in Hjelmstad's warping model for thin-walled beams [42]. Lopez-Anido and GangaRao [32] derived a similar parameter in their study of the shear lag problem in the context of Saint-Venant's principle (where the concept of a decay length was first introduced). The dependence upon this type of decay length upon the material properties and beam thickness for an anisotropic material was first established by Horgan [61].

2.2.4.6 Examples

To demonstrate the effect of warping on the maximum deflection of a beam, solutions for a few typical test geometries are derived. Solutions for solid rectangular isotropic beams are given, followed by the equivalent for thin-walled laminated beams. Note that the shear correction factor is replaced by a value of 5/6 which appears naturally with GA in the solid beam equations; this is the classical value of k as derived by Cowper [13]. The equivalent expression in TLBT is

$$\frac{D_{xx}^2\left(A_{xz} - 2D_{xz}\beta + F_{xz}\beta^2\right)}{\left(D_{xx} - \alpha F_{xx}\right)^2} \tag{2-34}$$

which yields *(5/6)GA* for the case of a solid rectangular isotropic beam. In the solutions below, the first term is the Euler bending deflection, the second term is the Timoshenko shear deformation, and the third term is the correction on the shear deflection due to warping. In each case, *L* is the span length and *P* is the total applied load, except where noted:

- *Three-Point Loading of a Simply-Supported Beam with a Central Load of P*
  Solid rectangular isotropic beam:

$$\delta_{max} = \frac{PL^3}{48EI} + \frac{PL}{4(\frac{5}{6})GA} - \frac{P\tanh\left(\frac{\omega L}{2}\right)}{2(\frac{5}{6})(GA)\omega} \tag{2-35}$$

Thin-Walled Laminated Beam:

$$\delta_{max} = \frac{PL^3}{48D_{xx}} + \frac{PL\left(D_{xx} - \alpha F_{xx}\right)^2}{4D_{xx}^2\left(A_{xz} - 2D_{xz}\beta + F_{xz}\beta^2\right)} - \frac{P\left(D_{xx} - \alpha F_{xx}\right)^2 \tanh\left(\frac{\omega L}{2}\right)}{2\omega D_{xx}^2\left(A_{xz} - 2D_{xz}\beta + F_{xz}\beta^2\right)} \tag{2-36}$$

- *Four-Point Loading of a Simply-Supported Beam with Loads P Applied at the Third Points*
  Solid rectangular isotropic beam:

$$\delta_{max} = \frac{23PL^3}{648EI} + \frac{PL}{3(\frac{5}{6})GA} - \frac{2P\text{Sinh}\left(\frac{\omega L}{6}\right)}{(\frac{5}{6})(GA)\omega\left(2\text{Cosh}\left(\frac{\omega L}{3}\right)-1\right)} \tag{2-37}$$

Thin-Walled Laminated Beam:

$$\delta_{max} = \frac{23PL^3}{648D_{xx}} + \frac{PL\left(D_{xx} - \alpha F_{xx}\right)^2}{3D_{xx}^2\left(A_{xz} - 2D_{xz}\beta + F_{xz}\beta^2\right)} - \frac{2P\left(D_{xx} - \alpha F_{xx}\right)^2 \text{Sinh}\left(\frac{\omega L}{6}\right)}{D_{xx}^2\left(A_{xz} - 2D_{xz}\beta + F_{xz}\beta^2\right)\omega\left(2\text{Cosh}\left(\frac{\omega L}{3}\right)-1\right)}$$

$$(2-38)$$

- *Uniform Distributed Load q = P/L Applied to a Simply-Supported Beam*

  Solid rectangular isotropic beam:

$$\delta_{max} = \frac{5qL^4}{384EI} + \frac{qL^2}{8(\frac{5}{6})GA} - \frac{q(1 - Sech(\omega \frac{1}{2}))}{(\frac{5}{6})(GA)\omega^2} \tag{2-39}$$

  Thin-Walled Laminated Beam:

$$\delta_{max} = \frac{5qL^4}{384D_{xx}} + \frac{qL^2(D_{xx} - \alpha F_{xx})^2}{8D_{xx}^2(A_{xz} - 2D_{xz}\beta + F_{xz}\beta^2)} - \frac{q(D_{xx} - \alpha F_{xx})^2(1 - Sech(\frac{\omega L}{2}))}{D_{xx}^2(A_{xz} - 2D_{xz}\beta + F_{xz}\beta^2)\omega^2} \tag{2-40}$$

- *Tip-Loaded Cantilever Beam (fixed at x = 0, load applied at x = L)*

  Solid rectangular isotropic beam:

$$\delta_{max} = \frac{PL^3}{3EI} + \frac{PL}{(\frac{5}{6})GA} - \frac{PTanh(\omega L)}{(\frac{5}{6})(GA)\omega} \tag{2-41}$$

  Thin-Walled Laminated Beam:

$$\delta_{max} = \frac{PL^3}{3D_{xx}} + \frac{PL(D_{xx} - \alpha F_{xx})^2}{D_{xx}^2(A_{xz} - 2D_{xz}\beta + F_{xz}\beta^2)} - \frac{P(D_{xx} - \alpha F_{xx})^2 Tanh(\omega L)}{\omega D_{xx}^2(A_{xz} - 2D_{xz}\beta + F_{xz}\beta^2)} \tag{2-42}$$

2.2.4.7 Application to the DWB

The TLBT model was programmed using *Mathematica*® software. First order laminated plate theory was used to calculate the panel stiffness values. The global stiffness coefficients were then calculated using Equations (2-24), and the governing equations were solved for the various loading examples above, as well as for the case of four-point bending using patch loads. The predicted response was then compared to the experimental data and finite element results. Specifically, the shear strain profiles near the load patches were compared to the finite element results and experimental data.

Finally, to estimate the error in the measured *kGA* value due to warping, the maximum deflections and bending stiffness were calculated using TLBT, and then the back calculation method was applied using the appropriate Timoshenko equation. The resulting effective *kGA* values were then compared to those obtained in the same manner using the FE results. The results of the TLBT analysis were also used to assess the influence of test geometry and span length on *kGA*. Next, the TLBT solutions for different loading geometries were used to actually quantify the effects of warping and warping restraint. Specifically, the influence of loading, span, and beam design (orthotropy) were examined.

2.2.4.8 Simple Beam Test Case

In addition to modeling the DWB, a simple test case was examined to understand the capabilities and limitations of the TLBT. This model was designed to ensure a high degree of mesh refinement and to eliminate any width or *y*-direction variations. A solid rectangular beam was modeled for aspect ratios varying from 3 to 30 and orthotropy ratios *E/G* varying from 2.5 to 37. The first orthotropy ratio corresponds to the ratio of the effective bending modulus of the DWB to its effective shear modulus, as calculated using the MLB model. The second orthotropy ratio corresponds to the properties of a carbon/vinyl ester uni-directional ply with a volume fraction of 55%. This is the material used in the DWB, and it is similar to the material used in the example of Dufort et al. [37].

Finite element models of the beam under four-point loading at varying span lengths were also constructed for the two cases of nodal fixity boundary conditions considered previously. The FE models were constructed in ANSYS™ using the PLANE42 element type, a 2-D planar 4-noded element for modeling plane stress problems. The beam was modeled with a 2.54 cm x 2.54 cm (1 inch x 1 inch) square cross-section and lengths ranging from 7.62 cm to 76.2 cm (3 inch to 30 inches). An element size of 1.27 mm x 1.27 mm (0.05 in x 0.05 in) was selected to provide a high degree of mesh refinement. The shear strain distributions of TLBT solution were compared to the FE results, and the back-calculated *kGA* values were computed.

2.2.5 Transverse Compressibility

Based on the results of the simple beam test case above, the influence of transverse flexibility on the global deformation and therefore the effective Timoshenko shear stiffness was also investigated. The influence of the transverse stiffness was considered for both the simple

beam and DWB using the FE models. The higher order sandwich theory of Frostig was then applied to both cases to further explore the transverse flexibility effect.

2.2.5.1 Solid Beam Test Case

To check for a transverse compressibility effect, a simple parametric study using the solid beam FE model was conducted. The transverse modulus E_z was varied between 5 and 445 MPa (1.11 Msi and 100 Msi), the modulus of the carbon/vinyl ester ply and the modulus of a nearly "infinitely stiff" material, respectively. The effective kGA was back-calculated as usual and compared to the TLBT and theoretical values. This analysis was conducted for both orthotropy cases considered previously.

2.2.5.2 DWB

A similar parametric study was undertaken to assess the influence of the transverse stiffness on the behavior of the DWB. Initially, the use of external stiffeners which would be bonded to the DWB was explored. However, the procedure proved difficult as x-direction stiffening could not be avoided. An alternate approach was adopted: the fiber-direction modulus E_{11} of the 90° plies in the web panels was increased to 689 GPa and 6.89e6 GPa (100 Msi and 1e6 Msi) to increase the panel stiffness in the z-direction from 14.8 GPa (2.15 Msi) to 138 GPa and 1296 GPa (20 Msi and 188 Msi), respectively. This approach does not affect the shear stiffness of the panels; an observation that can easily be verified by CLT. A check of the FE predicted shear strains also confirmed this.

2.2.5.3 Higher Order Sandwich Theory

The 2-D higher order sandwich theory of Frostig was reviewed previously in Sections 1.2.5.1 and 1.2.6, but the basic assumptions are reviewed here. The theory models the core as an elastic medium with no pre-prescribed kinematics. However, to permit a closed-form solution, the core is assumed to carry no axial stress – only shear and transverse stress. The result is that, like Timoshenko beam theory, the shear stress is predicted to be linear through the thickness of the beam. The theory is, however, able to predict x-direction variations in the shear stress.

The governing equations are developed by modeling the face sheets as Euler beams. The governing equations are found using the Principle of Minimum Potential Energy and by enforcing continuity at the face sheet/core interfaces. The governing equations are not given here; they can be found in Frostig et al. [36] and Swanson [54] for the case of symmetric face

35

sheets and in [52, 53] and Swanson [53]for the case of orthotropic laminated sheets. As noted previously, this model is able to capture more realistic loading and support conditions. For example, the applied load can be modeled as a traction on the top face, and the supports can be modeled as boundary conditions on the bottom face sheets.

In the current study, the procedure of Swanson [54] was used to obtain solutions for the cases of three- and four-point bending under discrete concentrated loads. The three-point solution was then applied to a sandwich beam test case used by Swanson. The effective Timoshenko shear stiffness was then back-calculated from the maximum predicted deflection for various spans. As in the FEA of the solid beam test case, the transverse modulus was varied to assess the effect on the effective kGA value.

Solutions for patch loads (modeled as uniform distributed loads) were then applied to the DWB, by modeling the DWB as a sandwich beam[2]. This was accomplished by neglecting the sub-flanges and assuming that the flange has a constant uniform thickness equal to the maximum thickness (2.62 cm or 1.032 inches). The web panels were represented as a uniform core with a width equal to that of the flanges. An effective core shear modulus was calculated by equating the core shear stiffness GA_{core} to the total web shear stiffness GA_{web}, and solving for G_{core}. The effective core transverse modulus $E_{z,core}$ was found in a similar manner. The effective Timoshenko shear stiffness was then back-calculated from the maximum predicted deflection for various spans. Again, the transverse modulus was varied to assess the effect on the effective kGA value. The results were then compared to the FE results.

---

[2] This is a reasonable assumption since the web panels and sub-flanges contribute only 9% of the total bending stiffness as determined using laminated beam theory.

3   Results

3.1   Shear Stiffness Determination

3.1.1   Thin-Walled Laminated Beam Theory

Using the MLB model, the total shear stiffness (neglecting flange and sub-flange contributions) was found to be $GA = 176$ MPa-m^2 (39.6 Msi-in^2). The double web feature of the DWB forces k to 0.997. Thus, the Timoshenko shear stiffness kGA is calculated to be 175 MPa-m^2 (39.5 Msi-in^2) (see Table 3). Henceforth, this value will be referred to as the <u>reference value</u> for comparison purposes.

3.1.2   Cowper/Bank Approach

Bank's equation for an I-section [10, 21] was applied to the DWB by neglecting the sub-flanges and modeling the double web panels as a single web panel of double thickness. The flanges were assumed to have a constant thickness equal to the average thickness over the entire width. Following this approach, k was calculated to be 0.7360. The resulting Timoshenko shear stiffness becomes 203 MPa-m^2 (45.7 Msi-in^2). This value is 16% larger than the MLB-predicted reference value. Using the box-beam equation, kGA was calculated as 209 MPa-m^2 (47.0 Msi-in^2). Accounting for the DWB's actual flange geometry and the presence of sub-flanges would likely improve the prediction for k, but these details were not considered in this study. Furthermore, the DWB flange is moderately thick with an aspect ratio (flange width divided by thickness) of 17, possibly violating the thin-flange assumption inherent in Bank's derivation [10].

3.1.3   Finite Element Analysis

The shear strain distribution through the depth of the beam in the far-field (at the quarter point) as predicted using the FE model is shown in Figure 7. The maximum strain predicted by Timoshenko beam theory using the MLB model matches the FE prediction quite well. The FE model predicts a very flat distribution in the web between the two sub-flanges (see Figure 1), and then a slow decrease as we approach the flange-web interface. It is also interesting to note that the shear strain within the flange is fairly significant, confirming the hypothesis that the flanges' contribution to the transverse shear stiffness is not negligible for this particular beam. Experimental measurements are also shown in Figure 7, and the shear strains appear to be

smaller than predicted suggesting a higher shear stiffness, and the distribution is less uniform. Part of the irregularity may be due to the fact that the outer surfaces of the web panels contain glass roving. Strain readings over or near the rovings may not be representative of the bulk web material.

Applying the approach of Barbero et al. [22] described in Section 2.1.3 to the FE results, k was computed to be 0.985. This value is in good agreement with the MLB value of $k = 0.997$. If the entire area and entire shear force is considered in the integration, k is computed to be 0.872.

3.2 Effects of Non-Classical Behavior

3.2.1 Sensitivity Analysis

The errors in back-calculated kGA values due to an error of 10% in the measured mid-span deflection for various loading geometries are summarized in Table 4. The results demonstrate the importance of accurate deflection measurements. A 10% error in measured deflection, which corresponds to between 0.254 and 0.685 cm (0.1 and 0.27 inch), results in an error in kGA of 36 to 53%.

3.2.2 Finite Element Results

3.2.2.1 12.2 m (40 ft) Results

The results of the finite element model solutions for a 12.2 m (40 ft) beam modeled using nodal fixity and pad supports, with and without overhang, are summarized in Table 5. In the case of the nodal fixity at the neutral axis, the predicted deflection is 10.7 cm (4.20 inches). Using the Timoshenko equation for point loads (the usual practice) leads to a back-calculated kGA value of 173 MPa-m^2 (38.9 Msi-in^2). This is only 2% less than the analytical reference value of 175 MPa-m^2 (39.5 Msi-in^2). Using nodal fixity at the bottom edge, the deflection is 10.9 cm (4.27 inches), which yields a kGA value of 146 MPa-m^2 (32.8 Msi-in^2). The "error" with respect to the reference value is -17%. This result highlights the inability of ordinary beam theory to capture boundary condition effects.

Inclusion of the support pads in the FE models complicates the analysis, generally increasing the error in "measured" kGA values. For example, for the case of a pad support and no overhang, the error varies from -4% to 29%, depending upon how the span is defined. If the span is defined as center-of-bearing pad to center-of-bearing pad, and the average pad

displacement is subtracted from the maximum deflection to calculate the net deflection ("COB-1" in Table 5), then the error is -2%. Using the average pad displacement along the centerline ("COB-2") yields nearly the same result (-1% error). If, however, the span is defined as the clear span, i.e. the distance from the inside edge of one pad to the inside edge of the other pad, the error is -4 to 29% again depending upon how the pad deflection is calculated. In the first case ("clear-1" in Table 5), the displacements at the inner corners of the pad were used to determine net deflection. This procedure was followed in the laboratory. The second case ("clear-2") demonstrates the effect of using the average displacement over the entire inner edge of the pad. The difference between these two latter cases is a result of non-uniform compression of the pad. The bottom flanges of the beam tend to bend upward, so that most of the pressure on the pad is introduced through the web panels.

3.2.2.2 Shear Strain Distribution

To understand the effects of the boundary conditions on the effective *kGA* values, it is useful to observe the behavior of the beam in the vicinity of the supports and the loading points. Figure 8 shows the mid-plane shear strain along half of the length of a 6.1 m (20 ft) long beam for the two models using discrete nodal boundary conditions to represent the supports. The shear strain undergoes a smooth decay at the load patch as the resultant shear force decreases from *P*/2 to 0. Similarly, the shear strain near the support decays towards zero. In the case of the fixity at the neutral axis, the nodes experience a high strain concentration. Figure 9 shows the mid-plane shear strain profiles for the two models which include the pad supports. The results show that the pad supports have nearly the same effect as the loading patches, while the effect of overhang is minimal. The decay patterns are identical for longer spans, but the 6.1 m (20 ft) cases shown demonstrate that this non-classical effect can impact a significant portion of the beam span at shorter spans.

To further understand the beam response, the shear strain profiles through the depth of the DWB at various positions along the length are given in Figure 10. The FE results demonstrate a decrease in the shear strain magnitudes in the vicinity of the load patch, as well as a complex warping effect at the top surface caused by the applied traction. This highly non-linear deformation field is not predictable using third order beam theory, and it may have an impact on the beam deflection and therefore the *kGA* calculation.

39

3.2.2.3   Effective kGA vs. Span Length and Comparison to Experimental Results

The back calculation method was applied to four additional span lengths in the manner described above. The resulting effective *kGA* values versus span length are shown in Figure 11 and Figure 12, for the cases of nodal fixity and pad supports, respectively. The results from the former case show a clear trend of increasing *kGA* with span. This trend is contrary to the hypothesized increase in effective *kGA* with decreasing span due to warping. The case of the boundary conditions applied at the bottom edge yields a *kGA* value 14 to 26% lower than the case where the boundary conditions applied at the neutral axis.

When the pad supports are modeled, the results are less clear. Defining the span as center-of-bearing to center-of-bearing, the same type of increasing trend is evident with the values being slightly higher than the case of neutral axis fixity at longer spans. The match with the analytical reference value is quite good (Figure 12). Using the clear span and the average inside pad deflections ("clear-2"), the results are very close to the "COB" case and the analytical value. However, using only the insider corner pad deflections ("clear-1", which is similar to experiments), the values are 29 to 44% higher than the reference value, and *kGA* decreases slightly with increasing span.

The experimental results also show a slightly decreasing trend with span length, and they compare reasonably well with the FE prediction based on the clear span and corner pad deflections ("clear-1"), as shown in Figure 13. This trend of decreasing *kGA* with increasing span is expected in light of the previous discussion concerning apparent and effective shear stiffness. As demonstrated by Figure 8 and Figure 9, the apparent shear stiffness in the vicinity of the loads and reactions is greater. Therefore, the integrated effect of these local increases in the apparent shear stiffness should be an increased effective shear stiffness of the beam as a whole. At lower span lengths, the region of beam affected by the loading- or reaction-induced disturbances comprises a greater percentage of the beam length. However, the increasing linear trend in effective *kGA* versus span length for the simple boundary condition cases (Figure 11 and Figure 12) suggests that other factors may counteract the warping effects in some cases.

3.2.2.4   Model Error and Pad Deformation

The previous results once again demonstrate the sensitivity of the *kGA* calculation to small errors in deflection. The calculation of net deflection is obviously important when dealing with a deformable support such as a pad. To highlight the difficulty in calculating the net beam

deflection, the sensitivity of the pad deflection calculation to the method used is shown in Figure 14. Furthermore, the finite element representation of the pad may also be introducing error in this study. In reality, the rubber is non-linear, so a non-linear finite element analysis would be more appropriate. As mentioned in Section 2.1.3.2, the actual pad strains were calculated to be as high as 340% (at the longest span), suggesting that the linear assumption is invalid. The predicted pad deflections are compared with the experimental measurements in Figure 15 and Figure 16. When all four corner displacements are averaged to calculate the pad deflection, the results show good agreement at the moderate 12.2 m (40 ft) span, but poor correlation at the other spans. When only the two inside corners are used, the agreement is reasonable for the 12.2, 15.2, 18.3 m spans, but poor for the shorter spans.

Other causes of slight error may include the effect of the overhang, and the use of point-load Timoshenko equations instead of patch-load equations. The above calculations were repeated for the case of a 53.3 cm (21 inch) overhang, but in most cases the resulting kGA value differed by only a few percent. The largest difference between the overhang and no-overhang case was 6%. Differences of 5 to 6% were observed at both the shortest and longest spans for the cases when span was defined as center-of-bearing to center-of-bearing. In general, an overhang has a slight stiffening effect. The use of patch load equations also has a negligible effect (<1%) on the back-calculated kGA values.

3.2.3   Shear Warping - Third Order Laminated Beam Theory

In order to understand what factors are influencing the effective kGA calculations, the results of the Third Order Laminate Beam Theory (TLBT) for the simple beam test case and the DWB are reviewed next. The relative warping effects for different loading types are then compared using the warping terms in the TLBT solutions. Finally, the importance of warping in other off-the-shelf FRP products is considered.

3.2.3.1   Simple Beam Example

For both orthotropy ratio cases, the far-field shear strain distributions through the beam thickness show excellent agreement (not shown). The resulting mid-surface shear strain decay profiles for the two orthotropy ratio cases are shown in Figure 17 and Figure 18. For the case of $E/G = 37$, good agreement between the FEA and TLBT predictions is observed with the TLBT model predicting a slightly shorter decay length. For the much lower E/G ratio equal to 2.5, the

agreement is observed to be much poorer, as the TLBT model predicts a much shorter decay length.

The back-calculated kGA values determined using the two nodal fixity boundary conditions for the low orthotropy example are shown in Figure 19. Both FEA and TLBT results are shown. The TLBT predicted value is found to be essentially constant and equal to the theoretical (reference) value of $(5/6)GA = 8.90$ MPa-m^2 (2.00 Msi-in^2), suggesting that warping has no effect. However, in the FEA results for the case of nodal fixity at the neutral axis, the effective kGA value is much lower than the theoretical value at short spans and then overshoots the theoretical value at longer spans. When nodal fixity is enforced at the bottom edge of the beam, kGA is reduced by 20 to 50%, approaching the theoretical value at longer span lengths.

These results suggest a significant effect of non-classical behavior on the effective kGA value, especially at shorter spans. For instance, at an aspect ratio of 10, the model using nodal fixity at the bottom edge yields an effective kGA value which is 40% less than the theoretical value. The source of this effect does not appear to be warping, since the TLBT model shows no span dependence. The increasing kGA versus span trend is similar to that observed in the DWB FEA modeling and, again, is contrary to the hypothesized decrease in effective kGA versus span.

In Figure 20, the kGA versus span curves for the high orthotropy example are shown. In this case, the TLBT model predicts a slight increase in kGA at shorter spans as expected, but the increase is only minor. The FE results again yield a low kGA value at short spans which then approaches the theoretical value at longer spans. However, longer spans are required to achieve a match with the theoretical value.

3.2.3.2 DWB

Next, the results from the DWB predictions are reviewed. In light of the previous findings and the low degree of orthotropy in the DWB, warping is not expected to play a role in the effective kGA calculation. However, the warping analysis and results are shown for completeness.

The TLBT predicted shear strain distribution through the depth of the beam in the far-field is compared to the finite element and experimental results in Figure 7. Recall that in the TLBT model, the total beam shear stiffness is used to determine the global response. As a result, the shear strain distribution is continuously parabolic like a solid section, and no jump in shear strain is predicted at the flange-web interface. This limitation leads to an erroneous shear strain

distribution, and the model cannot capture the flat character within the web panels. Still, the TLBT model overshoots the MLB and FE predictions by only 7% at the mid-surface. The actual distribution as predicted using FEA is bracketed by the Timoshenko/MLB and TLBT predictions.

The TLBT predicted shear strain profiles at various positions along the length of the beam are compared with the FE results in Figure 10. As observed previously, the FE results demonstrate a decrease in the shear strain magnitudes in the vicinity of the load patch, as well as a complex warping effect at the top surface near the load patch. Like Euler and Timoshenko beam theories, the TLBT model is not able to capture this traction-induced effect. The TLBT model is, however, able to capture the decay in shear strain magnitude near the load patch, and the maximum value follows the FE results quite well.

To better illustrate this, the mid-surface shear strain along the length of the beam as computed in the FE and TLBT models is compared to experimental readings by Schniepp in Figure 21. Recall that the shape of this shear decay is determined by the third order beam theory parameter, ω. Using Equation (2-28), ω for the 36 inch DWB is found to be 0.8 cm^{-1} (0.315 in^{-1}), and δ = 8.05 cm (3.17 inches). Nearly complete decay (99%) is predicted to occur over a distance of 6δ = 48.3 cm (19.0 inches) for the 36 inch DWB under three-point concentrated loading. Note that the TLBT decay distance is closer to 70-80 cm (Figure 17), because the results are for the case of a patch load under four-point loading. Still, the actual strain measurements suggest a longer decay length than both the FEA and TLBT predictions.

Using Equation (2-37), the mid-span deflection of the 36 inch DWB is predicted to be 1 to 4% less than the Timoshenko prediction, for spans from 18.3 m down to 9.14 m (60 ft to 30 ft). The result of this change in deflection is that the back-calculated kGA increases to 233 MPa-m^2 (52.3 Msi-in^2). This value differs by 32% from the reference value and 29% from the higher FE value, although the TLBT predicted deflection is only 1% less than the FE prediction! This result is included in Table 3. It is important to note that the decrease in deflection is not due to warping effects, but rather to a higher calculated shear stiffness (as compared to MLB) that results from including the flange contributions. This can be checked by observing that the warping term in Equation (2-37) decays to zero at $x = L/2$ (mid-span). This is explored further in the next section.

3.2.3.3 Effective kGA for Different Loading Types

Dufort et al. [37] claim that for a beam loaded in three-point bending, warping can affect the maximum deflection by as much as 6% using third order theory. As we have seen, a 6% change in deflection can greatly affect the measured kGA value. However, the results from the solid beam test case suggest that the effect is much less significant for lower degrees of orthotropy such as that of the DWB. Therefore, the purpose of this section is to investigate the magnitude of the warping effects for the DWB tested in various geometries at spans between 9.14 and 18.3 m.

The warping terms in Equations (2-35), (2-37), (2-39), and (2-41) can be rewritten as

3-pt:
$$-\frac{P\tanh(\lambda)}{2(\tfrac{5}{6})(GA)\omega}$$

4-pt:
$$\frac{2P\operatorname{Sinh}\left(\tfrac{\lambda}{6}\right)}{(\tfrac{5}{6})(GA)\omega\left(1-2\operatorname{Cosh}\left(\tfrac{\lambda}{3}\right)\right)}$$

Uniform:
$$-\frac{q\left(1-\operatorname{Sech}\left(\tfrac{\lambda}{2}\right)\right)}{(\tfrac{5}{6})(GA)\omega^2}$$

Cantilever:
$$-\frac{\tanh(\lambda)}{(\tfrac{5}{6})(GA)\omega}$$

$$(3\text{-}1)$$

where $\lambda = \omega L$ is a non-dimensional parameter. Next, recognizing that $q = P/L$, each term can be expressed as

$$-\frac{P}{2(\tfrac{5}{6})(GA)\omega}f(\lambda) \qquad (3\text{-}2)$$

where $f(\lambda)$ is a hyperbolic function which depends upon the type of loading. Using the TLBT form, the warping term can be rewritten as

$$-\frac{P(D_{xx}-\alpha F_{xx})^2 f(\lambda)}{2D_{xx}^2\left(A_{xz}-2D_{xz}\beta+F_{xz}\beta^2\right)\omega} \qquad (3\text{-}3)$$

44

Halving the load for the case of a cantilever beam so that the maximum shear resultant is $P/2$ for all load cases, the multipliers $f(\lambda)$ become:

3-pt: $\qquad\qquad\qquad\qquad\qquad\qquad \tanh(\lambda)$

4-pt: $\qquad\qquad\qquad\qquad \dfrac{-4\,\text{Sinh}\left(\frac{\lambda}{6}\right)}{\left(1-2\,\text{Cosh}\left(\frac{\lambda}{3}\right)\right)} \quad \text{or} \quad \dfrac{2\,\text{Sinh}\left(\frac{\lambda}{3}\right)}{\text{Cosh}\left(\frac{\lambda}{2}\right)}$ $\qquad\qquad\qquad$ (3-4)

Uniform: $\qquad\qquad\qquad\qquad \dfrac{2\left(1-\text{Sech}\left(\frac{\lambda}{2}\right)\right)}{\lambda}$

Cantilever: $\qquad\qquad\qquad\qquad\qquad \tanh(\lambda)$

These multipliers are plotted in Figure 22 for comparison. Above a non-dimensional span length of about $\lambda = 30$, the warping contributions for the four-point and uniform loading cases are negligible. For the 36 inch DWB, this corresponds to about 3.05 m (10 ft), so for span lengths greater than this, these results imply that warping is not a factor for the four-point test geometry with loads applied at the third points.

However, in the case of three-point loading or cantilever tip-loading, the warping effect is non-zero and constant above $\lambda \cong 5$. Thus, for all reasonable span lengths, the deflection or a thin-walled beam will differ from the Timoshenko prediction by

$$-\frac{P\left(D_{xx}-\alpha F_{xx}\right)^{2} Tanh(\omega L)}{2 D_{xx}^{2}\left(A_{xz}-2 D_{xz}\beta+F_{xz}\beta^{2}\right)\omega}$$

In the case of the 36 inch DWB, this quantity equals only (7.65e-8)*P cm. At a span of 9.14 m (30 ft), the shortest allowable length for the DWB as determined by Schniepp [9], this is only 0.2% of the maximum deflection predicted using Timoshenko beam theory. Despite such a small error, the back-calculated kGA value is 233 MPa-m^2 (52.3 Msi-in^2), which is 32% greater than the reference value of 175 MPa-m^2 (39.5 Msi-in^2).

Revisiting the four-point loading case, if the loads are applied at $x = a$, then Equation (3-4) becomes

$$f(\lambda) = \frac{2\operatorname{Sinh}\left(\lambda\,\frac{a}{L}\right)}{\operatorname{Cosh}\left(\frac{\lambda}{2}\right)}$$

This function is plotted in Figure 23, and it is observed that as a increases, i.e. the load points are moved closer to mid-span, the coefficient $f(\lambda)$ approaches a value of 2 and the three-point loading case is recovered. For the DWB at spans greater than 9.14 m (30 ft), Figure 23 suggests that warping does not become significant until $a = 0.48L$. Thus, warping will have no significant effect for any four-point geometry.

Since the warping contribution in the three-point and cantilever loading cases is constant at reasonable spans, it will comprise a greater percentage of the total deflection at shorter spans. Therefore, these results suggest that the back-calculated effective Timoshenko shear stiffness will vary with span length. However, as shown in Figure 24, the variation is very small for the case of the DWB: only 3% difference between the 6.1 m span and longer spans for the three-point loading case, and only 1% for the cantilever loading case. Therefore, the use of the third order laminated beam theory confirms that warping has a negligible effect on the effective kGA of the 36 inch DWB for all spans and test geometries.

3.2.3.4 Other FRP Beams

The DWB is a unique structural beam due to the use of carbon fiber in the flanges and the double web design. Therefore, the degree of orthotropy in this beam may be different than that of more common FRP beams. To assess the magnitude of the warping for standard, off-the-shelf FRP sections, the shear decay parameter ω was calculated for a series of wide-flange beams, I-beams, and box-beams manufactured by Strongwell, Inc. The section properties were taken from the EXTREN Design Guide [4], and ω was calculated using the TLBT equations. The 99% decay distance 5δ was normalized by the beam height h and plotted versus the quantity $EI/(GA\,h^2)$, a measure of the orthotropy of the beam (Figure 25). The predicted shear decay lengths for the standard FRP shapes are 12 to 34% less than that of the DWB, implying that warping will have a negligible effect on the measurement of kGA for standard FRP shapes.

On the other hand, because off-the-shelf pultruded products typically utilize a high volume fraction of continuous strand mat, the compressive modulus will be less than that of the DWB. Data from the Strongwell Design Guide indicate that their standard EXTREN beams have a transverse compressive modulus equal to 6.89 GPa (1 Msi), compared to the 14.8 GPa

(2.15 Msi) modulus of the DWB web panels. Thus, transverse deformation is expected to have an even larger impact on the *kGA* measurement for standard FRP shapes.

One can expect even greater error when dealing with sandwich panels. Sandwich panels typically have very soft cores, which possess a low shear modulus and low compressive modulus. In addition to significant transverse deformation, warping should become significant. The low shear modulus of the core will yield a very high degree of orthotropy, so that the shear decay length can be many times the thickness of the panel or beam. For instance, the sandwich panels used in the examples by Frostig [36] and Swanson [54] yield values of *5δ/h* = 12 to 15, which are around 30 times greater than that of the DWB.

3.2.4 Transverse Compressibility

3.2.4.1 Solid Beam Example

The results of the four-point loading FEA parametric study for the high orthotropy case are shown Figure 26. The results clearly indicate that as the transverse stiffness is increased, the effective *kGA* value increases and approaches the theoretical value. Furthermore, as E_z becomes very large, the TLBT solution is recovered and the slight short span stiffening effect is observed. Note that the FEA predicted value is less than 1% greater than the TLBT/theoretical value. Thus, it appears that the reduction in *kGA* at short spans can be explained by transverse compression.

The amount of transverse deformation should depend upon how the loads and boundary conditions are applied, and this effect is confirmed by the behavior observed previously in Figure 19 and Figure 20 for the two orthotropy cases. Incidentally, the location where the mid-span deflection is taken or measured is also important. In the previous results, the deflection was taken from the bottom surface. However, if the absolute maximum deflection is used instead, the resulting *kGA* values are shifted, as shown in Figure 27 and Figure 28 for the case of E/G = 2.5.

3.2.4.2 DWB

The effect of the transverse stiffness on the back-calculated *kGA* value of the DWB is shown in Figure 29. The results clearly show an increase in *kGA* with transverse stiffness, and while the curves do appear to be approaching some limit, this limit is higher than the theoretical value determined from laminated beam theory. This effect is addressed in the following section.

3.2.4.3 Higher Order Sandwich Theory

The variation of the effective kGA value of the sandwich beam considered by Swanson [54] for the three- and four-point loading cases determined using Frostig's higher order sandwich theory is shown in Figure 30. Contrary to the warping effect, the four-point loading case is observed to cause greater error than the three-point loading case as compared to the theoretical value of $(5/6)(GA)_{core}$. Furthermore, the choice of deflection to be used in the calculation has an effect for the case of three-point loading, since the load is applied at the same location as the measurement. It is also interesting to note that in both loading cases, the effective shear stiffness approaches the "uncorrected" or true shear stiffness GA, rather than the Timoshenko value of $(5/6)GA$. This is similar to the behavior observed in Figure 29. This can be explained by the fact that higher order models predict the deflection more accurately than Timoshenko beam theory which always over predicts the maximum deflection. Thus, the back-calculated shear stiffness is closer to the actual value than the Timoshenko value. The results of increasing the transverse core modulus are demonstrated in Figure 31. Again, we see that as the transverse stiffness increases, the true theoretical value is obtained at shorter spans, and again, as the transverse stiffness approaches infinity, the shear warping solution is realized.

Next, the results of applying the higher order sandwich theory to the DWB are presented. The resulting effective kGA values for the three- and four-point loading cases are shown in Figure 32. Unlike the sandwich beam case, the four-point loading geometry appears to cause less error in the effective kGA value for the DWB. This is the same trend observed with the warping effect. The reason for the discrepancy is unclear. Figure 32 includes results for span lengths up to 107 m (350 ft); these unrealistic spans were considered simply to verify that the theoretical true value is obtained. (Note that in the case of the DWB, $kGA \approx GA$ since k $\approx$ 1.)

Actually, the effective shear stiffness again approaches a value slightly greater than the theoretical value as the transverse stiffness increases. This higher value may be the true shear stiffness of the DWB, accounting for the flanges and sub-flanges. Note that the total web area is actually 3232 cm^2 (50.1 in^2) and assuming a uniform shear modulus of 5.96 GPa (0.864 Msi), the true shear stiffness GA is estimated to be 193 MPa-m^2 (43.3 Msi-in^2). The effect of increasing the transverse stiffness is shown in Figure 33, and again kGA approaches a slightly higher value than the MLB theoretical value.

Finally, the sandwich theory results are compared to the FEA results for the two lower E_z cases in Figure 34. (Note that the sandwich theory results for the higher modulus value at longer spans could not be computed due to numerical problems.) While the trends are of course the same, the predicted effective kGA values are slightly different using the two methods. Furthermore, the FEA values approach a higher value at long spans. Possible sources of error in the sandwich theory calculations include: 1) the assumption of symmetric face sheets/flanges, 2) the assumption of a uniform flange thickness, and 3) the assumption that the web carries no axial stress.

3.2.4.4   Comparison of Transverse Strain

To quantify the amount of transverse compression under the load patches and above the supports, Schniepp [9] measured compressive strains on the outer surface of the web underneath one load patch in a 133 kN (30 kip) test of a 12.2 m (40 ft) beam. A line of gages directly below the center of the pad was used. He also placed a line of gages 11.4 cm (4.5 inches) away from the edge of the pad. Predicted strains were extracted from the FE results and the higher order sandwich model results at the same locations. In addition, strains above the supports were calculated for the case of a pad support.

The results are compared in Figure 35 through Figure 37 by scaling all strains to 445 kN (100 kips). The FEA prediction and experimental results show only fair correlation, but in both cases, the strains are found to be fairly high. Note these measurements may also be influenced by the presence of roving on the outer web panel surfaces. For comparison, the maximum axial strain for this geometry is around 3000 microstrain at 445 kN. The transverse strains under the load patch are predicted by Frostig's higher order sandwich theory to be much higher at the top of the beam (3370 microstrain) and to become tensile at the bottom. Part of this discrepancy may be due to the restrictions on the stress state in the theory which are required to obtain a closed-form solution. Furthermore, the FEA results suggest that the stress distribution under the load patch may not be uniform in the x-direction, as shown in Figure 38. The stress concentration at the edges of the load patch occur as the rigid steel plate impinges upon the curved flanged. These factors may explain the lower effective kGA values predicted using the higher order sandwich theory as observed in Figure 34.

At a distance of 11.4 cm from the edge of the loading pad, the strains are still predicted to be fairly high using FEA. Furthermore, the strains near the top of the beam are predicted to

change sign, suggesting a beam on elastic foundation type of effect. Similar effects are observed in the FE predictions of the behavior above the pad supports, although the distribution is different and the maximum strains are predicted to be twice as large as the strains under the loading pads.

3.2.5 Summary

It has been shown that small changes or errors in the deflection measurement can significantly affect the back-calculated *kGA* values. The FE models results also suggest that boundary conditions may play a role through non-classical behavior effects. The difficulty in estimating the error is compounded by the uncertainty in the definition of span length and in accounting for pad deformation when using bearing pads at the supports.

The results of the FE model which include pad supports are inconclusive regarding the effect of span and boundary conditions on the effective *kGA* value. When the pad deformation is averaged over the entire pad or over the inside edge, the results suggest an increase in *kGA* with span, and the predictions closely match the reference value at the moderate span of 12.2 m (40 ft). However, when only the inside corner pad deflections are considered (like the experiments), the predicted effective shear stiffness is significantly higher than the reference value. The experimental data lie between the analytical value and this latter FE model. Furthermore, the data show a slight trend of decreasing effective *kGA* with increasing span. The third order laminated beam theory including warping predicts a similar trend, but the effect of shear warping was found to be negligible. Furthermore, the theory suggests that any warping effect can be avoided by simply avoiding the three-point geometry.

Yet the FE analyses of the 2-D simple beam and the DWB clearly indicate a span-dependence for the effective *kGA* value under four-point loading, with the effective shear stiffness actually decreasing at shorter spans. This effect is attributed to transverse flexibility. The parametric studies indicate that as the transverse stiffness approaches infinity, the error in the effective *kGA* is reduced and the warping solution is obtained. The experimental strain measurements confirm that large transverse deformations occur under the load patches and above the supports. The higher order sandwich theory of Frostig shows promise as a means to estimate the flexibility related error analytically. Further refinement of the application of this model to thin-walled beams may permit the future development of guidelines to estimate flexibility related error in the measured *kGA* values for use by the engineering community.

4 Conclusions and Future Work

The purpose of this study was to calculate the Timoshenko shear stiffness for a particular structural beam, the 36 inch DWB, and to identify factors which hinder accurate measurement of the shear stiffness. This study considered in great detail the issue of shear warping, which had been cited as a possible cause for kGA measurement errors by several sources. Specifically, an increase in the measured kGA value was expected at shorter spans. To investigate this hypothesis, a third order beam model was derived for thin-walled laminated beams. The results of the model suggest that warping has a negligible effect and only at very short spans and very high degrees of orthotropy. The follow-up investigation using a simple solid rectangular beam confirmed this conclusion.

Surprisingly, the parametric studies involving the solid beam test case and the DWB with varying values of transverse stiffness revealed that transverse compressibility had a significant softening effect on the beam and reduced the effective Timoshenko shear stiffness. This observation confirmed the trend found in the finite element analysis of the DWB with nodal fixity boundary conditions: a decrease in effective kGA with decreasing span length. Furthermore, the test case revealed that the boundary conditions and loading conditions can significantly impact the back-calculated kGA by affecting the amount of transverse deformation. The fact that transverse deformation can have such a significant effect on the kGA measurement represents a significant contribution to the current understanding of the problem.

The complications that arise when bearing pads are used at the supports were also studied using finite element analysis. The results suggested that the effective calculated shear stiffness value can be higher or lower than the theoretical value depending upon how the pad deformation is treated and how the span length is defined. Good agreement between experimental data and FEA predictions was obtained when only the inner pad deflections were used to calculate net beam deflection. However, this procedure does not capture the dependence of the effective kGA on span caused by transverse flexibility. The use of average pad deflection or average centerline deflection and the center-of-bearing span length appears to yield more reasonable results and is therefore recommended when bearing pads must be used. The best experimental results will likely be achieved when more traditional rollers and plates are used at the supports. Furthermore, the use of transverse stiffeners at the load and support points is recommended to reduce the transverse flexibility effect.

To build upon the results of this study, the author recommends the following additional work:

- The effective *kGA* calculations for the DWB should be repeated using the version of Frostig's higher order sandwich model developed for non-symmetric face sheets.

- Furthermore, the sandwich analysis of the DWB should be repeated using a reduced effective flange width to account for the tapers.

- To better understand the deformation of a bearing pad and its effect on the measured *kGA*, a non-linear FE analysis modeling the actual non-linear elastic behavior of the rubber pad is suggested.

- Although not considered in this study, shear testing of the web panel laminate has demonstrated a non-linear shear stress-strain curve suggesting material non-linearity. An investigation into the effects of material non-linearity should be pursued, using the non-linear load stepping capabilities in ANSYS® or a comparable finite element package.

While the original goal of developing guidelines for estimating error in the *kGA* measurements was not accomplished, considerable progress has been made to identify and quantify the sources of error which are related to non-classical behavior. The future development and use of analytical models such as the higher order sandwich theory may permit estimates of the error based on the transverse stiffness, the length of the load patch, the boundary conditions, and the test geometry.

Figures and Tables
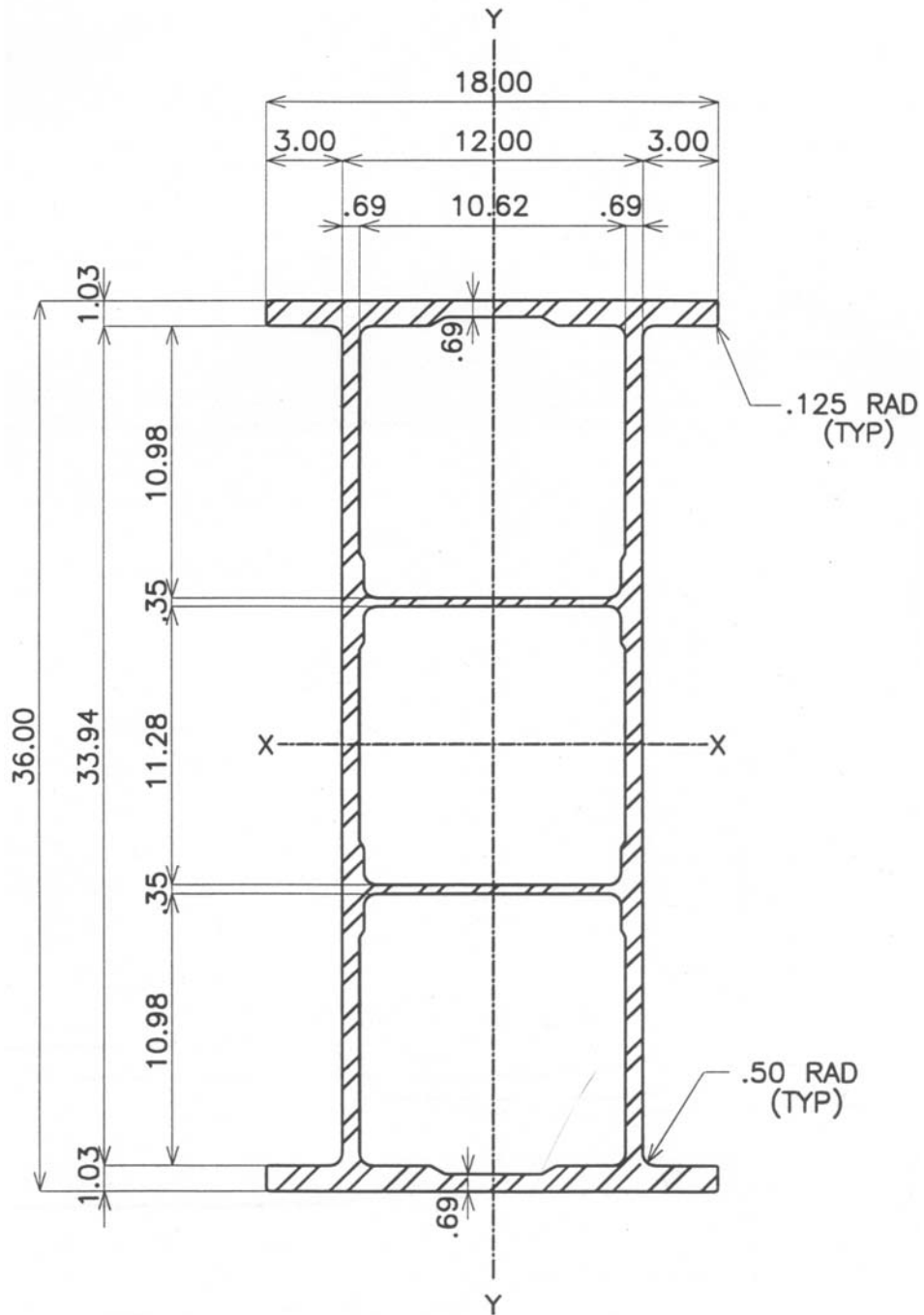
Figure 1. Strongwell's 36 inch DWB (dimensions in inches)**.**

53

Figure 2. The Route 601 Bridge over Dickey Creek in Smyth County, Virginia, employing eight 36 inch DWB FRP girders.
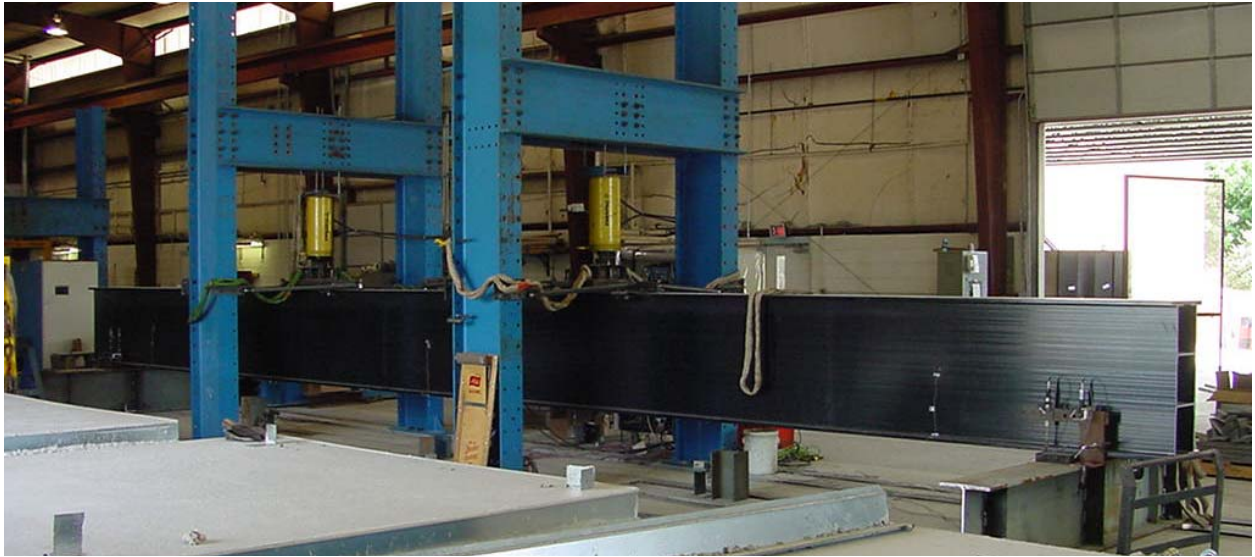
Figure 3. Four-point bend test set-up for 36 inch DWB (18.3 m or 60 ft span).

Table 1. Stiffness parameters of the 36 inch DWB determined by Schniepp.

span (m)	kGA (MPa-m^2)				E (GPa)			
	mean	st dev	B-allow.	A-allow.	mean	st dev	B-allow.	A-allow.
9.14	224	37.8	159	113	45.0	1.13	43.0	41.0
12.2	212	32.8	157	115	43.3	1.76	40.4	37.4
18.3	203	35.6	141	99.6	44.4	1.23	42.3	40.1
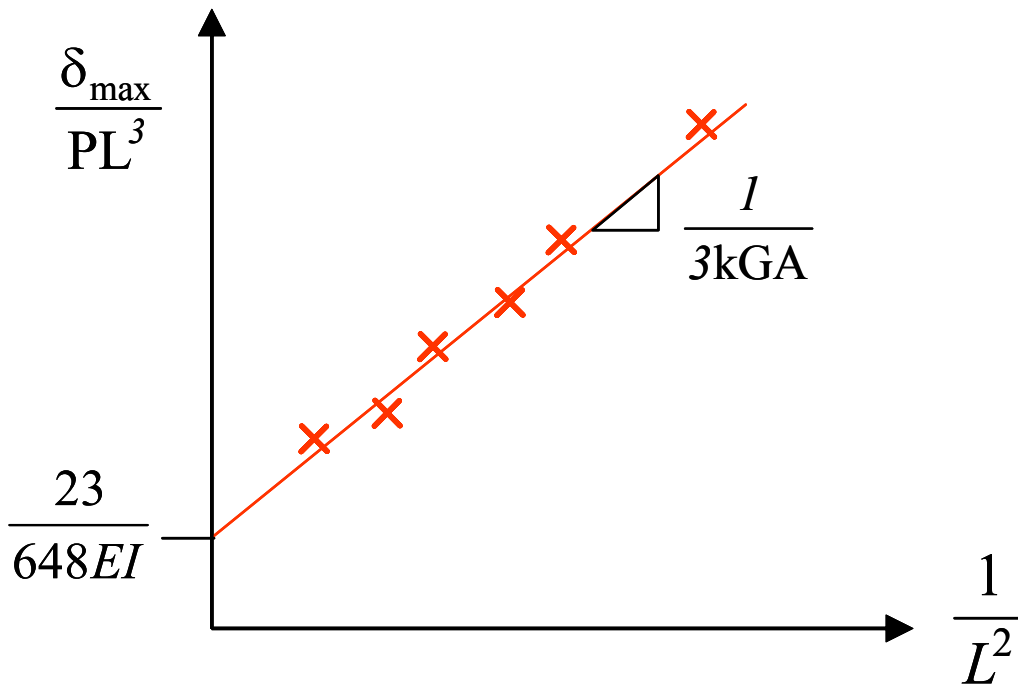
Figure 4. The graphical method used to calculate kGA. Slope and intercept quantities shown are for four-point bending with loads applied at the third points.

Table 2. Lamina properties used in the DWB models.

Property	Units	Method	1 carbon/VE	2 glass/VE	3 CSM
Fiber Vol. Fraction		---------	0.55	0.45	0.25
E_1	Msi	Rule of Mixtures	16.71	4.98	1.5148
E_2	Msi	Halpin-Tsai formula [62]	1.2780	1.3739	1.5148
E_3	Msi	Assume transverse isotropy	1.2780	1.3739	1.5148
ν_{12}		Rule of Mixtures	0.2168	0.2318	0.2951
ν_{23}		Assume transverse isotropy	0.5720	0.7585	0.6319
ν_{13}		Assume transverse isotropy	0.2168	0.2318	0.2951
G_{12}	Msi	Cylindrical Assemblage Model [62, 63]	0.4496	0.4506	0.5848
G_{23}	Msi	Stress-Partioning Parameter technique [62, 64]	0.4065	0.3906	0.4641
G_{13}	Msi	Assume transverse isotropy	0.4496	0.4506	0.5848
α_1	10^{-6} in/in	Tsai and Hahn [62, 64]	-0.0541	4.2937	11.7156
α_2	10^{-6} in/in	Tsai and Hahn [62, 64]	17.0998	21.8181	11.7156
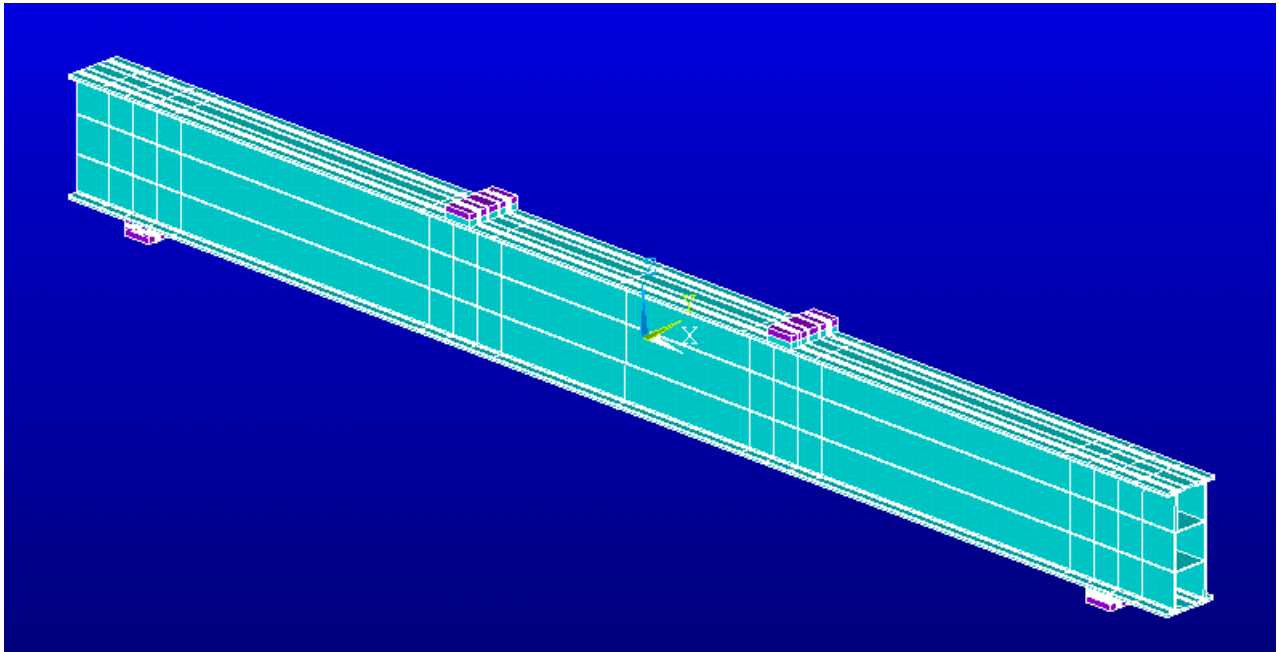
Figure 5. 12.2 m span FEA model of 36 inch DWB.
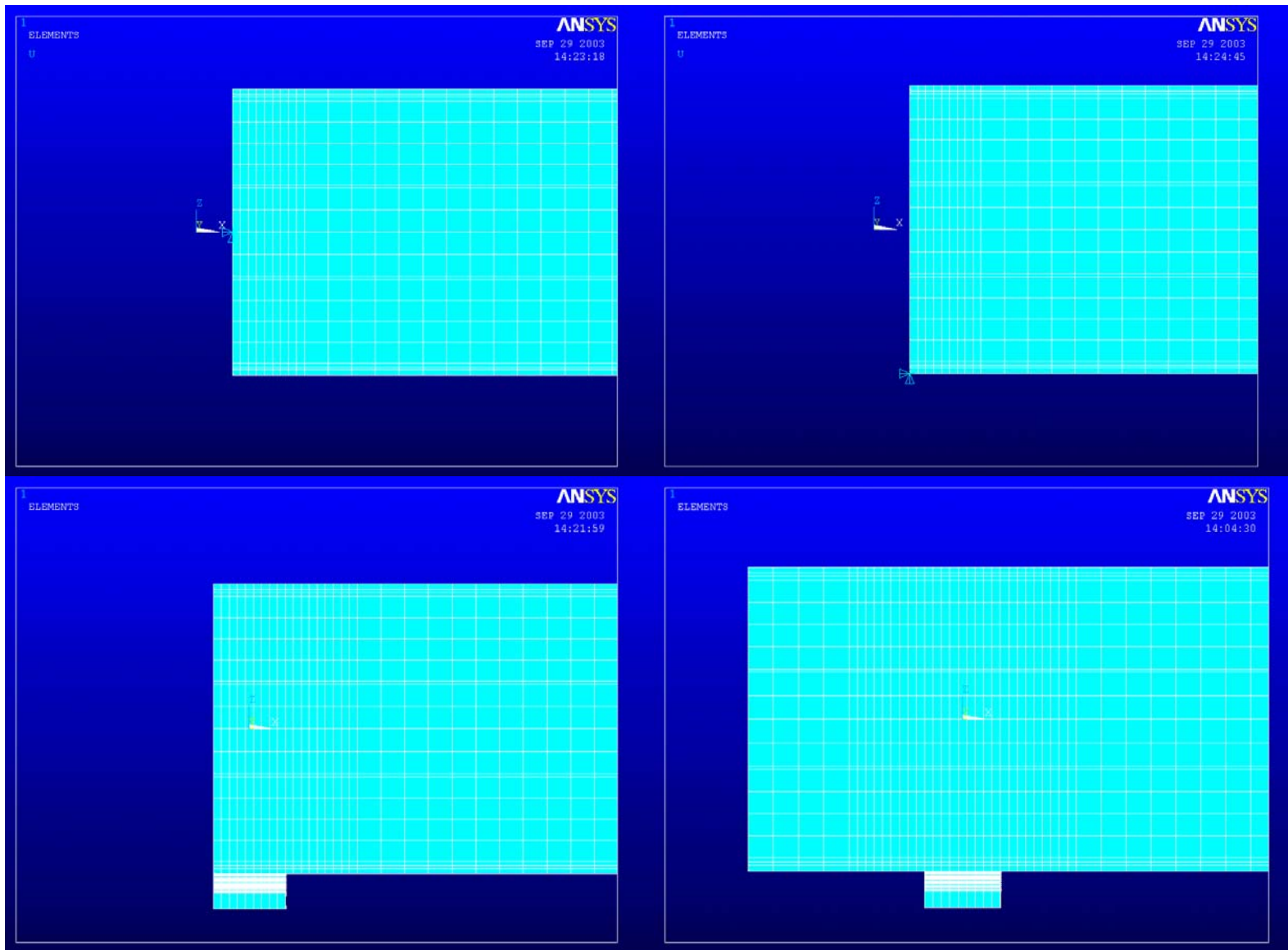
Figure 6. The four different boundary condition types employed in the finite element analysis of the DWB: nodal fixity at the neutral axis (top left), nodal fixity on the bottom edge (top right), pad support, no overhang (bottom left), and pad support, with overhang (bottom right).

Table 3. Summary of calculated *kGA* values.

Method	k	GA MPa-m² (Msi-in²)	kGA MPa-m² (Msi-in²)	error relative to reference value
THEORETICAL				
1. Reference value from MLB model (A_w = 45.9 in²)	0.997	176 (39.6)	175 (39.5)	---------
2. Cowper/Bank equations				
a. I-beam, average flange thickness	0.7360	276 (62.1)	203 (45.7)	16%
b. Box-Beam, average flange thickness	0.7566	276 (62.1)	209 (47.0)	19%
3. FEA (direct method)				
a. Idealized boundary conditions	------	------	167 (37.5)	-5%
b. Actual boundary conditions	------	------	139 (31.2)	-21%
4. TLBT (direct method)	------	------	233 (52.4)	33%
5. FEA to calc k, G = 864 ksi from MLB				
a. web area only (using A_w = 50.1 in²)	0.985	193 (43.3)	190 (42.6)	9%
b. total area (A_{total} = 91.2 in²)	0.872	189 (42.5)	165 (37.0)	-6%
EXPERIMENTAL				
Back-calculation method (Schniepp [9])	-------	-------	207 (46.5)	18%
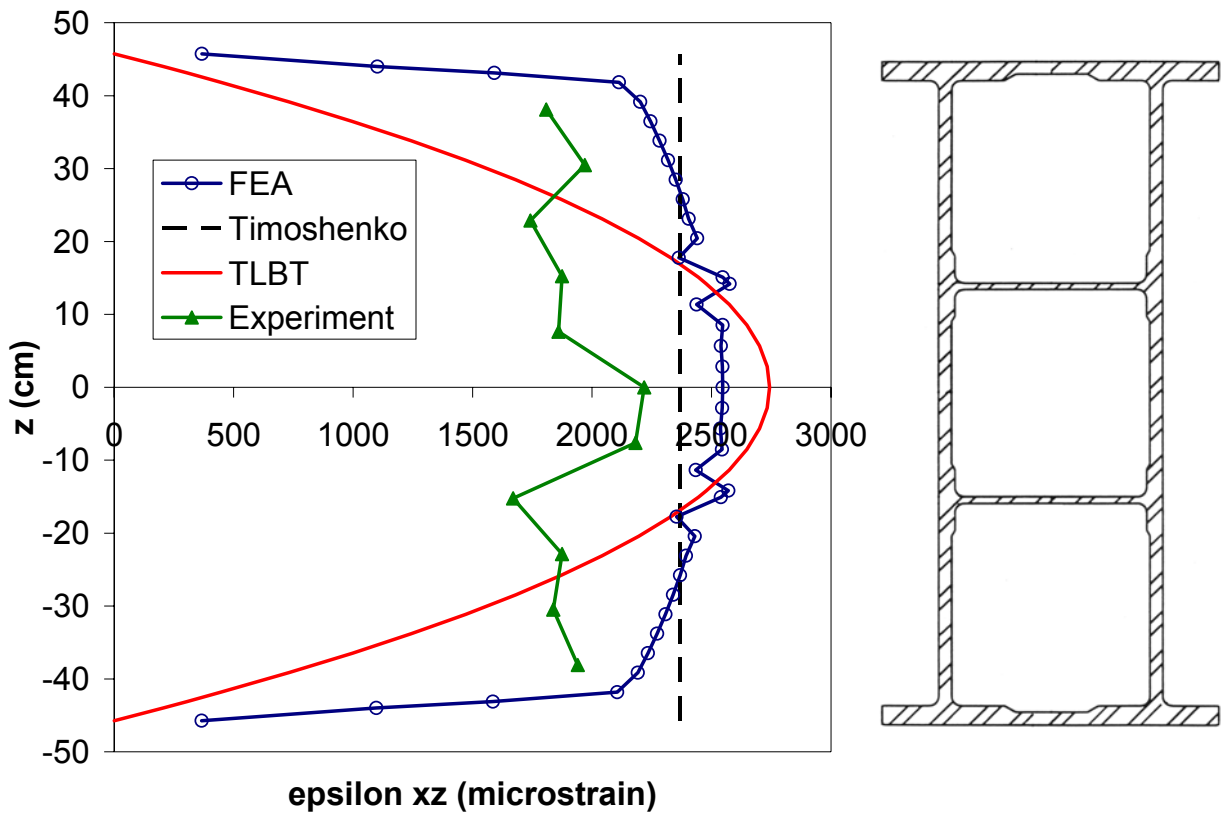
Figure 7. Far-field (x = 191 cm) shear strain distribution as predicted using the FE model, Timoshenko/first order laminated beam theory, and third order laminated beam theory (TLBT). Experimental measurements are also shown.

Table 4. Error in the back-calculated *kGA* values for various loading geometries for a 10% error in the deflection measurement.

type of loading	Total Span L (m)	Shear Span a (m)	Timoshenko Deflections (cm)			Defl incl. error	kGA (MPa-m^2)	Error
			Bending	Shear	Total			
4-pt, 222 kN	9.14	3.05	2.21	0.381	2.59	2.87	105	-40%
at each 3rd point	12.2	4.06	5.26	0.508	5.77	6.32	83.2	-53%
3-pt, 222 kN	9.14	4.57	2.59	0.584	3.18	3.51	114	-36%
center point load	12.2	6.10	6.17	0.762	6.93	7.62	93.0	-47%
uniform loading	9.14		1.63	0.279	1.91	2.12	106	-40%
(222 kN total)	12.2		3.86	0.381	4.24	4.65	84.1	-52%

Table 5. Summary of *kGA* values calculated for the 12.2 m (40 ft) four-point geometry via the back calculation method using various FE model results.

model type	span definition	max defl (cm)	pad defl (cm)	net defl (cm)	a (m)	L (m)	kGA (MPa-cm^2)	% error vs. reference
12.2 m (40 ft), pads centered at a = 4.11 m (13.5 ft)								
point supports (nodal fixity) at the neutral axis		10.668		10.668	3.96	11.89	**173**	-2%
point supports (nodal fixity)at the bottom flange		10.856		10.856	3.96	11.89	**146**	-17%
12.1 m (39.75 ft) beam, 11.9 m (39 ft) clear span, with pad supports (NO OVERHANG)	COB - 1	11.547	0.287	11.260	4.08	12.12	**178**	1%
	COB - 2	11.547	0.287	11.260	4.08	12.12	**178**	1%
	clear - 1	11.547	0.881	10.665	3.96	11.89	**227**	29%
	clear - 2	11.547	0.620	10.927	3.96	11.89	**170**	-4%
13.4 m (44 ft) beam, 11.9 m (39 ft) clear span, with pad supports (includes overhang)	COB - 1	11.582	0.295	11.287	4.08	12.12	**173**	-2%
	COB - 2	11.582	0.303	11.279	4.08	12.12	**174**	-1%
	clear - 1	11.582	0.922	10.660	3.96	11.89	**228**	29%
	clear - 2	11.582	0.652	10.930	3.96	11.89	**169**	-4%
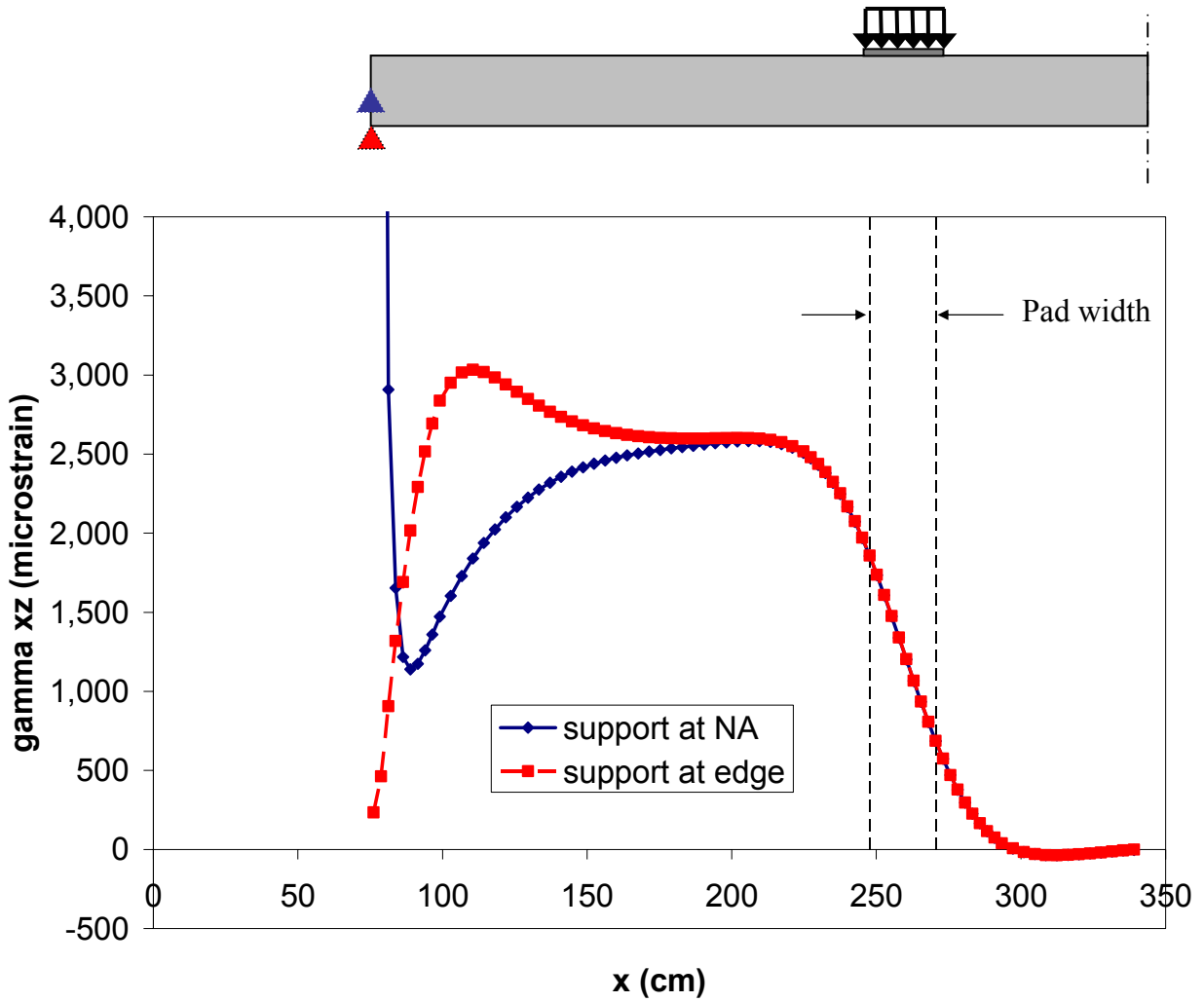
Figure 8. Shear strain profiles for the models with discrete nodal boundary conditions, showing the decay near a support and at a load patch. The load patch is located between x = 248 and 271 cm. Only half of the span is shown.
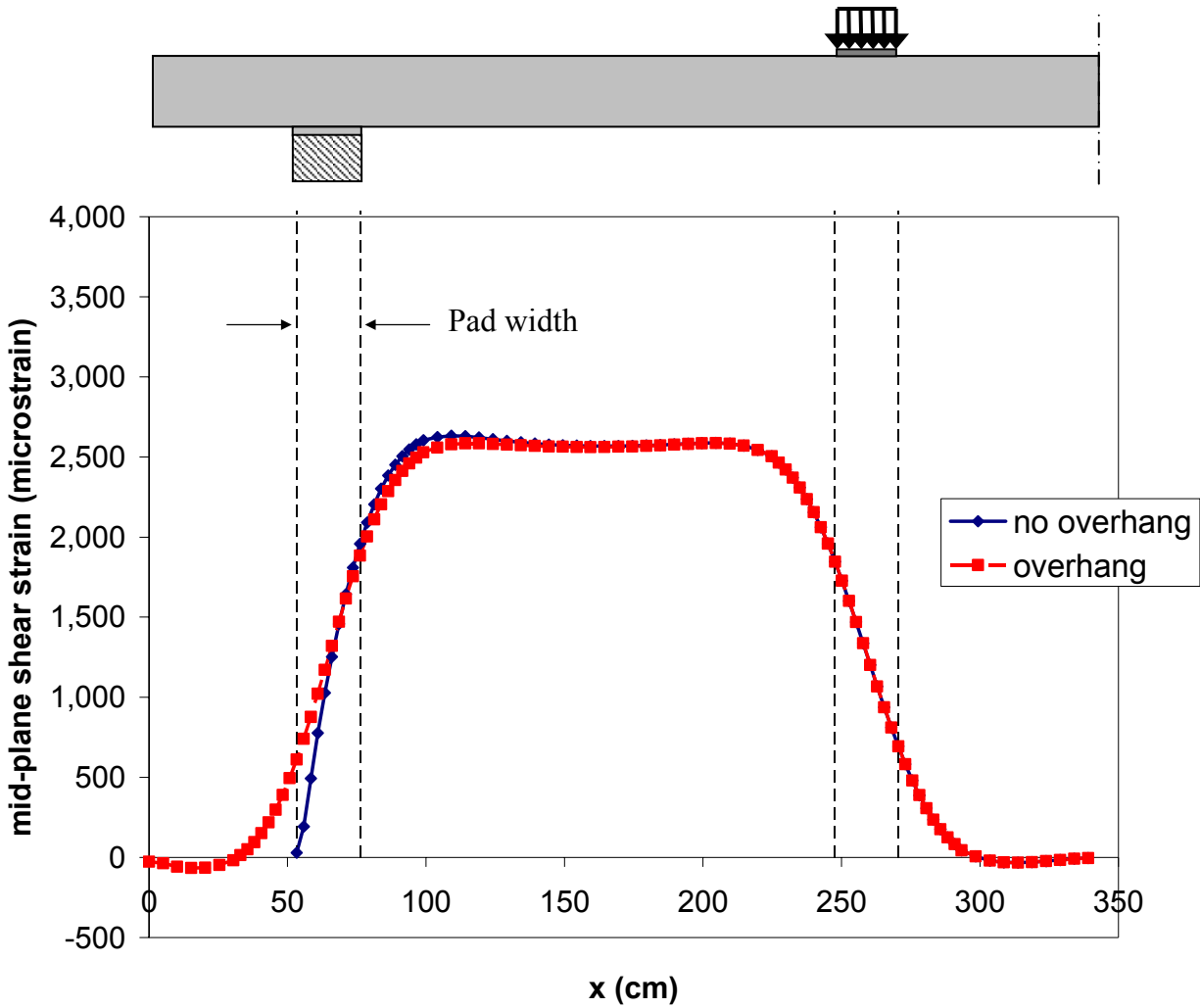
Figure 9. Shear strain profiles for the models with pad supports, showing the decay near a support and at a load patch. The support is located between x = 53.3 and 76.2 cm, while the load patch is located between x = 248 and 271 cm. Only half of the span is shown.
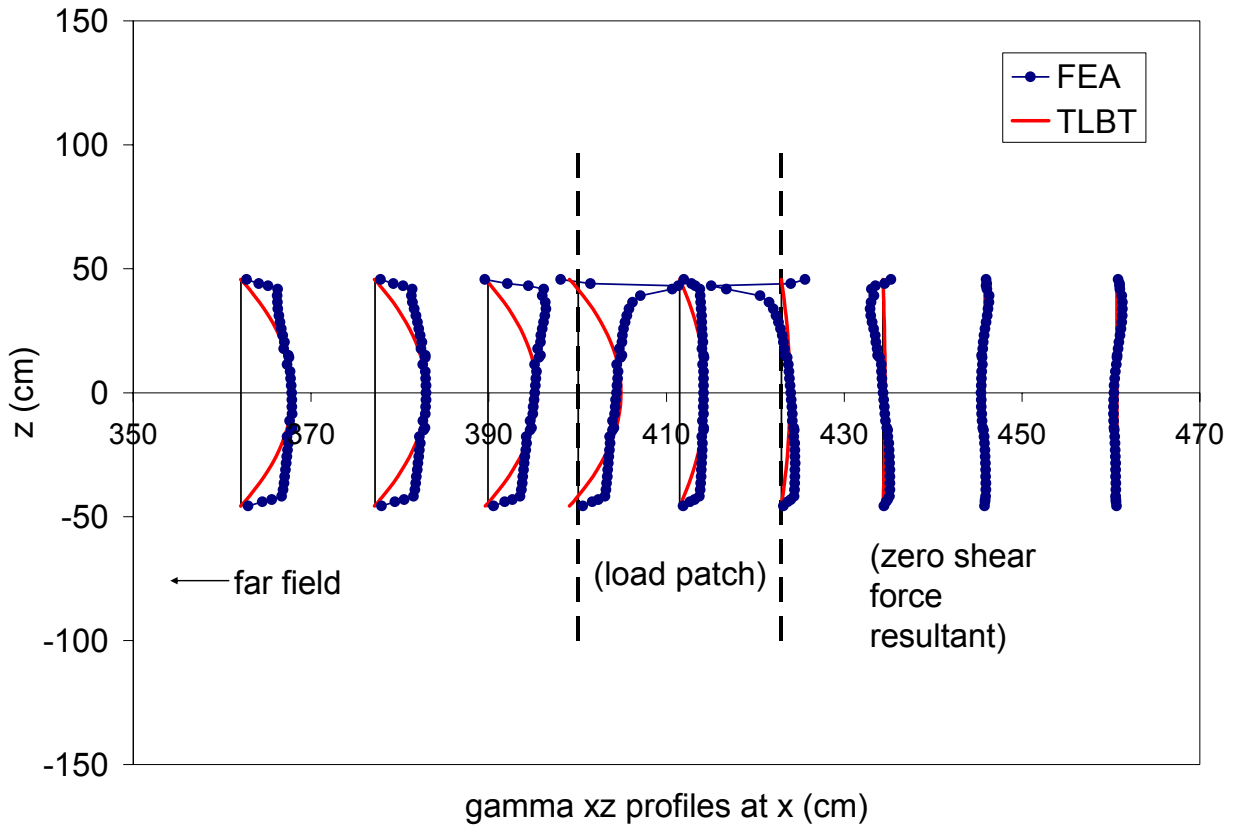
Figure 10. Shear strain profiles through the depth of the 36 inch DWB at various locations along the length of the beam (abscissa) as predicted by the TLBT model (solid curves) and the FE model. The load patch is denoted by the dashed lines.
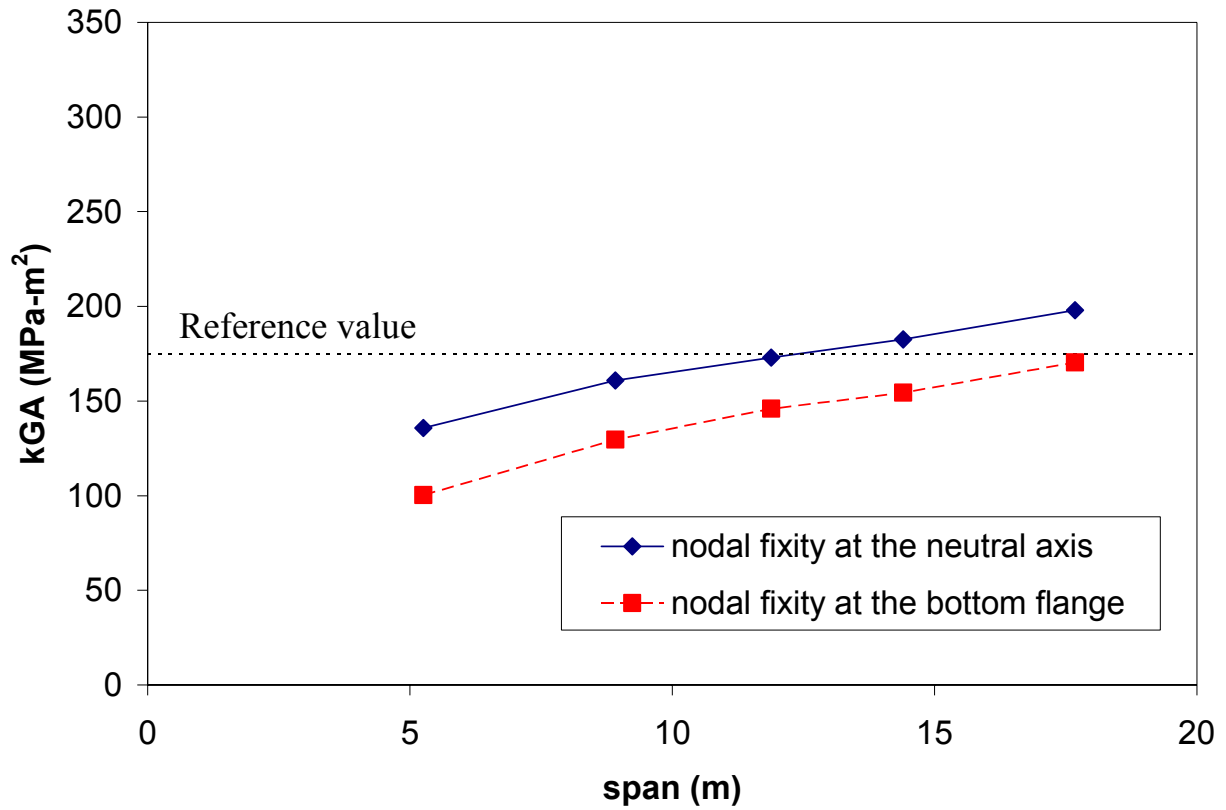
Figure 11. The effect of span on the effective *kGA* back-calculated from the FE results for the four-point loading geometry and the two cases of discrete supports.
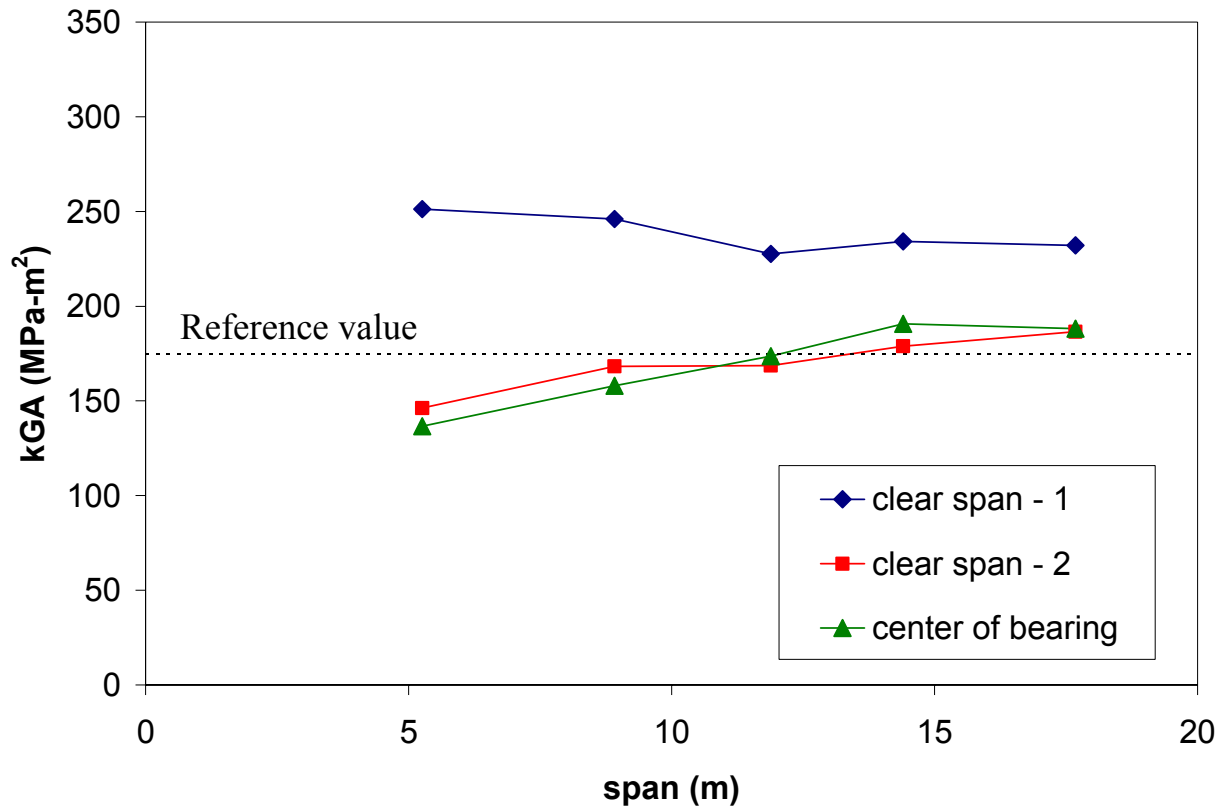
Figure 12. The effect of span on the effective *kGA* back-calculated from the FE results for the four-point loading geometry with pad supports.
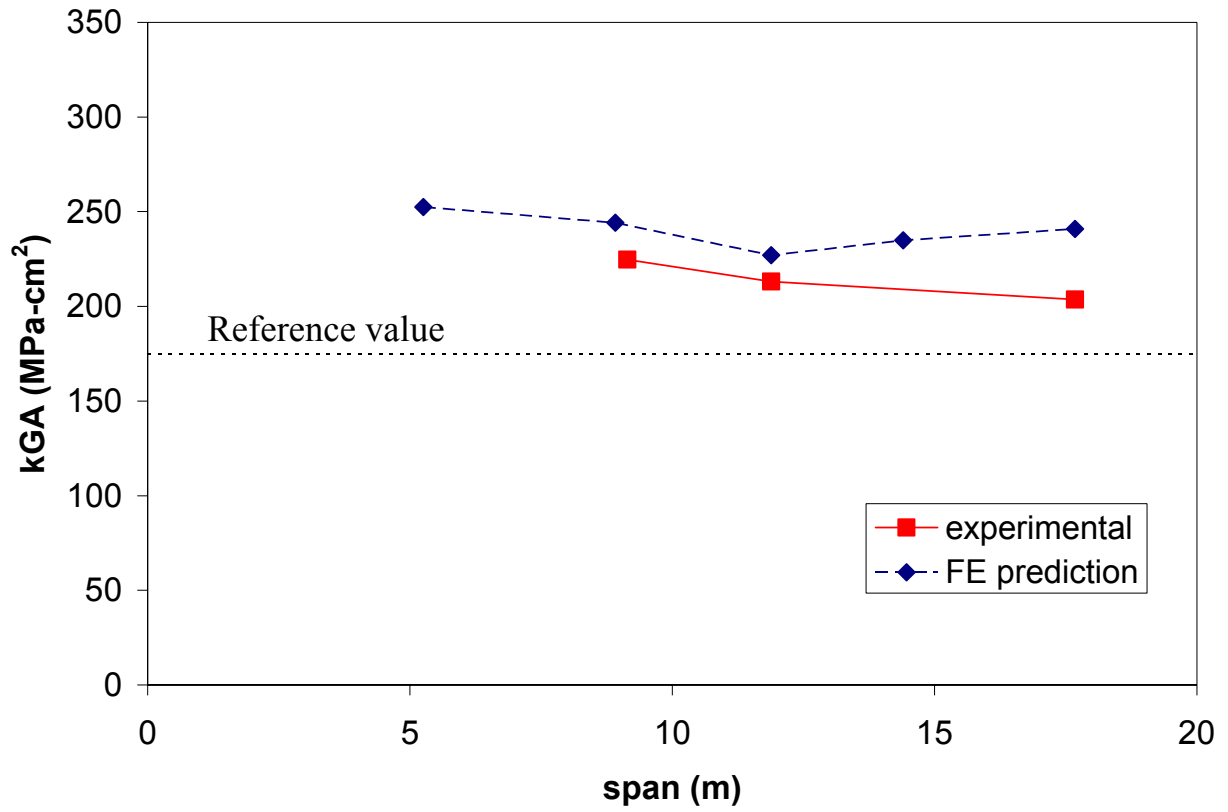
Figure 13. Comparison of *kGA* versus span trends as computed using both the FE model results and experimental results (four-point loading).
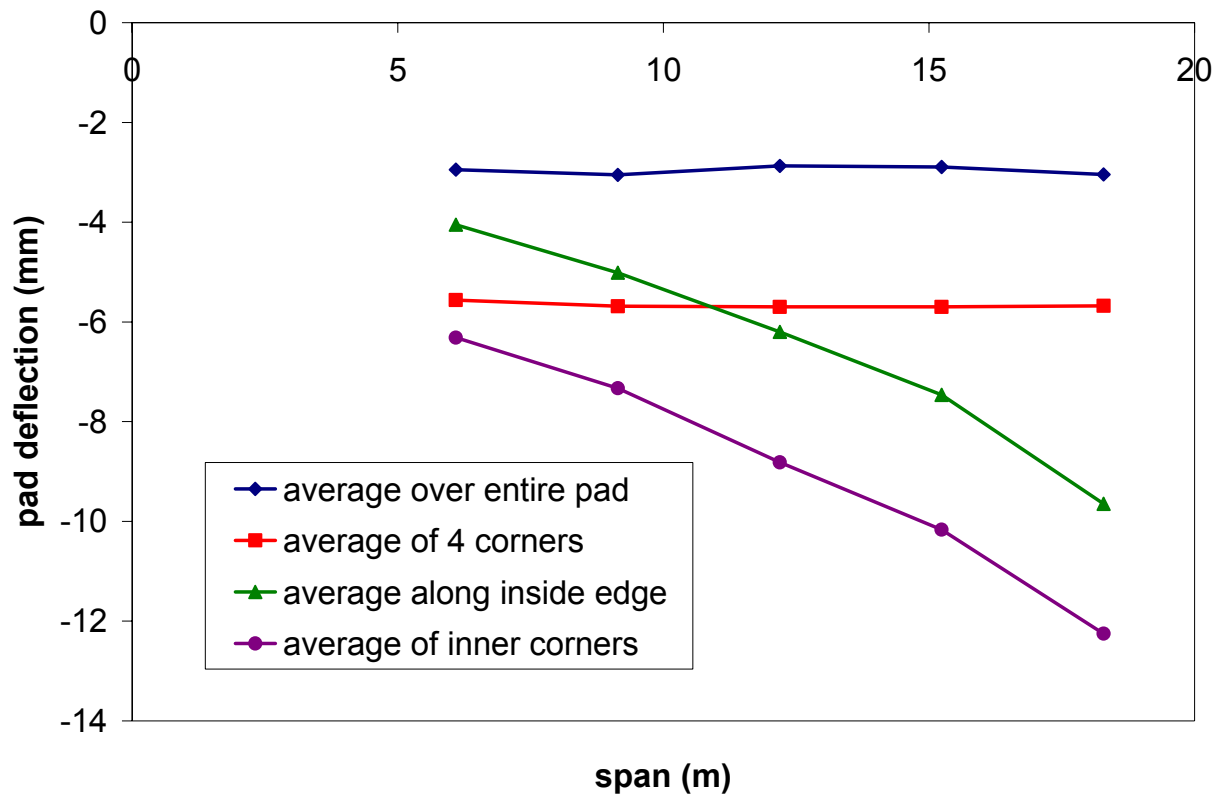
Figure 14. Average pad deflection versus span as predicted using FEA using four different averaging schemes (four-point loading).
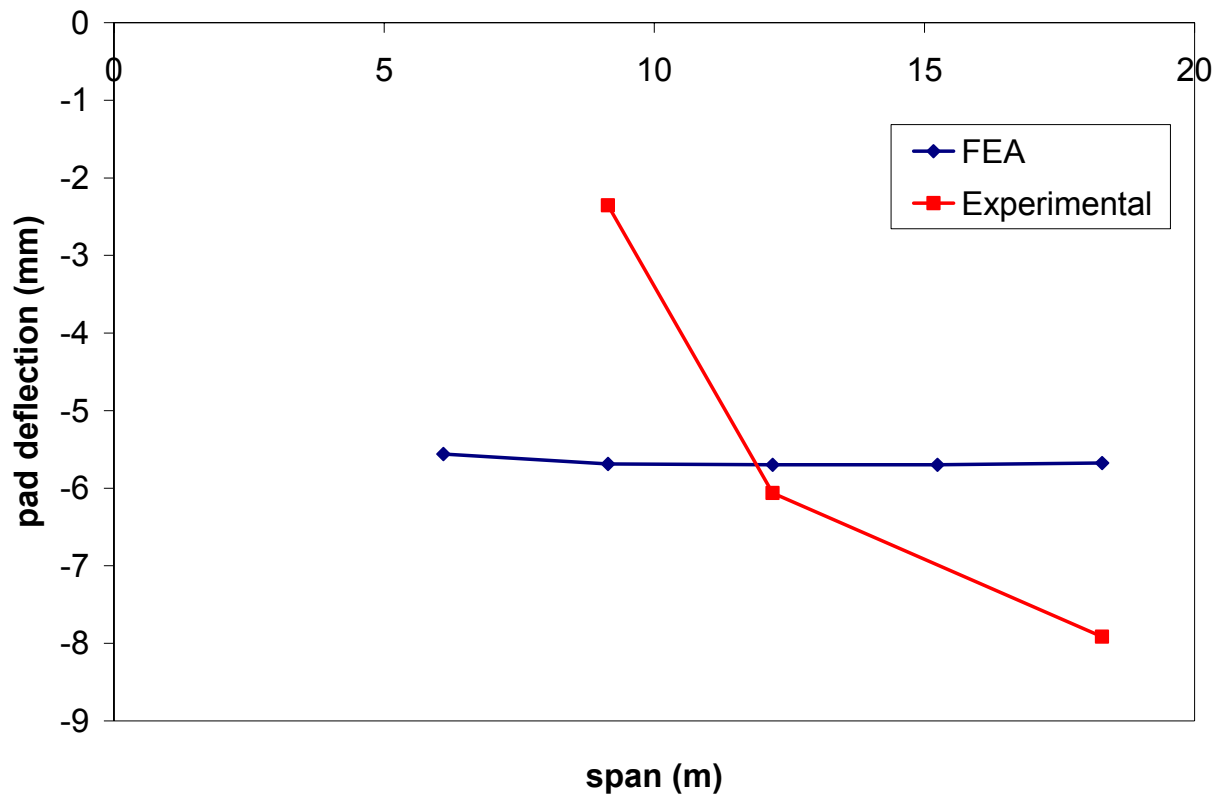
Figure 15. Comparison of the average pad deflection under four-point loading as predicted using FEA and as measured experimentally by Schniepp. The displacements at <u>all four corners</u> were averaged.
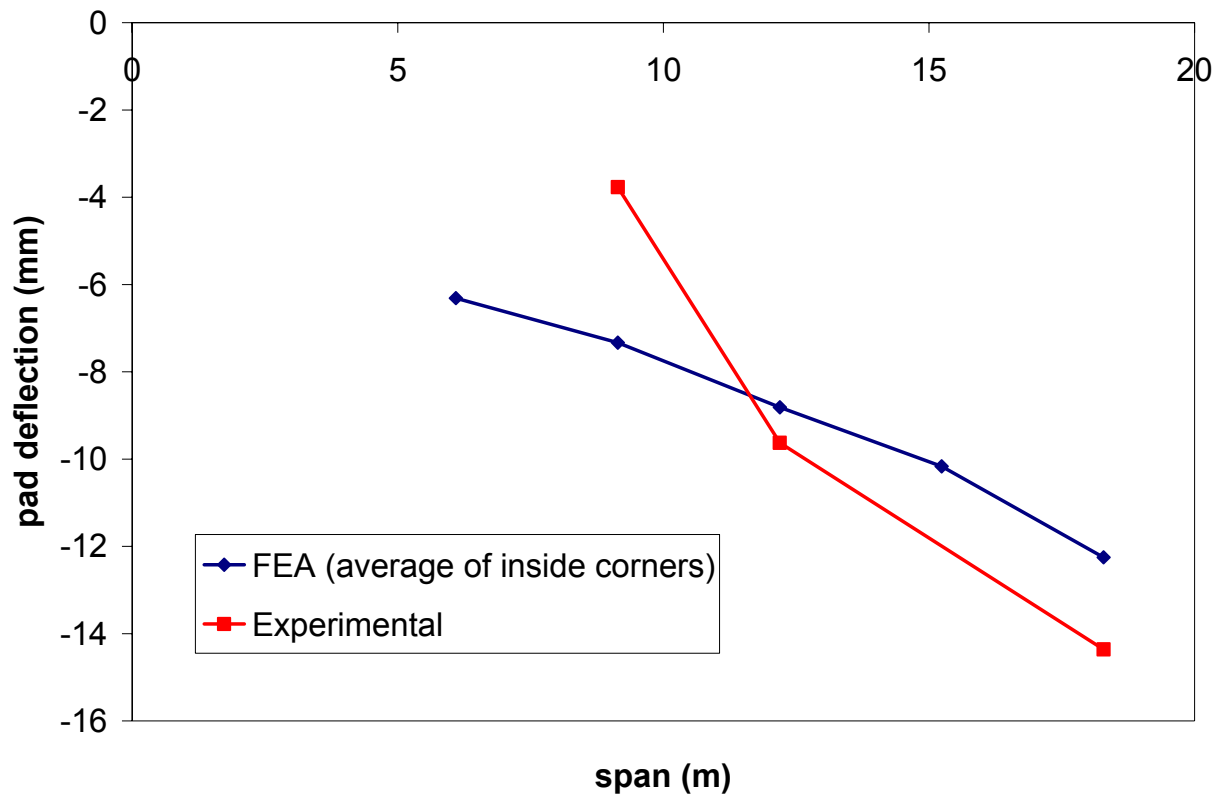
Figure 16. Comparison of the average pad deflection under four-point loading as predicted using FEA and as measured experimentally by Schniepp. The displacements at the <u>two inner corners</u> were averaged
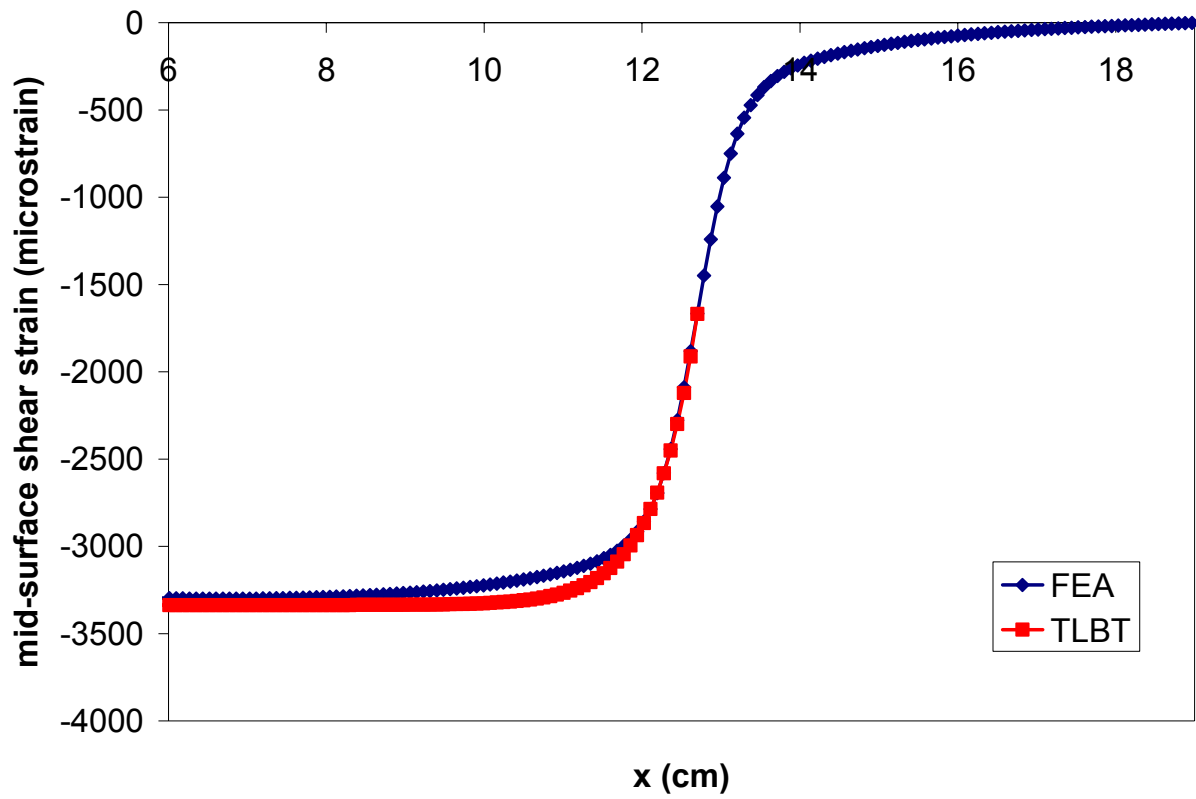
Figure 17. Mid-surface shear strains in the vicinity of a loading point for a solid rectangular beam with E/G = 37. Third-point loads are 4.45 kN (1 kip) each.
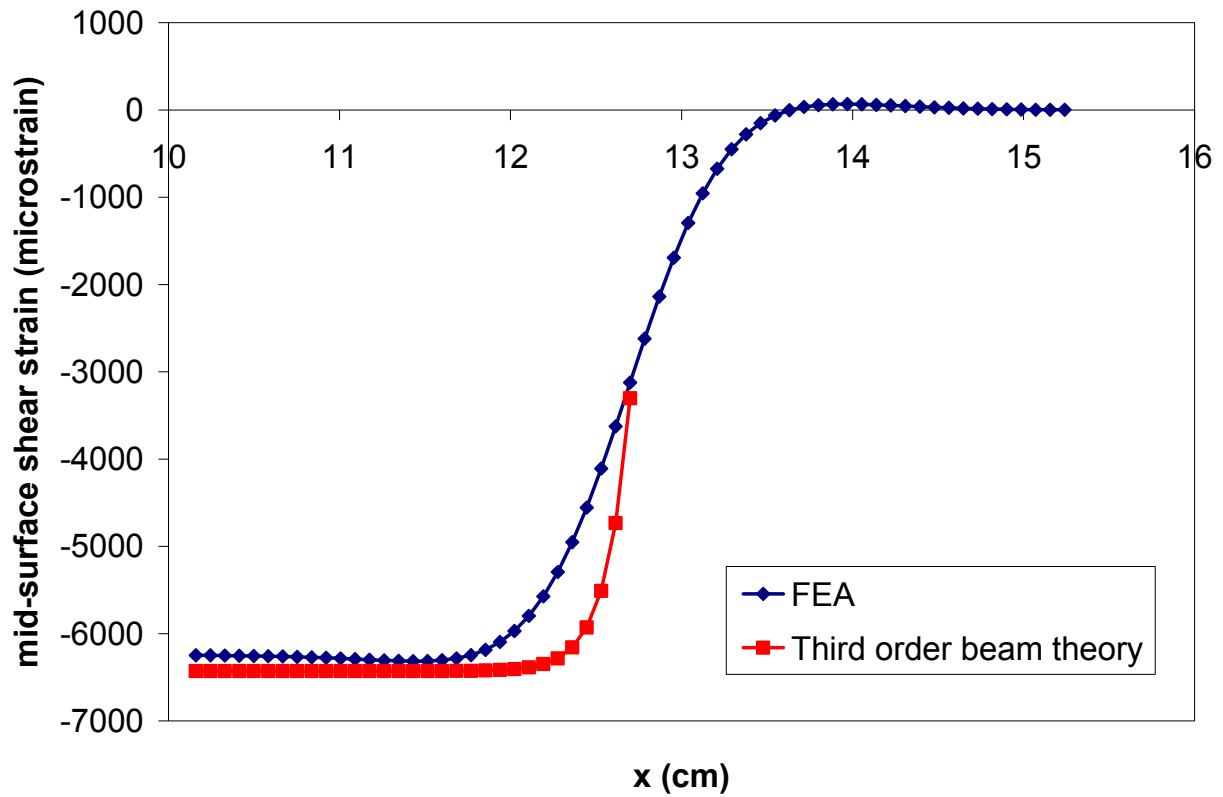
Figure 18. Mid-surface shear strains in the vicinity of a loading point for a solid rectangular beam with E/G = 2.5. Third-point loads are 44.5 kN (10 kips) each. (Note that only half of the TLBT profile is shown due to numerical problems in calculating the response between the load point and mid-span.)
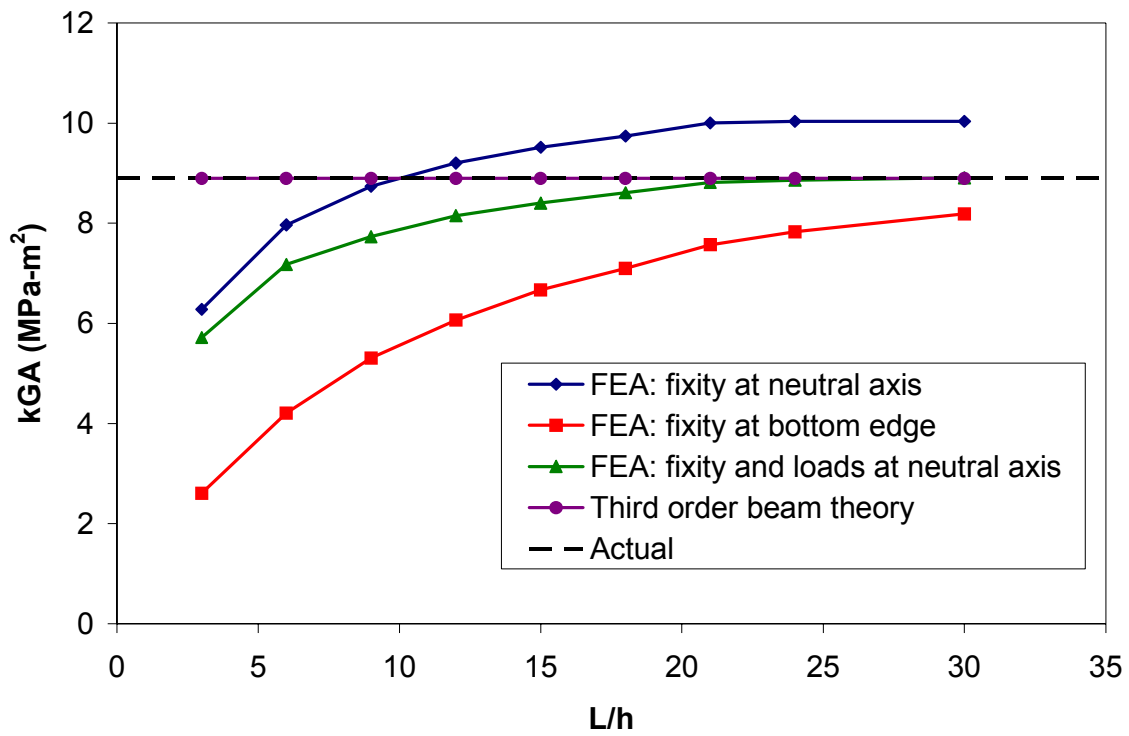
Figure 19. Back-calculated *kGA* values for a solid rectangular beam in four-point loading with E/G = 2.5 as determined from FEA and third order beam theory.
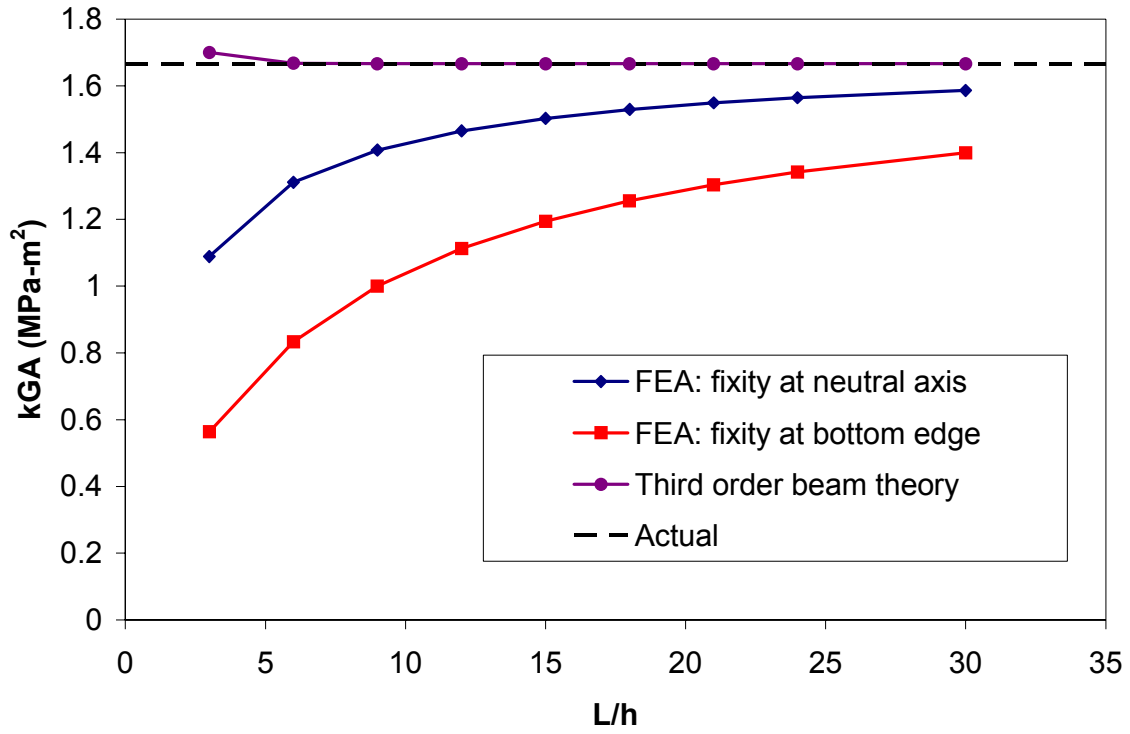
Figure 20. Back-calculated *kGA* values for a solid rectangular beam in four-point loading with E/G =37 as determined from FEA and third order beam theory.
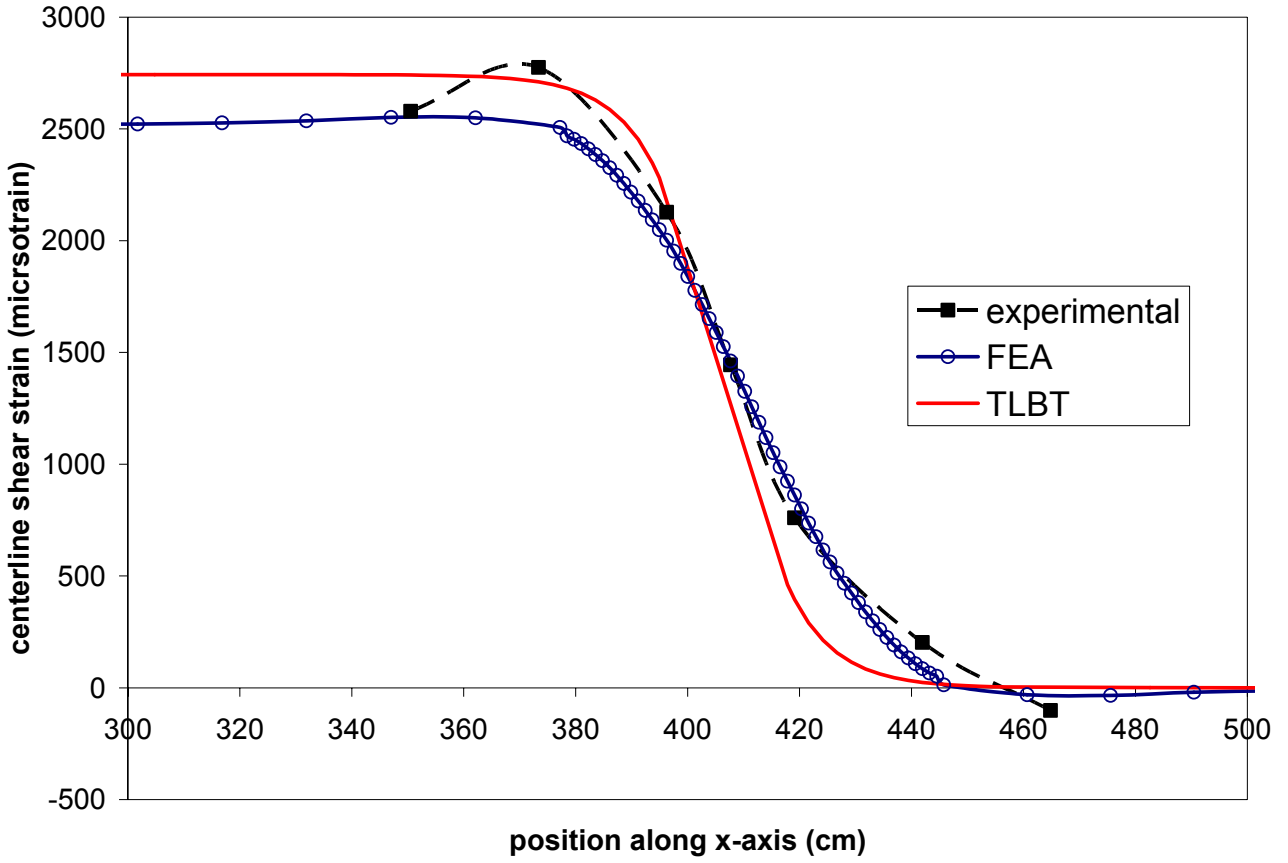
Figure 21. Mid-surface shear strain along the x-axis of a 12.2 m (40 ft) long beam subjected to four-point patch loading. (The patch load was located between x = 400 and 423 cm)
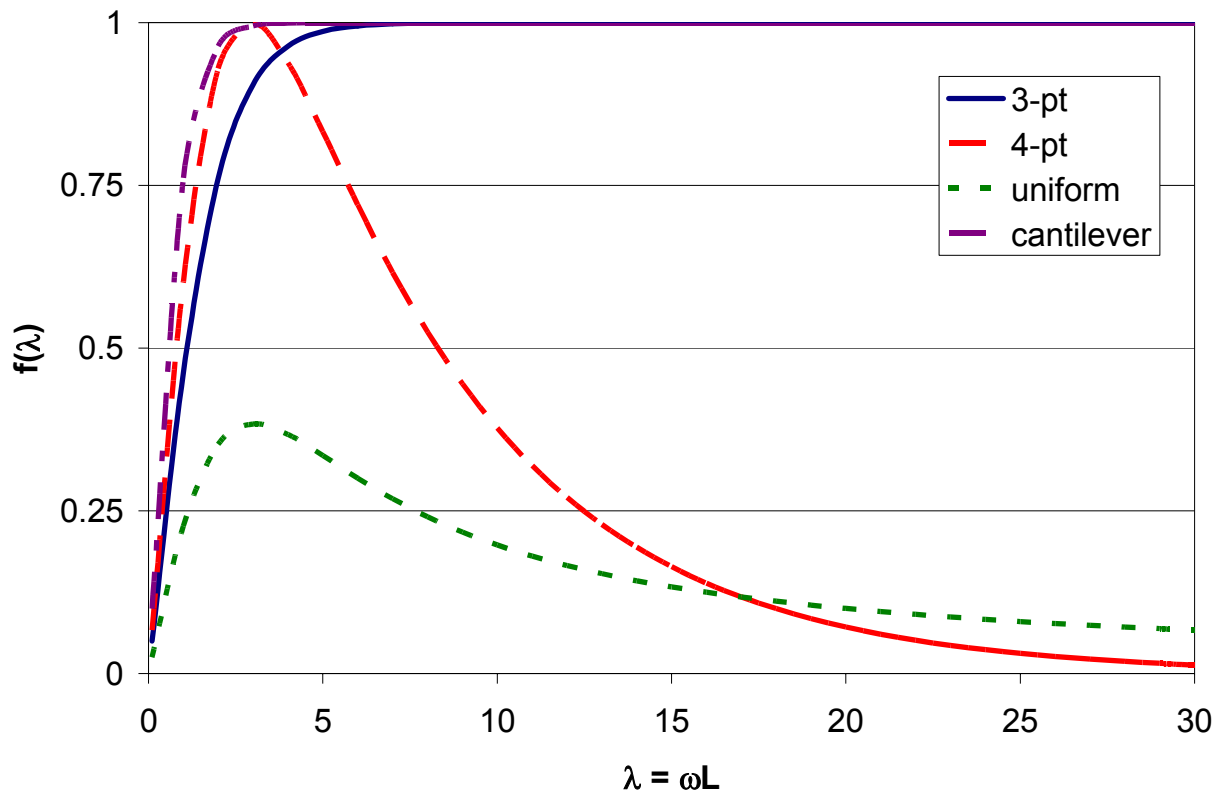
Figure 22. Warping term multiplier versus the non-dimensional span length, showing the relative contribution of warping for various loading geometries.
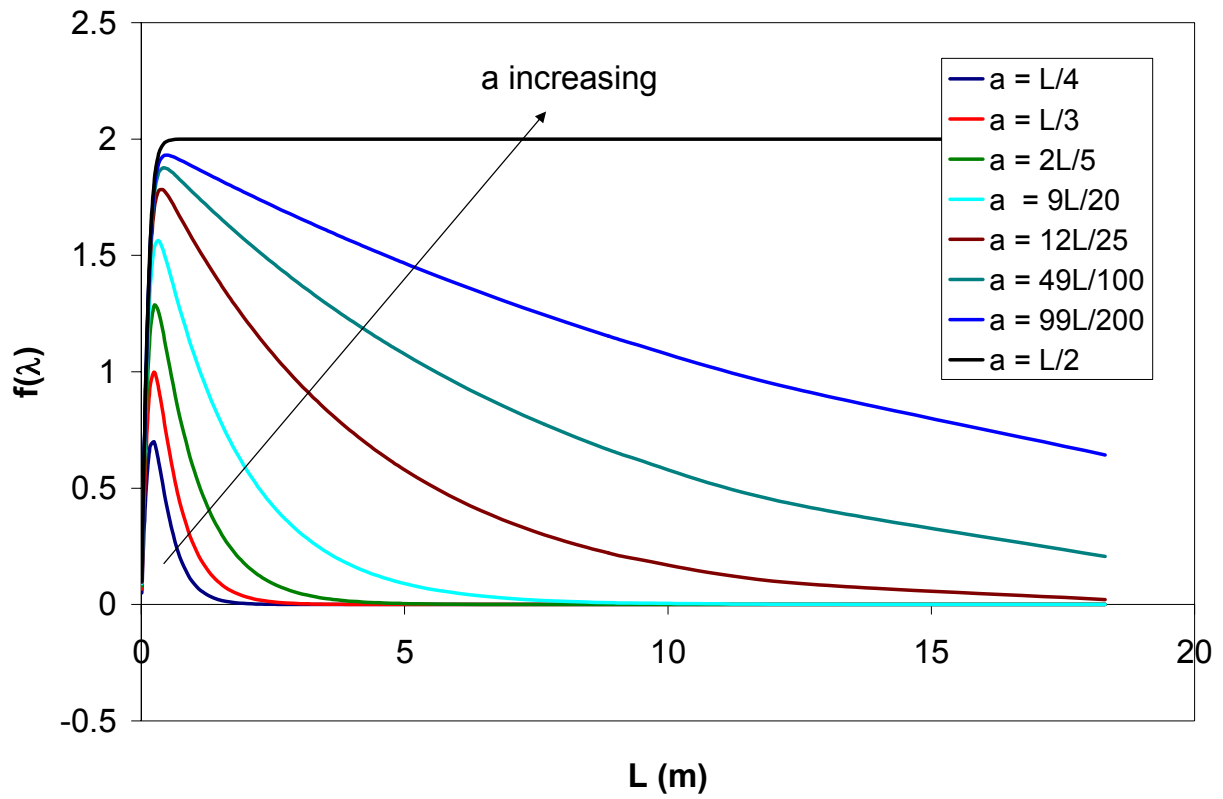
Figure 23. Effect of increasing the shear span length in a four-point test on the warping parameter, f(λ).
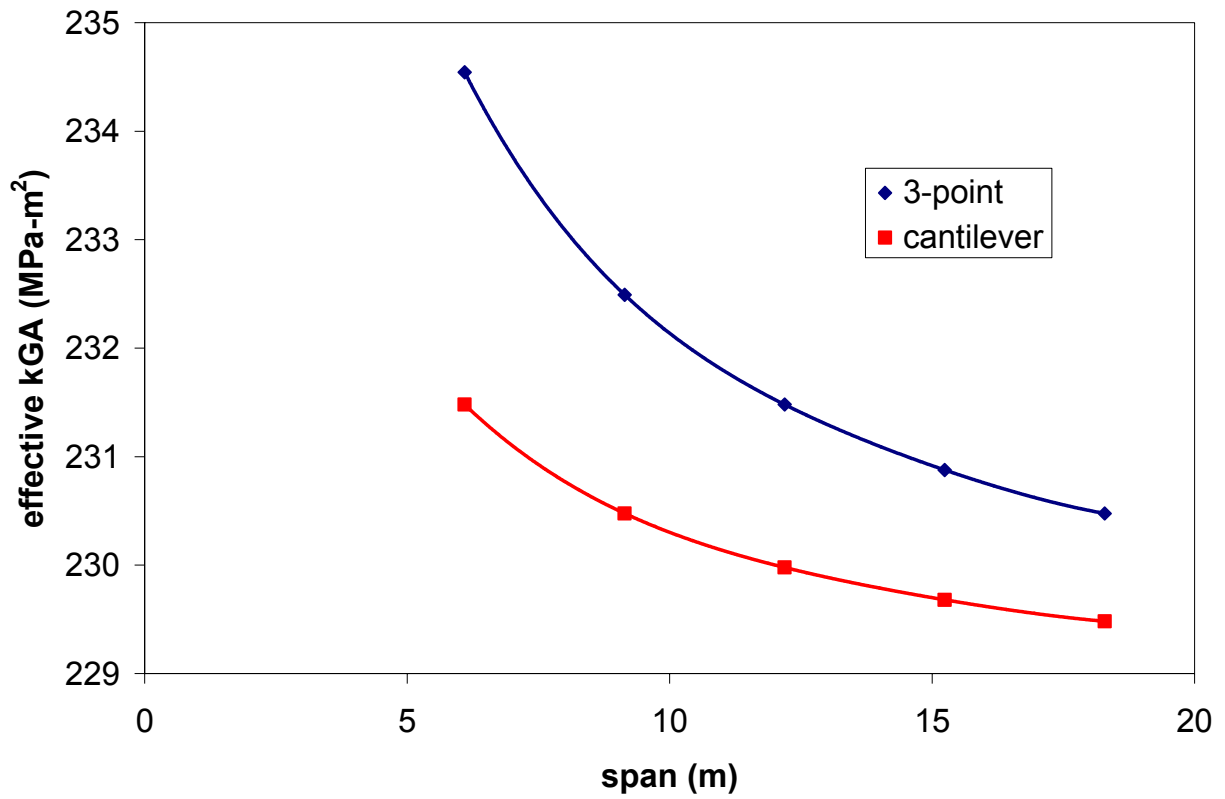
Figure 24. Effective shear stiffness versus span determined using the TLBT model for the three-point and cantilever load cases.
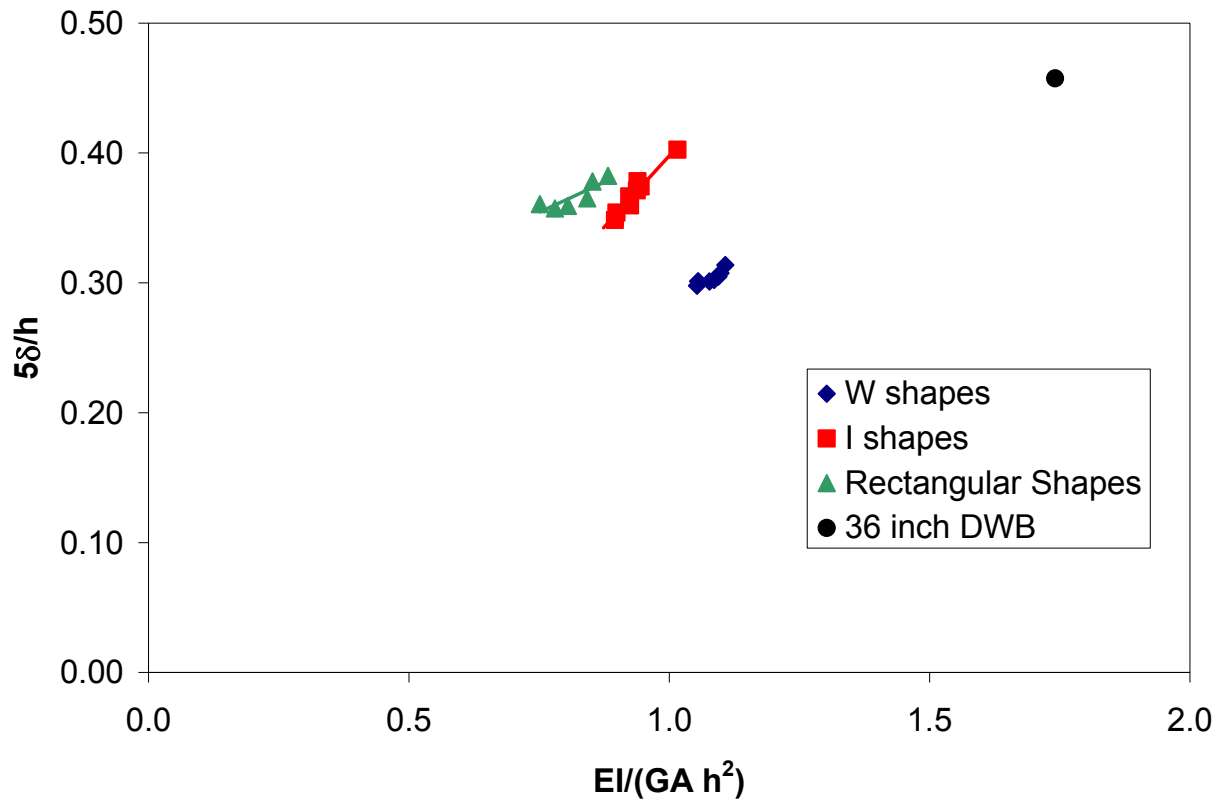
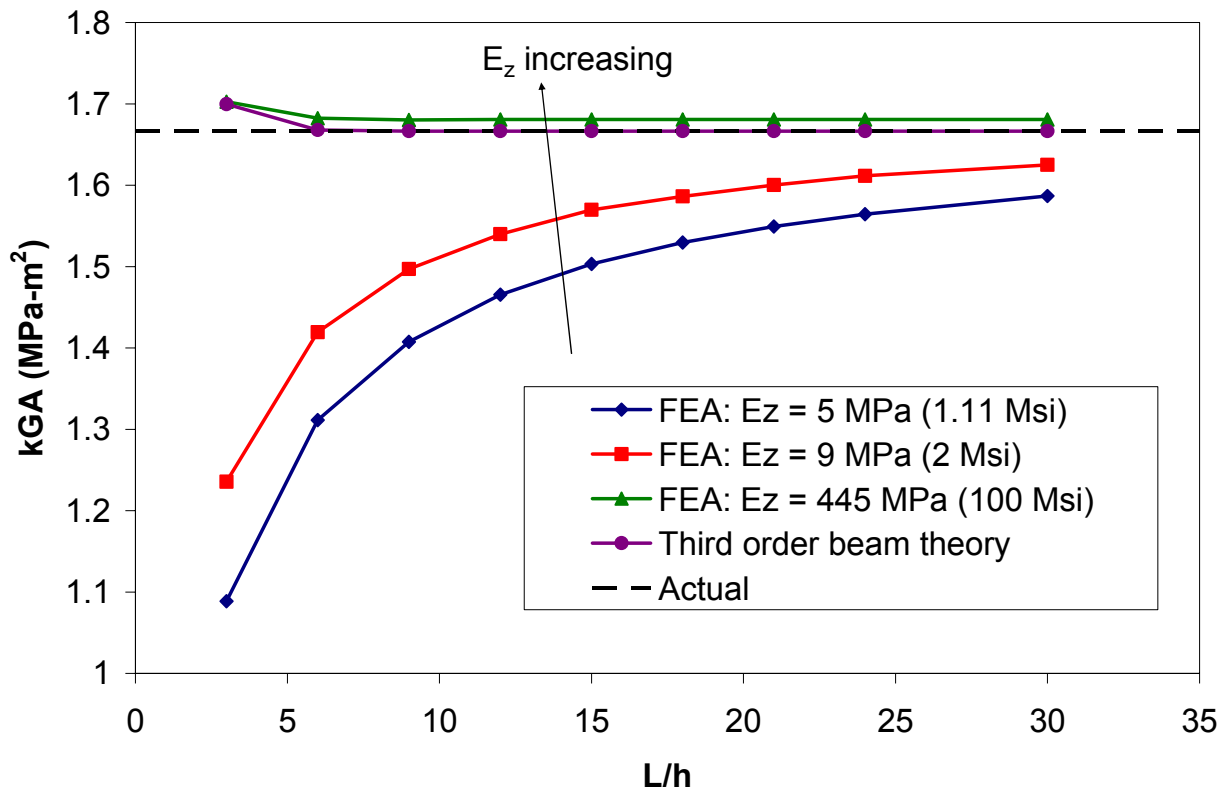Figure 25. Comparison of warping decay parameters for various fiberglass structural beams.

Figure 26. Influence of the transverse compressive modulus on the effective *kGA* value (solid beam test case, four-point loading).
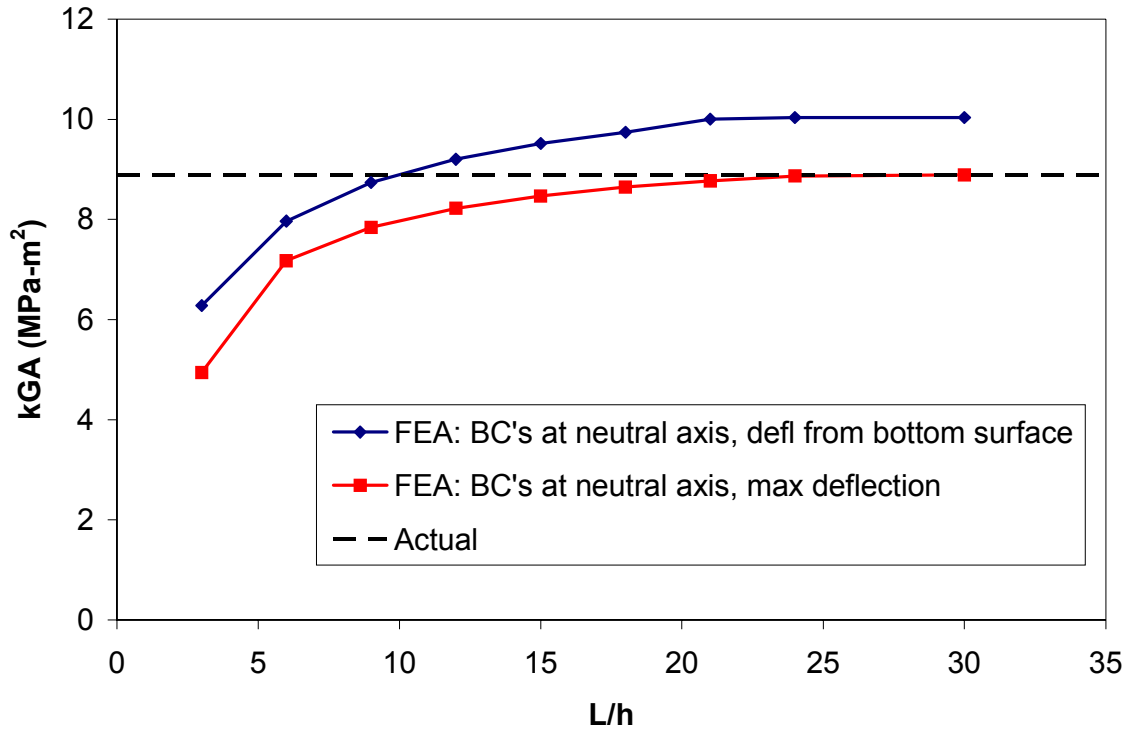
Figure 27. Sensitivity of the *kGA* measurement to the location where deflection is measured. (solid beam test case: E/G = 2.5, boundary conditions at the <u>neutral axis</u>)
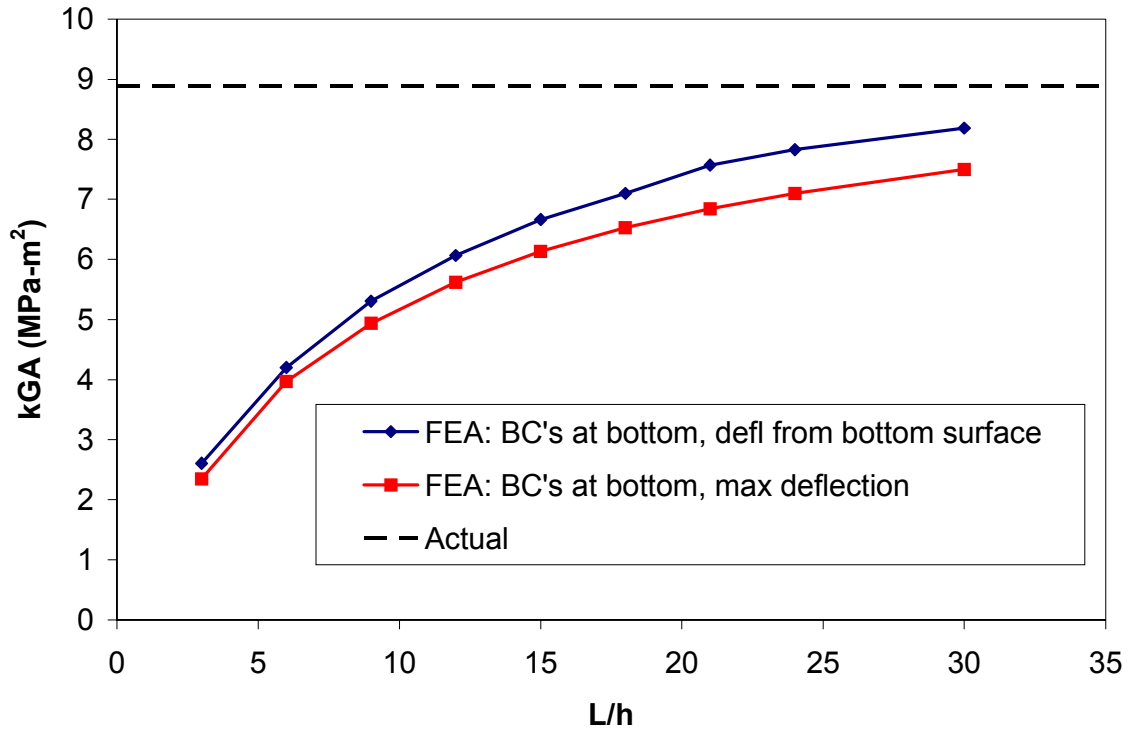
Figure 28. Sensitivity of the *kGA* measurement to the location where deflection is measured. (solid beam test case: E/G = 2.5, boundary conditions at the <u>bottom edge</u>).
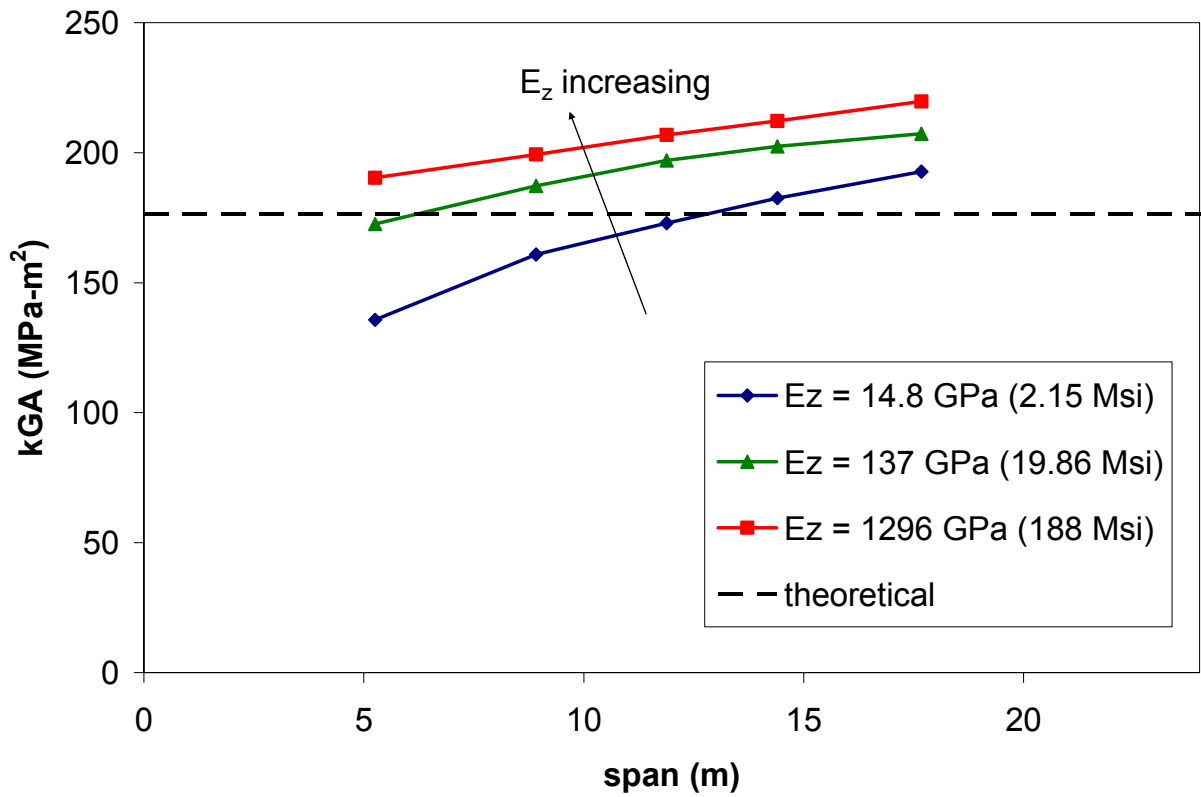
Figure 29. Effect of transverse stiffness on the effective *kGA* value of the DWB (finite element results).
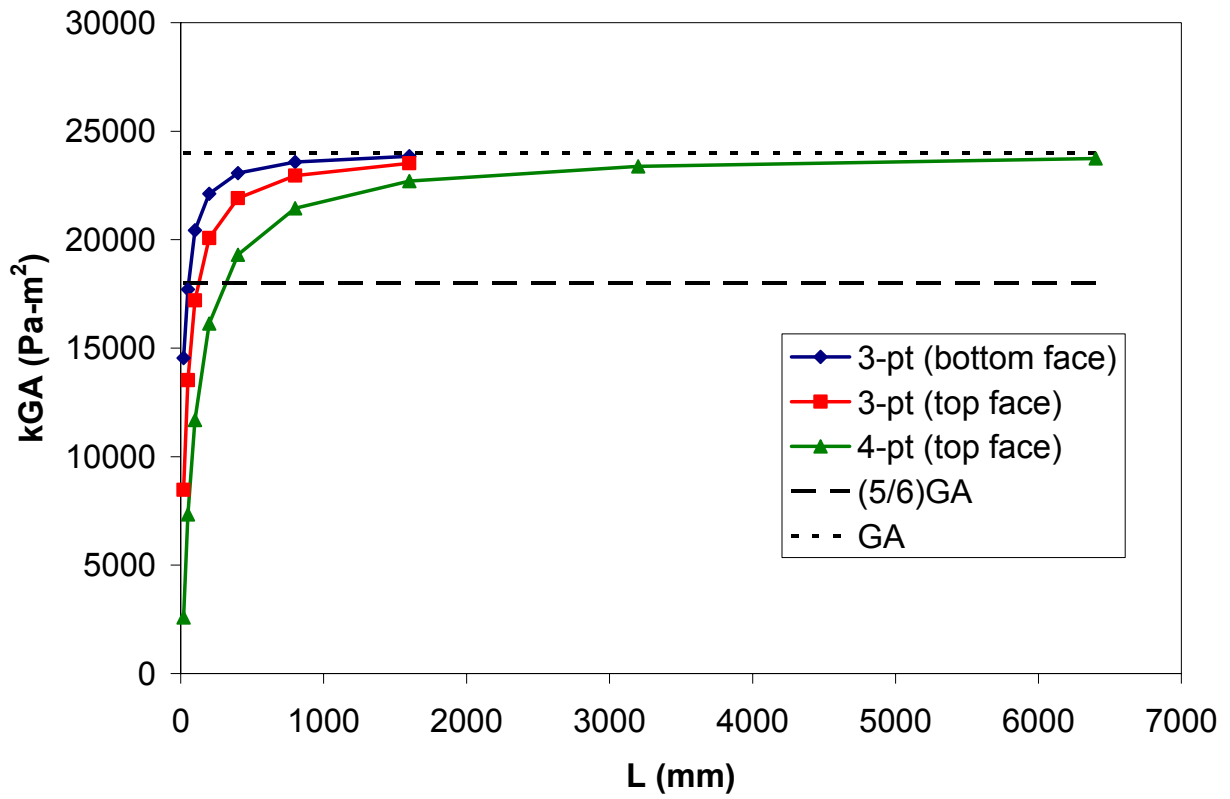
Figure 30. Effective *kGA* versus span for Swanson's sandwich beam under three- and four-pt loading (higher order sandwich theory).
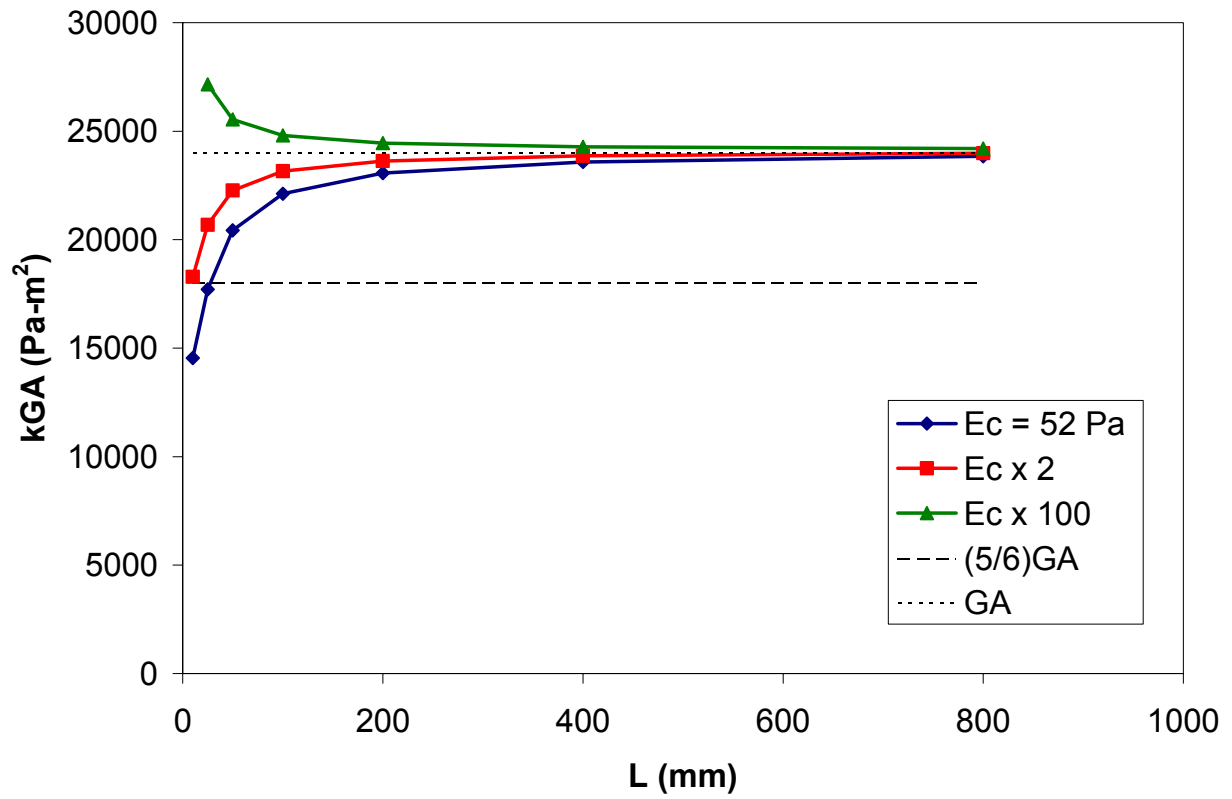
Figure 31. Effect of transverse core modulus on the effective *kGA* of Swanson's sandwich beam (higher order sandwich theory).
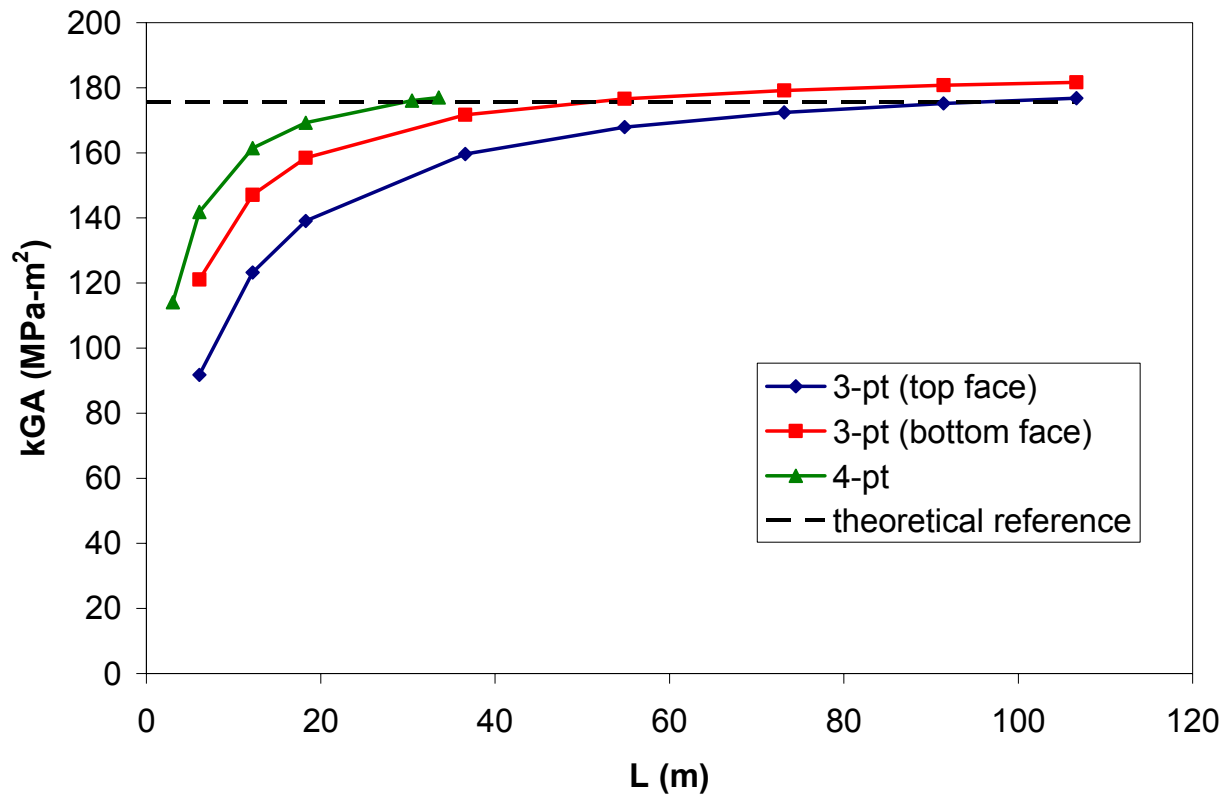
Figure 32. Effective *kGA* versus span for DWB under three- and four-point loading (higher order sandwich theory).
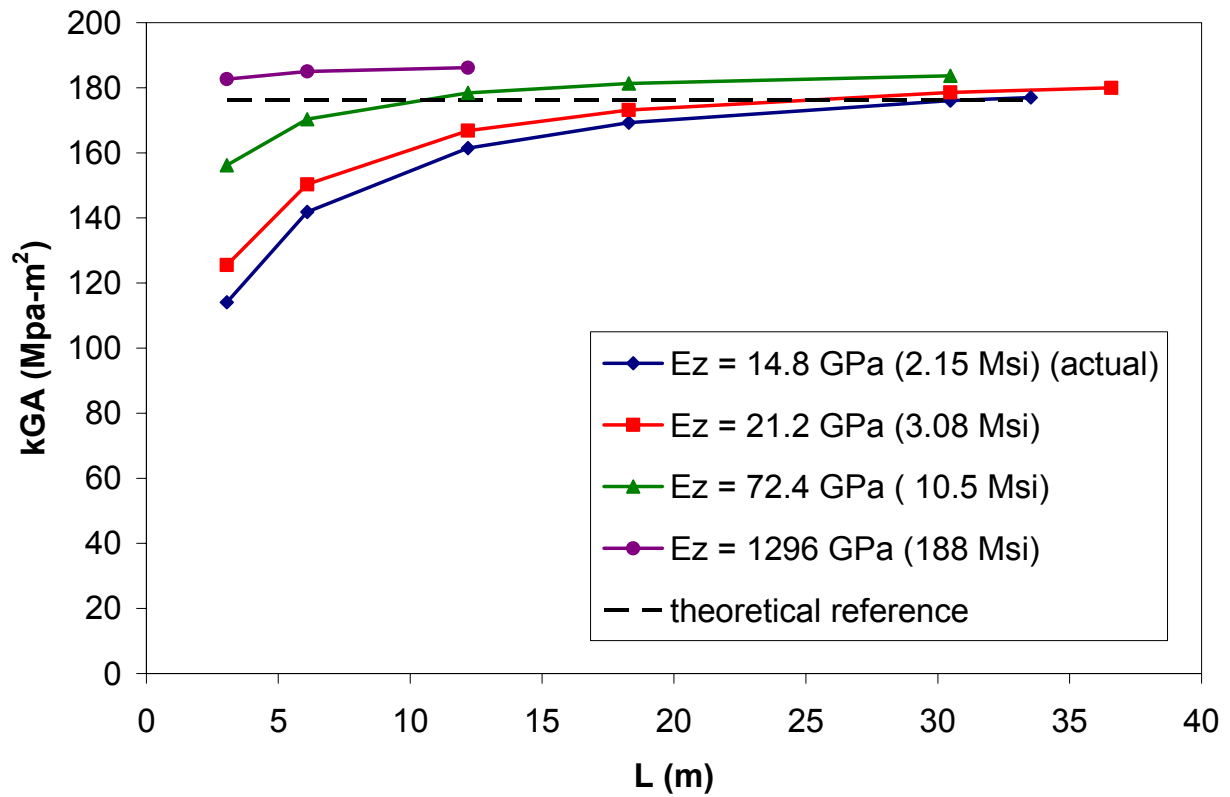
Figure 33. Effect of transverse stiffness on the effective *kGA* value of the DWB (higher order sandwich theory).
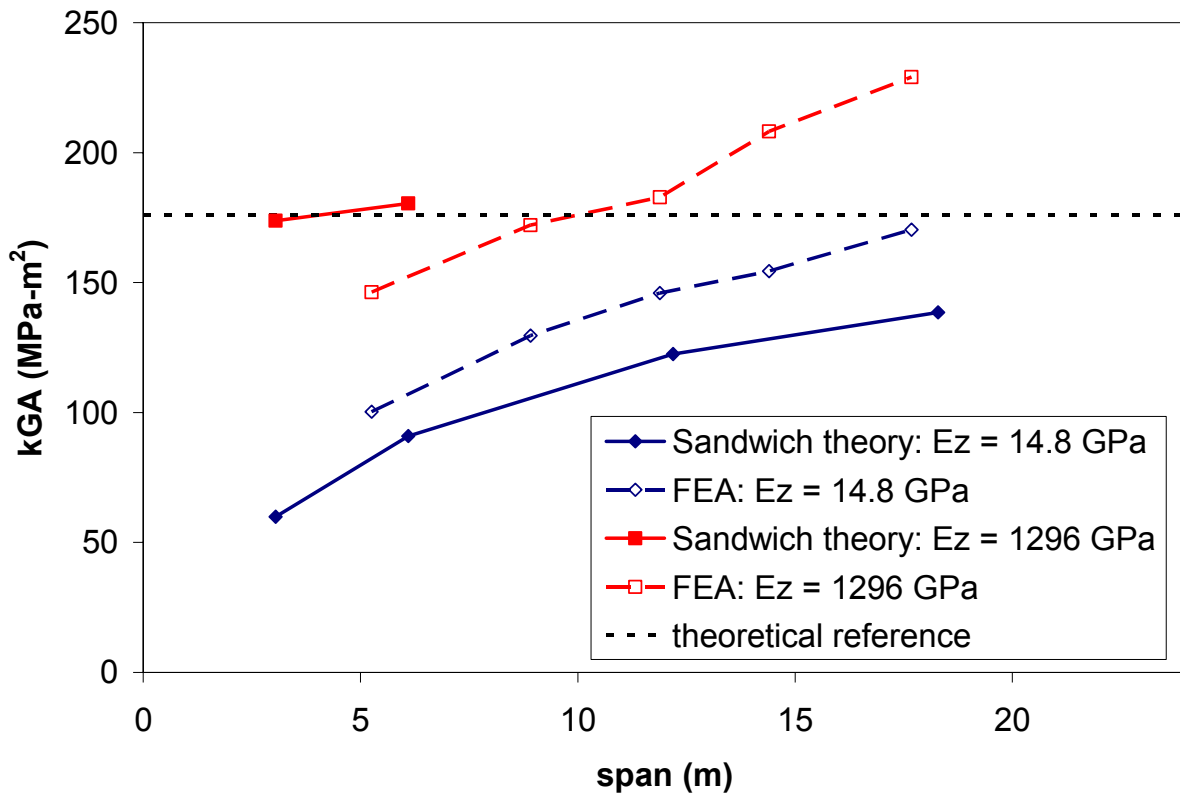
Figure 34. Variation of the effective *kGA* of the DWB with span and transverse stiffness: FEA vs. higher order sandwich theory.
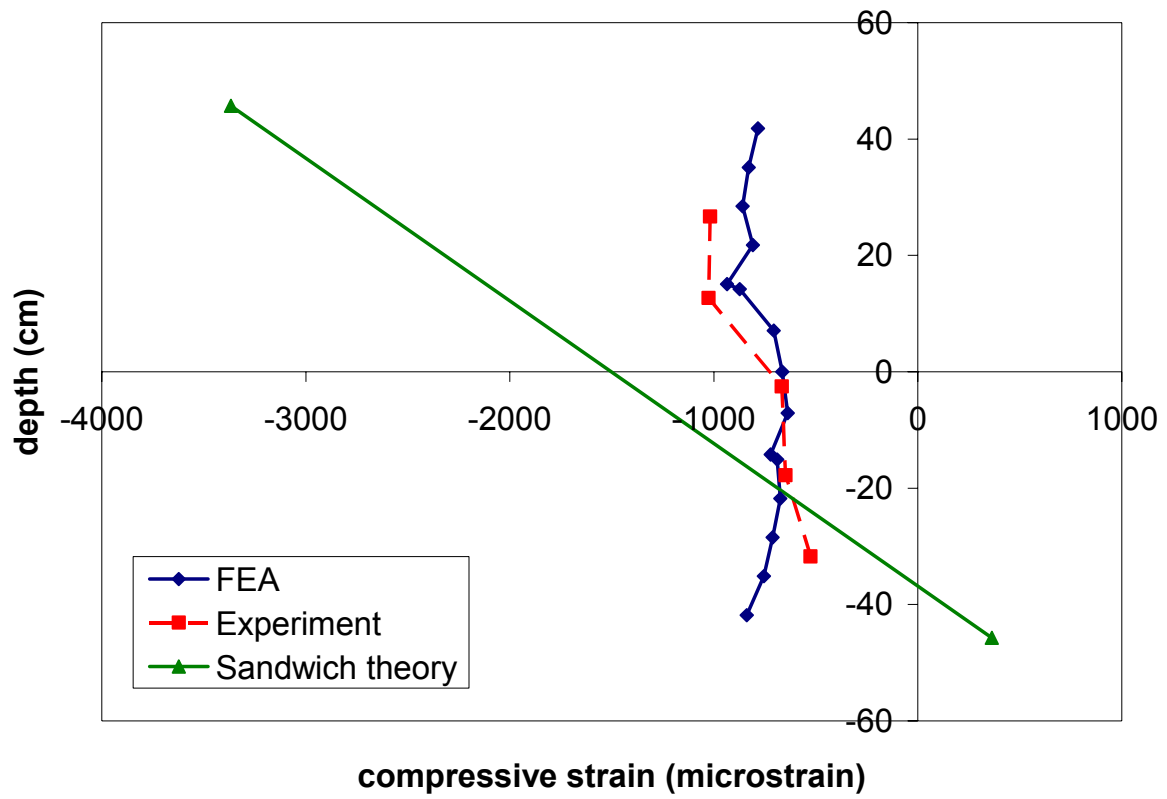
Figure 35. Compressive strains at 445 kN (100 kips) through the thickness of the DWB web, directly underneath the load patch.
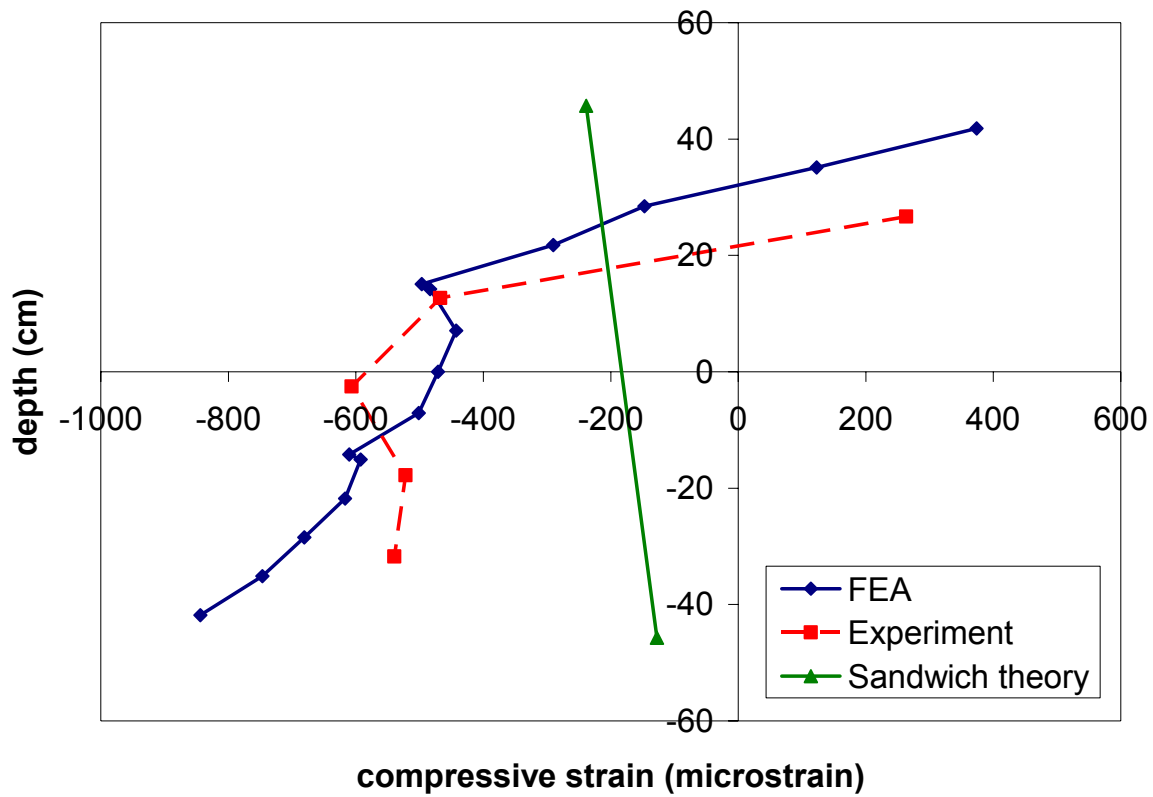
Figure 36. Compressive strains at 445 kN (100 kips) through the depth of the DWB web, at a distance of 11.4 cm outside the edge of the pad.

Figure 37. FE predicted compressive strains in the vicinity of the pad support (at 445 kN or 100 kips).

Figure 38. Compressive strains at the flange/web interface of a beam under four-point patch loading (444 kN or 100 kips) as predicted using FEA and the higher order sandwich theory.

References

1. Bank, L.C., *Flexural and shear moduli of full-section fiber reinforced plastic (FRP) pultruded beams.* Journal of Testing and Evaluation, 1989. **17**(1): p. 40-45.
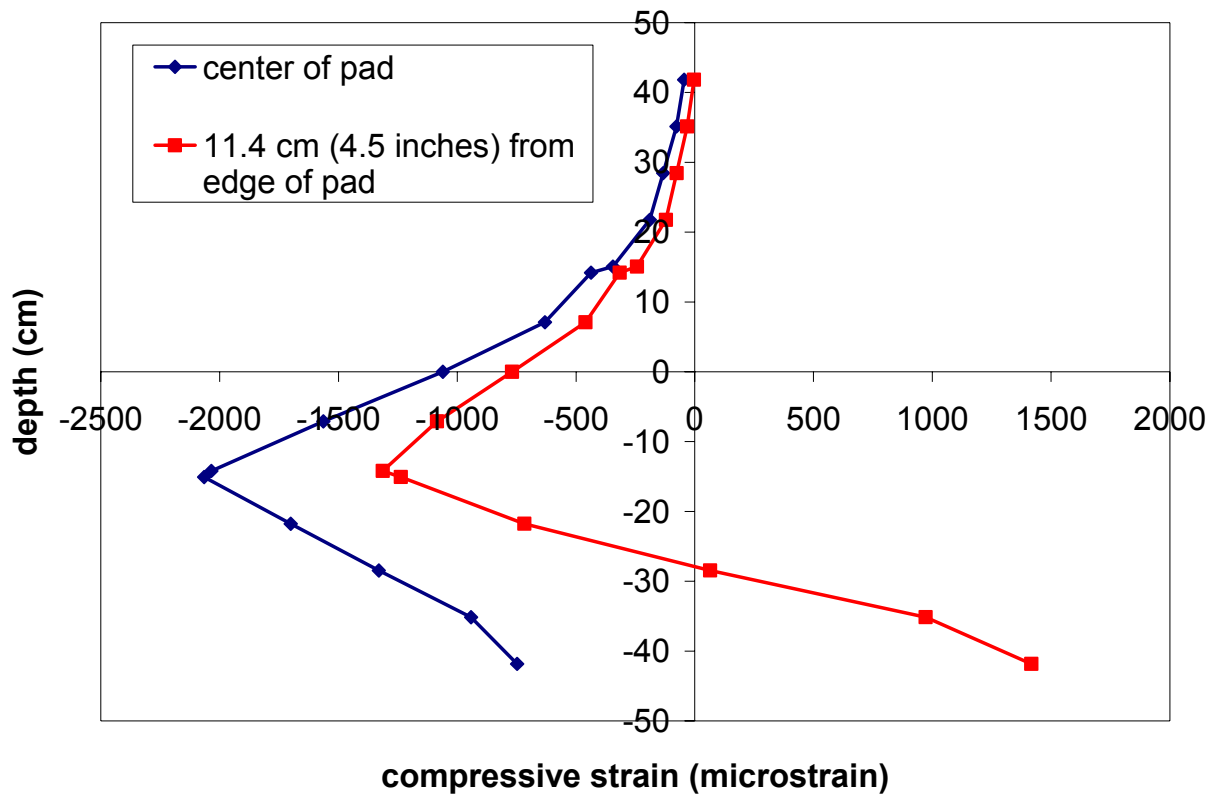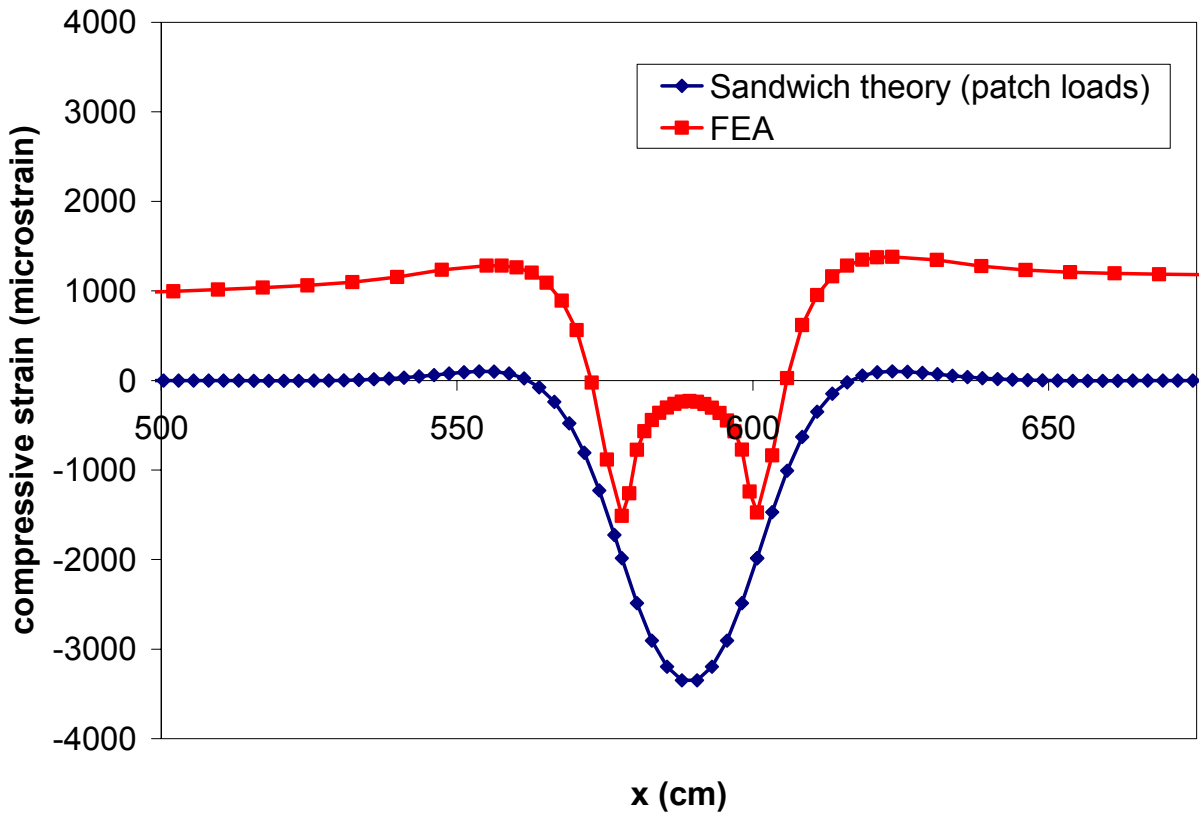
2. Hayes, M.D., et al., *Laboratory and field testing of composite bridge superstructure.* Journal of Composites for Construction, 2000. **4**(3 Aug): p. 120-128.

3. Hayes, M.D., *Characterization and Modeling of a Fiber-Reinforced Polymeric Composite Structural Beam and Bridge Structure for Use in the Tom's Creek Bridge Rehabilitation Project*, in *Engineering Mechanics*. 1998, Virginia Polytechnic Institute and State University: Blacksburg, Virginia.

4. Strongwell, *EXTREN DWB^{TM} Design Guide*. 2000.

5. Senne, J., *Fatigue Life of Hybrid FRP Composite Beams*, in *Engineering Science and Mechanics*. 2000, Virginia Tech: Blacksburg.

6. Seung Jo, K., Y. Ki Won, and J. Sung Nam, *Shear correction factors for thin-walled composite boxbeam considering nonclassical behaviors.* Journal of Composite Materials, 1996. **30**(10): p. 1132-49.

7. Restrepo, E.S., *Determination of AASHTO Bridge Design Paramters through Field Evaluation of the Rt. 601 Bridge: A Bridge Utilizing Strongwell 36 in. Fiber-Reinforced Polymer Double Web Beams as the Main Load Carrying Members*, in *Civil and Environmental Engineering*. 2002, Virginia Polytechnic Institute and State University: Blacksburg. p. 164.

8. Waldron, C., *Determination of the Design Parameters for the Route 601 Bridge: A Bridge Containing the Strongwell 36 inch Hybrid Composite Double Web Beam*, in *Civil Engineering*. 2001, Virginia Polytechnic Institute and State University: Blacksburg, VA.

9. Schniepp, T.J., *Design Manual Development for a Hybrid, FRP Double-Web Beam and Characterization of Shear Stiffness in FRP Composite Beams*, in *Engineering Mechanics*. 2002, Virginia Polytechnic Institute and State University: Blacksburg, Virginia.

10. Bank, L.C., *Shear coefficients for thin-walled composite beams.* Composite Structures, 1987. **8**(1): p. 47-61.

11. Timoshenko, S.P., *On the Correction for Shear of the Differential Equationfor Transverse Vibrations of Prismatic Bars.* Philosophical Magazine, 1921. **41**: p. 744-746.

12. Timoshenko, S.P., *On the Transverse Vibrations of Bars of Uniform Cross-Section.* Philosophical Magazine, 1922. **43**: p. 125-131.

13. Cowper, G.R., *The Shear Coefficient in Timoshenko's Beam Theory.* Journal of Applied Mechanics, 1966: p. 335-340.

14. Dharmarajan, S. and H. McCutchen, *Shear Coefficients for Orthotropic Beams*. Journal of Composite Materials, 1973. **7**: p. 530-535.

15. Teh, K.K. and C.C. Huang, *Shear Deformation Coefficient for Generally Orthotropic Beam*. Fiber Science and Technology, 1979. **12**: p. 73-80.

16. Madabhusi-Raman, P. and J.F. Davalos, *Static shear correction factor for laminated rectangular beams*. Composites Part B:Engineering, 1996. **27**(3-4): p. 285-293.

17. Jones, R.M., *Mechanics of Composite Materials*. 1975, New York: Hemisphere Publishing Corporation.

18. Hyer, M.W., *Stress Analysis of Fiber-Reinforced Composite Materials*. 1998, Boston: McGraw-Hill.

19. Nagaraj, V. and H.V.S. GangaRao, *Static Behavior of Pultruded GFRP beams*. Journal of Composites for Construction, 1997. **1**(3): p. 120-129.

20. Omidvar, B., *Shear coefficient in orthotropic thin-walled composite beams*. Journal of Composites for Construction, 1998. **2**(1): p. 46-56.

21. Bank, L.C. and T.P. Melehan, *Shear coefficients for multicelled thin-walled composite beams*. Composite Structures, 1989. **11**(4): p. 259-276.

22. Barbero, E.J., R. Lopez-Anido, and J.F. Davalos, *On the mechanics of thin-walled laminated composite beams*. Journal of Composite Materials, 1993. **27**(8): p. 806-29.

23. Kim, S.J., K.W. Yoon, and S.N. Jung, *Shear correction factors for thin-walled composite boxbeam considering nonclassical behaviors*. Journal of Composite Materials, 1996. **30**(10): p. 1132-1149.

24. Fischer, S., et al., *Simultaneous Determination of Shear and Young's Moduli in Composites*. Journal of Testing and Evaluation, 1981. **9**(5): p. 303-307.

25. Sims, G.D., A.F. Johnson, and R.D. Hill, *Mechanical and Structural Properties of a GRP Pultruded Section*. Composite Structures, 1987. **8**: p. 173-187.

26. Barbero, E.J., Fu, and Raftoyiannis, *Ultimate Bending Strength of Composite Beams*. Journal of Materials in Civil Engineering, 1991. **3**(4): p. 292-306.

27. Davalos, J.F., et al., *Analysis and design of pultruded FRP shapes under bending*. Composites Part B:Engineering, 1996. **27**(3-4): p. 295-305.

28. Cosenza, E., F. Lazzaro, and M. Peece. *Experimental Evaluation of Bending and Torsional Deformability of FRP Pultruded Beams*. in *Advanced Composite Materials in Bridges and Structures*. 1996. Montreal, Quebec.

29. Allen, H.G., *Analysis and design of structural sandwich panels*. 1969, Oxford: Pergamon Press.

30. Bauchau, O.A., *A Beam Theory for Anisotropic Materials.* Journal of Applied Mechanics-Transactions of the ASME, 1985. **52**: p. 416-421.

31. Dufort, L., M. Grediac, and Y. Surrel, *Experimental evidence of the cross-section warping in short composite beams under three point bending.* Composite Structures, 2001. **51**(1 Jan): p. 37-47.

32. Lopez-Anido, R. and H.V.S. GangaRao, *Warping Solution for Shear Lag in Thin-Walled Orthotropic Composite Beams.* Journal of Engineering Mechanics, 1996. **122**(5): p. 449-457.

33. Whitney, J.M., *Elasticity Analysis of Orthotropic Beams under Concentrated Loads.* Composites Science and Technology, 1985. **22**: p. 167-184.

34. Yoshida, H., T. Ogasa, and M. Uemura, *Local Stress Distribution in the Vicinity of Loading Points in Flexural Test of Orthotropic Beams.* Journal of Energy Resources Technology, 1991. **113**: p. 230-234.

35. Ming, X. and D.F. Adams, *Contact Finite Element Modeling of the Short Beam Shear Test for Composite Materials.* Computers & Structures, 1995. **57**(2): p. 183-191.

36. Frostig, Y., et al., *High-Order Theory for Sandwich-Beam Behavior with Transversely Flexible Core.* Journal of Engineering Mechanics-Asce, 1992. **118**(5): p. 1026-1043.

37. Dufort, L., S. Drapier, and M. Grediac, *Closed-form solution for the cross-section warping in short beams under three-point bending.* Composite Structures, 2001. **52**(2): p. 233-246.

38. Bauld, N.R. and L.S. Tzeng, *A Vlasov theory for fiber-reinforced beams with thin-walled open cross sections.* International Journal of Solids & Structures, 1984. **20**(3): p. 277-297.

39. Chandra, R. and I. Chopra, *Experimental and theoretical analysis of composite I-beams with elastic couplings.* AIAA Journal, 1991. **29**(12): p. 2197-2205.

40. Rehfield, L.W. *Design Analysis Methodology for Composite Rotor Blades.* in *Seventh DOD/NASA Conference on Fibrous Composites in Structural Design, AFWAL-TR-85-3094.* 1985.

41. Goetschel, D.B. and T.H. Hu, *Quantification of Saint-Venant's Principle for a General Prismatic Member.* Computers and Structures, 1985. **21**(5): p. 869- 874.

42. Hjelmstad, K.D., *Warping Effects in Transverse Bending of Thin-Walled Beams.* Journal of Engineering Mechanics, 1987. **113**(6): p. 907-924.

43. Foutch, D.A. and P.C. Chang, *A Shear Lag Anomaly.* Journal of the Structural Division, ASCE, 1982. **108**(7): p. 1653-1658.

44. Rehfield, L.W., A.R. Atilgan, and D.H. Hodges, *Nonclassical Behavior of Thin-Walled Composite Beams with Closed Cross-Sections.* Journal of the American Helicopter Society, 1990(May): p. 42-49.

45. Smith, E.C. and I. Chopra, *Formulation and evaluation of an analytical model for composite box-beams.* Collection of Technical Papers - AIAA/ASME/ASCE/AHS Structures, Structural Dynamics & Materials Conference. Publ by AIAA, New York, NY, USA, 1990: p. pt 2. p 759-782.

46. Hodges, D.H., et al., *Free-Vibration Analysis of Composite Beams.* Journal of the American Helicopter Society, 1991(July): p. 36-38.

47. Tripathy, A.K., H.J. Patel, and S.S. Pang, *Bending analysis of laminated composite box beams.* Journal of Engineering Materials & Technology-Transactions of the ASME, 1994. **116**(1 Jan): p. 121-129.

48. Song, O. and L. Librescu, *Refined theory and behavior of thin-walled beams made of advanced composite materials and incorporating non-classical effects*, in *Recent Advances in Structural Mechanics, American Society of Mechanical Engineers, Pressure Vessels and Piping Division.* 1991, ASME: New York. p. 111-119.

49. Kim, C. and S.R. White, *Laminated composite thin- and thick-walled beam theory and coupled deformations.* Recent Advances in Composite Materials American Society of Mechanical Engineers, Materials Division (Publication) MD, 1995. **56**: p. 167-182.

50. Plantema, F.J., *Sandwich construction; the bending and buckling of sandwich beams, plates, and shells*. 1966, New York: Wiley.

51. Thomsen, O.T., *Analysis of local bending effects in sandwich plates with orthotropic face layers subjected to localized loads.* Composite Structures, 1993. **25**(1-4): p. 511-520.

52. Frostig, Y. and Y. Shenhar, *High-Order Bending of Sandwich Beams with a Transversely Flexible Core and Unsymmetrical Laminated Composite Skins.* Composites Engineering, 1995. **5**(4): p. 405-414.

53. Swanson, S.R., *Response of Orthotropic Sandwich Plates to Concentrated Loading.* Journal of Sandwich Structures and Materials, 2000. **2**: p. 270-287.

54. Swanson, S.R., *An examination of a higher order theory for sandwich beams.* Composite Structures, 1999. **44**(2-3): p. 169-77.

55. Frostig, Y. and M. Baruch, *Localized load effects in high-order bending of sandwich panels with flexible core.* Journal of Engineering Mechanics-Asce, 1996. **122**(11): p. 1069-1076.

56. Pipes, R.B. and N.J. Pagano, *Interlaminar stresses in composite laminates under uniform axial extension.* Journal of Composite Materials, 1970. **4**: p. 538-48.

57. Srinivas, S. and A.K. Rao, *Bending, Vibration and Buckling of Simply Supported Thick Orthotropic Rectangular Plates and Laminates.* International Journal of Solids and Structures, 1970. **6**: p. 1463-1481.

58. *ANSYS 6.0 Documentation*.

59. Reddy, J.N., *Mechanics of Laminated Composite Plates: Theory and Analysis*. 1997, New York: CRC Press, Inc.

60. Reddy, J.N., C.M. Wang, and K.H. Lee, *Relationships between bending solutions of classical and shear deformation beam theories.* International Journal of Solids & Structures, 1997. **34**(26 Sep): p. 3373-3384.

61. Horgan, C.O., *On Saint-Venant's Principle in Plane Anisotropic Elasticity.* Journal of Elasticity, 1972. **2**: p. 169-180.

62. Barbero, E.J., *Introduction to Composite Materials Design*. 1999, New York: Taylor and Francis. 352.

63. Hashin, J. and B.W. Rosen, *The Elastic Moduli of Fiber-Reinforced Materials.* Journal of Applied Mechanics, 1964: p. 223-230.

64. Tsai, S.W. and H.T. Hahn, *Introduction to Composite Materials*. 1980, Lancaster, Pennsylvania: Technomic.